Three dimensional method for monitoring damage to dolos breakwaters

Purpose:

Thesis presented in fulfilment of the requirements for the degree of

Master of Science in the Faculty of Civil Engineering

at

Stellenbosch University

by:

Kishan Ramesh Tulsi

Supervisor:

Prof J S Schoonees

Civil Engineering

Stellenbosch University

December 2016

Declaration

By submitting this thesis electronically;
I declare that the entirety of the work contained therein is my own, original work, that I am the sole author thereof (save to the extent explicitly otherwise stated), that reproduction and publication thereof by Stellenbosch University will not infringe any third party rights and that I have not previously in its entirety or in part submitted it for obtaining another qualification. I have used the Harvard convention for citation and referencing.

Signature:.....
K. R. Tulsi

Date:.....

Abstract

Ports are frequently protected by breakwaters which are designed to withstand harsh environmental conditions over long periods of time. However, in most cases, they gradually or suddenly deteriorate before they reach their design life.

In order to extend the design life of breakwaters, regular damage investigations and timeous repairs are required. One of the important aspects is calculating the severity of damage to breakwaters. Traditionally, breakwater inspection has been done using aerial photographs and underwater imaging to accomplish these investigations. Breakwaters are systematically divided into inspection stations and photographs are taken to inspect and assess the damage. The photographs are then visually compared with the previous inspection photographs to identify changes. This is difficult to achieve as it is not always possible to get the helicopter exactly in the same position on every survey and highly dependent on the skill of the helicopter pilot. Another difficulty is taking underwater images near the breakwater due to poor visibility and wave breaking.

A major disadvantage of the aerial photographic method is that it only provides a two dimensional (2D) picture of the breakwater above water. The inter-tidal zone on a breakwater slope is where damage usually occurs. It is difficult to capture data in this zone, particularly due to wave action, which results in poor visibility. Ideally, a method is required to capture and assess damage above and below water. High resolution laser scanning and acoustic technologies are available to inspect breakwaters above and below water. These are light detection and ranging (LIDAR) and multibeam echo sounders respectively.

The South African coastline has few significant embayments' that can provide natural shelter from the high energy wave regime on the coastline. Consequently, South African ports require protection in the form of heavy armoured breakwaters and seawalls. Maintenance of these defences is critical for the safe functioning of these ports. Rapid assessment of damage to breakwaters and seawalls which is cost effective is necessary to ensure that repairs are undertaken timeously. This study explores the use of LIDAR and multibeam echo sounders, instead of the traditional aerial photography, to assess damage to breakwaters in general.

Three dimensional (3D) data analysis using LIDAR and multibeam echo-soundings (as investigated in this thesis) is aimed at providing a more realistic method to quantify damage above and below water rather than two dimensional (2D) photographs.

The objective of this study was to evaluate the accuracy of a 3D method using the LIDAR and multi-beam echo sounder data to quantify damage to dolos breakwaters above and below the water surface (including the inter-tidal zone). This was aimed towards the development of the 3D eroded volume method (3D method).

The investigation began with an idealized undamaged model breakwater slope in a laboratory experiment comparing the repeatability of the 3D method with sequential scans and the photographic method in an attempt to compare the deviation in repeatability of data captured. Thereafter three degrees of artificial damage were created to the slope of the model breakwater in the form of settlement, intermediate damage and failure of a localized area of the dolos armour layer.

The 3D method was then applied to a 3D physical model study of the spur breakwater at the root of the Table Bay main breakwater. Field data of the spur breakwater were then captured with the 3D method and compared with the most recent 2D aerial photographic survey. More than two decades of 2D aerial photography damage assessment data of the spur breakwater were available to establish a baseline.

The 3D method data captured were compared with the visual 2D field data to determine the 3D methods accuracy. The comparison of the cumulative damage progression monitored by the visual 2D photographic method with that calculated by the 3D method, showed that there is a good correlation between the two damage quantification methods. The cumulative percentage damage obtained from the 2D visual analysis records has a mean difference of 10% in comparison to the 3D method. The results of the 2D and 3D methods differ in cases of small settlements and larger displacements.

This study has led to an advance in the quantitative 3D assessment of different degrees of damage to breakwaters with dolos armour units above and below water. The 3D method used to assess the extent of damage to a breakwater was compared against the conventional visual method described by Phelp (1995). A marginal variation between the two methods was found, however the 3D method which quantifies 3D eroded volume is recommended for future breakwater investigations to provide a better quantifiable above and below water assessment.

Opsomming

Hawens word gewoonlik beskerm deur golfbrekers wat ontwerp word om storm toestande oor n lang tydperk te weerstaan. Weens moeilik voorspelbare golftoestande gebeur dit dat golfbrekers (veral rotsvul tipe golfbrekers) geleidelik of skielik skade ondevind voor hul ontwerp leeftyd.

Om te verseker dat golfbrekers hul stabiliteit behou, is dit belangrik dat gereelde inspeksies/opnames gedoen word om moontlike skade te identifiseer om sodoende tydige herstelwerk te kan doen. Van uiterse belang met die inspeksies is dat skade gekwantifiseer word om die graad van skade te definieer.. Tradisionele metodes om die skade van golfbrekers bo water (en gedeeltelik onder water) te dokumenteer sluit in lugfotos vanaf voorafbepaalde vaste posisies vanuit n helikopter. Hierdie opnames word dan visueel vergelyk met vorige opnames om veranderinge tussen opnames te identifiseer. Hierdie metode het bepaalde leemtes soos byvoorbeeld dat die voorafbepaalde vaste posisies van waar fotos geneem moet word, moeilik deur deur n helicopter gehandhaaf kan word. Verder is dit moeilik om goeie kwaliteit fotos te verkry in die onderwater gedeeltes weens golfbreking en swak sigbaarheid deur die water.

'n Groot leemte van die lugfoto-metode is dat dit slegs 'n twee-dimensionele beeld (2D) van die golfbreker dokumenteer. Die inter-getysone op 'n golfbreker helling is die gebied waar die meeste skade gewoonlik voorkom. In die sone is dit moeilik om die data op betroubare inligting te bekom weens golf aksie en swak sigbaarheid. Daarom is dit nodig om 'n metode te ontwikkel wat skade beide bo en onder water effektief en kwantitatief kan bepaal.

Ho resolusie laser skandering en akoestiese tegnologie is beskikbaar om die golfbrekers bo en onder die water in drie dimensies (3D) op te meet. Dit sluit in die sogenaamde LIDAR metode (wat bebruik maak van laser posisie bepaling) en die "Multi-beam echo sounder" metode.

Suid Afrika se kuslyn het net 'n paar beduidende baai-gebiede wat natuurlike beskerming teen ho energie golwe vanuit die suidelike oseaan bied. As gevolg hiervan benodig Suid Afrikaanse hawens grootskaalse gofbreker beskerming in die vorm van bewapende golfbrekers en see mure. Onderhoud van die stukture is van uiterse belang om veilige gebruik van die hawens te verseker. Dit is daarom nodig dat hierdie gofbreker strukture dikwels en op n gereelde basis ondersoek word vir moontlike skade om derhalwe herstelwerk, waar nodig, betyds te doen.

Hierdie studie het die gebruik van LIDAR en multi-straal eggo-peiling metode ondersoek om die skade aan golfbrekers in 3D te bepaal. Hierdie metodes is gebruik omdat dit veranderinge in die oppervlakte van n golfbreker in 3D kan opmeet die ontblote oppervlakte van n golfbreker kan met hierdie metodes baie na aan kontinu in die x-, y- en z-vlakke vasgel word.

Die doel van hierdie studie was om die akkuraatheid te evalueer van n 3D metode deur gebruik te maak van die LIDAR en multi eggo peilings data om die skade van n Dolos (golfbreker) bo en onder die water oppervlakte te kwantifiseer (insluitend die getysone). Hierdie ondersoek was gerig om n 3D erosie volume metode (3D metode) te ontwikkel.

Die ondersoek is begin met n ge-idialiseerde onbeskadigde Dolos model golfbreker helling in 'n laboratorium eksperiment waar die herhaalbaarheid van die 3D metode saam met die fotografiese metode bepaal is. Dieselfde heraalbaarheids evaluering is gedoen met drie grade van skade wat kunsmatig aan die model golfbreker se helling aangebringsis nl. versakking, tussen stadium skade en faling van n lokale gedeelte van die Dolos beskermingslaag.

Die 3D metode was hierna toegepas op 'n 3D fisiese model van n gedeelte van die bestaande Tafelbaai se hoof golfbreker. Veld-data van dieselfde gedeelte van die Tafelbaai se golfbreker was daarna versamel met die 3D metode en vergelyk met die mees onlangse lugfotos van dieselfde gedeelte van die golfbreker. Meer as twee dekades se lug-fotografiese data van die golfbreker skade was beskikbaar om 'n grondslag te vestig vir die ondersoek.

Die data van die 3D metode en die data verkry van die lugfotos (2D metode) is hierna vergelyk om die akkuraatheid van die 3D metode te bepaal. Hierdie vergelyking het getoon dat daar 'n sterk korrelasie tussen die 3D metode en die lugfoto metode is. Die kumulatiewe persentasie skade verkry van die 2D lug-foto metode het 'n gemiddelde verskil van 10 persent met dit verkry van die 3D metode. Die resultate het wel afwykings tussen die twee data stelle getoon. Die afwykings was gevind waar daar klein versakkings en groot verplasings voorgekom het.

Die studie het gelei to die verbetering in die kwantifisering van skade aan Dolos golfbrekers deur middel van n 3D metode wat die skade aan n golfbreker in terme van die volume skade bo en onder water bepaal. Hierdie 3D metode is vergelyk met die konvensionele visuele metode, wat beskryf word deur Phelp (1995). 'n Minimale variasie tussen die twee metodes was gevind. Aangesien die 3D metode n beter kwantitatiewe skade bepaal in terme van volume skade bo en onder water, word dit aanbeveel vir toekomstige golfbreker monitering.

Acknowledgments

To my mentors;
The first person that deserves my gratitude is the Late Mr David Thomas Phelp. My journey in coastal engineering started in July 2000 when I met Dave. His inspirational, and energetic attitude on the subject lead me to test the waters.

"A meeting with Dave would invigorate enthusiasm and raise anyone's spirit immeasurably". My wife and family always knew, whenever I was spilling over with excitement and new adventures, it was partnered with Dave. Dave's steadfast support and intellectual guidance has been invaluable over the years and I feel incredibly privileged to have met him in the earlier years of my career. This thesis closes a chapter in my life's journey and is dedicated to Dave.

To my family;
I have been blessed with a very loving and supportive family. To my wife, Jasmita Tulsi, thank you for the constant and unconditional love for as long as I can remember in supporting me in my endeavours. Without your love and support, I would be lost. The two little people in my life that bring me joy and happiness, my daughters, Priyal and Kriya. Their bright little smiles and laughter eased the stress of the task at hand and made every worry in the world fade away. Thank you to mom, dad, mom-in-law, brothers and brother-in-law, for their love and encouragement and help with the girls while I just stared at the computer screen. I appreciate all the sacrifices that you have made.

I have also benefited greatly from other mentors, at the Council for Scientific and Industrial Research (CSIR) and Stellenbosch University. Eddie Bosman, who, convinced me to enrol at the Stellenbosch University for a PDE in Coastal Engineering and who lectured the undergraduate course to me. To his successor Geoff Toms, who lectured the Coastal and Port Engineering coursework, giving in-depth knowledge on best practises internationally and then later through his successor Prof J. S. Schoonees who helped find closure to my thesis. I want to also thank Laurie Barwell, Pat Morant, Hans Moes, and Marten Grundlingh for their insightful career advice in our brief meetings. I am grateful for the knowledge and wisdom.

On the Geographic and survey technology side, Melanie Luck-Vogel, Robert Vonk, Francois Stroch, Ashley Pearce, Nic Herrington, Andrew Turner have all been brilliant information sources. Together with your intellectual knowledge on the subject it provided the constructive feedback that has helped me gain knowledge on this topic. Thank you for your help; I am extremely grateful for the discussions.

To my financial supporters;
I would like to thank the CSIR for providing me with generous financial support throughout my career. I would also like to thank Transnet National Port Authority (TNPA) for providing the research funding to CSIR in order for the data to be gathered. The CSIR has been very patient with me, and I am thankful for the financial support.

To my friends and colleagues at the CSIR;
Cornelius Ruiters, Gregory Davids, Hlubi Mzamo, Jatin Harribhai, Juanita van Heerden, Johan Kieviet, Lee Koekemoor, Lesego Nkhumise, Louise Watt, Louisa van der Merwe, Mario August, Martinius Koopman, Patrick Hlabela, Reagan Solomons, Raffick Jappie, Simphiwe Mashalaba, Sonwabiso Yoyo, Steven Pieterson, Terence Hendricks, Ursula von St Ange, and many others whom allowed me time to work on my studies.

Contents

Figures **xiv**

Tables **xvi**

Abbreviations and Acronyms **xvii**

Symbols **xviii**

1 Introduction **1**

1.1 Background 1

1.1.1 Objective of the study 4

1.1.2 Methodology 4

1.1.3 Schematic of methodology 5

2 Literature review **6**

2.1 Definitions of breakwaters and damage concepts 6

2.1.1 Rubble mound breakwater 6

2.1.2 Armour stability 8

2.1.3 Stability formula for dolosse 9

2.1.4 Breakwater failure modes 10

2.1.5 Damage index 11

2.1.6 Digital dolos movement analysis for model tests 18

2.1.7 Correlation between prototype and model damage 19

2.1.8 Damage classification related to damage parameters D, N_{od} and S . 21

2.2 Review of literature on breakwater investigations 22

2.2.1 Visual inspection 22

2.2.2 Photographic survey from a boat 23

2.2.3 Close-up photography 25

2.2.4 Crane and Ball survey method 25

2.2.5 Aerial, LIDAR and sonar monitoring 26

2.2.6 Summary 30

3 Experimental verification **31**

3.1 General 31

3.2 Accuracy test 31

3.2.1 3D Laser scanner 32

3.2.2 Repeatability 34

3.2.3 Cross-sectional analysis 36

3.2.4 Displacement, rotation and settlement quantification 38

3.2.5 Erosion quantification comparison using visual analysis and 3D laser scanning technique 41

3.2.6 Measurement Accuracy 47

3.3 Summary 49

4 3D Physical model of the Cape Town Spur breakwater **51**

4.1 Background 51

4.2 3D Physical model facility and equipment 51

4.3 Basin boundaries and absorbing beach 51

4.4 Wave generation 53

4.5 Wave climate 54

4.5.1 Consideration for the physical model 57

4.6 Model scale effects 58

4.7 Viscous flow effects 59

4.8 Friction effects 59

4.9 Aeration effects 59

4.10 Set-up of the experiments 60

4.11 The 3D method and visual analysis method 62

4.12 Summary 66

5 Aerial photographic monitoring and three dimensional monitoring experiment 68

5.1 Aerial photographic data monitoring 68

5.1.1 Background 68

5.1.2 Set-up of the photographic monitoring data gathering 70

5.1.3 Data analysis 72

5.2 Cape Town Breakwater aerial photographic data 74

5.3 Cape Town spur laser scanning and multi-beam sonar 80

5.3.1 Set-up to gather hydrographic and topographic data 82

5.4 Multi-beam and LIDAR prototype survey data 84

6 Discussion of results 92

6.1 General 92

6.2 Accuracy measurements 93

7 Summary, conclusions and recommendations 97

7.1 Summary 97

7.2 Conclusions 99

7.3 Recommendations 101

A Appendix A 107

A.1 Field Data Aerial Photographic survey 107

B Appendix B 118

B.1 Field data mobile LIDAR multi-beam survey 118

B.2 Cross-section of the spur breakwater from LIDAR Multi-beam scan for the S-Spur 120

C Appendix C 124

C.1 Data from model study 124

C.1.1 Data from spur breakwater model tests 124

C.1.2 Sensitivity test comparing scanned data to photographic method . 130

D Appendix D 139

D.1 Conference abstract 139

List of Figures

1.1 Aerial view of the Port of East London dolos breakwater and harbour taken in December 2015. Photo: K. Tulsi 2

1.2 3D image of Point data collected from scanning 20 tonne dolos units on a breakwater 3

1.3 Schematic of methodology 5

2.1 Typical cross-section of a breakwater 7

2.2 Typical breakwater failure modes (USACE (2006);(Part VI-2-22)) 11

2.3 Profile of a rubble mound revetment showing eroded area (USACE (2006)) 13

2.4 Typical armour layer failure modes, Burcharth (1993) 15

2.5 Damage parameters for structure armour layer, (Melby and Kobayashi, 1998) 16

2.6 Recorded displacement using the Armour Tracking software 19

2.7 Broken dolos units at the Port of Ngqura contributing to slope cover, Photo: K. Tulsi 21

2.8 Visual inspection of rock armoured breakwater, Photo: K. Tulsi 23

2.9 Photographic survey from a boat (a) equipment, (b) breakwater, (c) station view, Photo: R. Vonk 24

2.10 Close-up photography in a storm, Mykonos breakwater, Saldanha, September 2008, Photo: R Vonk 25

2.11 Image from the 2014 aerial photographic investigation undertaken at spring low tide. Photo: K Tulsi 27

2.12 Airborne LIDAR for topography and bathymetry (RIEGL, 2012) 28

3.1 Laser scanner and fixed camera positioned over test section 33

3.2 Camera image of slope as reference 34

3.3 3D laser scanner image 34

3.4 Volume calculation by filling the meshed surface voids beneath the artificial water surface. 35

3.5 Image showing lines spaced equally (1 D_n) apart on the meshed surface for scan 1 and scan 3 36

3.6 Image of mesh and profile at 1Dn spacing of scan 1 and scan 3 37

3.7 Image of profiles from Scan 1 and scan 3 excluding mesh 37

3.8 Profile of scan 1 and scan 3 showing no significant deviation 38

3.9 Image of slope with profiles taken every 0.25Dn 38

3.10 Image of slope with profiles taken every 0.125Dn 38

3.11 Definition of 3D eroded volume method 41

3.12 Visual image from scaned method T1.1 42

3.13 Visual image from scaned method T1.6 42

3.14 Visual image from scaned method T2.1 42

3.15 Visual image from scaned method T2.9 42

3.16 Visual image from scaned method T3.1 43

3.17 Visual image from scaned method T3.3 43

3.18 Visual image from scaned method T4.1 43

3.19 Visual image from scaned method T4.5 43

3.20 Comparison of damage percentage determined using photographic and scanned data 45

3.21 Model dolos units used for the mean absolute error measurements 47

4.1 3D Wave basin, spur model structure, profle of the test section and wave-maker position 52

4.2 The model with scanner (left) and calibration box (foreground) 53

4.3 The PM and JONSWAP spectra source: (USACE, 2006) 55

4.4 Model output showing wave height contour and direction (CSIR, 2015) . 56

4.5 Wave refraction around Green Point, Cape Town (Google Earth image 2010) 56

4.6 Construction of the Cape Town spur breakwater scale model 61

4.7 Placement of model dolos using the grid spacing 61

4.8 View of breakwater stability test for damage accuracy assessment using the two methods 63

4.9 Recorded displacement for Test 3.1 64

4.10 Scan of displacement for Test 3.1 66

4.11 Comparison between visual analysis and 3D surface volume extraction . . 67

5.1 Location of the Cape Town breakwater protected with dolosse (Google Earth image 2010) 68

5.2 Image of helicopter over section of breakwater. The area of interest is indicated by the dashed lines 69

5.3 Aerial photographic stations at 25 m intervals starting at the breakwater head 71

5.4 Analysed aerial photographic survey 2002 station South Spur (above) . . 73

5.5 Dolos placement grid overlay on 2014 Google Earth image 74

5.6 Aerial photographic survey 1991 station south spur(above) 75

5.7 Aerial photographic survey 1997 station south spur(above) 75

5.8 South spur damage progression according to photographic method 77

5.9 Legend used in identifying damage for Figure 5.10 and Figure 5.11 77

5.10 2002 Aerial photographic survey station south spur 78

5.11 2012 Aerial photographic survey station south spur 78

5.12 South spur damage relative displacement 80

5.13 Multibeam and mobile laser scanner capture area 81

5.14 Multibeam and mobile laser scanner on boat set-up for the breakwater survey 84

5.15 Multibeam and laser scanner south west aerial view 85

5.16 Multibeam and mobile laser scan processed with as-built cross-section overlay 86

5.17 Cross-section view through station providing depth of cover 87

5.18 Prototype scan capture of 10 mm by 10 mm and mesh resolution 87

5.19 Smooth+wire mesh of dolos surface 88

5.20 As-built station design (transparent pink) and scanned station surface (red and blue) in 3D 89

5.21 South spur damage progression determined according to the eroded volume method 91

6.1 3D surface volume overlay of before test 3(blue) and after test 3(red) . . 94

List of Tables

1 Abbreviations and acronyms xvii

2 Symbols xviii

3 Symbols continued xix

2.1 Typical mass relation to primary armour for a breakwater 8

2.2 Damage level by N_{od} for two layer armour Van der Meer (1988) 14

2.3 Damage level by D for two-layer armour 22

3.1 Riegl VZ-400 Laser scanner specification 32

3.2 Repeatability deviation error results of scans in laboratory 35

3.3 Comparison of cross-sectional spacing and volume calculation 38

3.4 Visual displacement criteria used to categorise H and Dn for the armour track software at model scale 1:75 39

3.5 Damage Level assumption and Test conditions for 3D method 39

3.6 Damage calculation by *camera* images using visual assessment 44

3.7 Damage calculation by *scanned* images using visual assessment 44

3.8 Damage calculation by 3D eroded volume 45

3.9 Absolute error of model dolos units 48

3.10 Absolute error of LIDAR scanned model dolos units 48

3.11 Mean absolute error of model dolos units 48

3.12 Mean absolute error of LIDAR scanned model units 48

4.1 Test condition selected for damage assessment 55

4.2 Design water level for MHWS and MLWS 55

4.3 Placement grid for model dolos units 60

4.4 Visual displacement criteria used to categorise H and Dn for the armour track software 64

4.5 Damage table using visual analysis 65

4.6 Damage table using 3D data eroded volume extraction 65

5.1 Cumulative percentage damage for the south spur station 76

5.2 South spur damage table according to photographic analysis method . . 79

5.3 Manufacturers Specifications for the Reson SeaBat 7125 multi-beam echo sounder 82

5.4 Manufacturers specification for the Valeport Sound velocity probe (SVP 70) 82

5.5 Manufactures specifications of the Applanix POS MV 320 inertial mesurement unit 83

5.6 Station volume calculation 89

5.7 Scanned percentage eroded volume 89

Abbreviations and Acronyms

Table 1: Abbreviations and acronyms

Abbreviation	Definition
2D	Two-dimensional
3D	Three-dimensional
CAD	Computer-aided design
CSIR	Council for Scientific and Industrial Research
GPS	Global positioning system
JONSWAP	Joint North Sea Wave Project
LIDAR	Light detection and ranging
MHWN	Mean High Water Neap
MHWS	Mean High Water Spring
MLWN	Mean Low Water Neap
MLWS	Mean Low Water Spring
MSL	Mean sea level
PDE	Postgraduate Diploma in Engineering
SANHO	South African Navy Hydrographic Office
SLR	Single Lens reflex
SU	Stellenbosch University
SWL	Still Water Level
TNPA	Transnet National Ports Authority

Symbols

Table 2: Symbols

Symbol	Definition	Unit
A_e	eroded area	m^2
α	slope angle of breakwater	-
B	structure width	m
D	proportion of displaced units relative to the total number of units	-
D_{ball}	ball diameter for concrete armour units	m
d_c	cover depth	m
d_e	eroded depth	m
D_{rock}	ball diameter for concrete armour units	m
D_n	nominal diameter	-
D_n	equivalent cube length	-
D_n	nominal diameter of the armour unit	-
D_{n50}	equivalent cube length of median rock	-
$E_{JONSWAP}$ (f)	variance density with unit	m^2/s
f	frequency	Hz
F_D	drag force	N
F_G	gravity as a stabilising force	N
F_I	inertia force	N
F_L	lift force	N
f_{peak}	frequency peak	Hz
F_r	Froude number	-
g	acceleration due to gravity	m/s^2
γ	peak enhancement factor	-
γ_a	specific weight of armour	kg/m^3
γ_w	specific weight of water	kg/m^3
G_c	width of armour berm at crest	m
H	design wave height	m
H_b	breaking wave height	m
h_c	breakwater crest elevation above the bottom	m
h_t	water depth at toe	m
h_a	length (height) of the unit	m
h_c	capping crest level relative to the seabed	m
H_s	significant wave height in front of breakwater	m

Symbols continued

Table 3: Symbols continued

Symbol	Definition	Unit
h_t	depth of the toe	m
KD	Hudson stability coeficient	-
l	length	m
l_e	slope eroded length	m
L_om	deepwater wavelength corresponding to mean wave period	m
μ	characteristic flow velocity	m/s
μ	flow velocity	m/s
N_a	total number of units within a strip of horizontal width Dn	-
N_d	number of units displaced	-
N_{od}	number of displaced units within a strip with width Dn	-
N_{or}	number of units rocking	-
n_x	prototype to model scale ratio	m
N_s	stability parameter	-
N_z	number of waves	-
P	notational permeability	m^2
R_e	Reynolds number	-
Rc	crest freeboard	m
rho_s	mass density of rocks	kg/m^3
rho_w	mass density of water	kg/m^3
S	relative eroded area	-
S_a	specific gravity of armour unit relative to water	-
S_m	wave steepness	-
t_a	thickness of armour layer	m
Θ	angle of the structure slope measured from horizontal	-
t_u	thickness of underlayer	m
μ	absolute viscosity	-
ν	viscosity of seawater	-
V_e	average eroded volume	m^3
W	mass of primary armour unit	kg
w_c	the crest width	m
W_a	weight of an individual armour unit	kg
x_m	model scale	m
x_p	prototype scale	m
$E_{JONSWAP}$ (f)	variance density of a JONSWAP spectrum	m^2/s

Chapter 1

Introduction

1.1 Background

The longevity of breakwaters built worldwide relies not only on sound design but also on regular maintenance and repairs to maintain their original functionality. The design and service life performance of breakwaters are the main cause of concern as breakwater longevity depends largely on the local wave climate. In the case of harbour breakwaters, port authorities generally adopt monitoring programmes to assess the condition of their breakwaters on a periodic basis.

Monitoring techniques include visual surveys, photogrammetry, land based topographic surveys, airborne LIDAR (light detection and ranging) laser techniques, profile surveys (crane and ball), underwater surveys (side-scan sonar, laser scanning, multi-beam and diver inspection).

The significance of monitoring is that it provides a record of the serviceability of the breakwater as deterioration often goes undetected when minor deformations become hidden due to the size of these mega structures. Consequently, if left uncorrected, continual deterioration can lead to catastrophic failure of the structure resulting in higher expenditure if complete replacement of the structure is required.

Pope (1992) describes the main types of deterioration of coastal structures as settlement or lateral displacement of the structure, loss of slope toe support, partial slope failure, loss of core or backfill material, and loss of armour units.

Long term monitoring provides information on the condition and early detection and isolation of damage and allows timeous repairs over the lifetime of the structure. Traditional methods of breakwater monitoring are described in the Coastal Engineering Manual ((USACE, 2006)) classifying damage to armour layers either by counting the number of displaced units or by measurement of the eroded surface profile of the armour slope. Armour unit displacement parameters are referenced to D_n, the nominal diameter or h_a, where h_a is the length (height) of the unit. Displacements can be in terms of units being removed from the layer or units sliding along the slope to fill in a gap, USACE (2006).

Methods are needed to quantify the state of the structure so that:

1. Damage to the structure caused by particular events can be assessed;
2. The future working life of the structure can be predicted; and
3. Maintenance or rehabilitation of the structure can be planned.

The dolos armour unit was developed in South Africa in 1963 and has been used extensively ever since. The unit was first designed in East London as a means to reduce the cost of repairing the Port of East London breakwater (Figure 1.1). The breakwater is still protected by some of the original dolos units. The individual mass of a dolos unit ranges between 5 tonnes and 30 tonnes. Monitoring of these units has been done in the past using the available technologies of each decade and has evolved over time from visual inspections, photographic, 2D cross-sectional and now using the 3D volumetric quantifications method being investigated in this study.

Figure 1.1: Aerial view of the Port of East London dolos breakwater and harbour taken in December 2015. Photo: K. Tulsi

Recent advancements in technology have assisted in combining two survey instruments for use in monitoring of breakwaters. These are the laser scanner which is primarily used for terrestrial surface mapping, and the multi-beam echo sounder used for mapping of bridges in navigation channels to identify safe navigable vessel clearance (Thies, 2011). These technologies have been used in this study in a new application to track damage of dolos armour units on breakwaters, described further in Section 3.

These two technologies combined provide a novel method of monitoring breakwaters (the 3D method). Detailed profiles and 3D models of the entire above water structure can be evaluated by high definition land based scanning and the underwater surfaces by the multi-beam echo sounding equipment. By using both techniques, a detailed geo-referenced data file is created of the structure by means of computer-aided design (CAD) software. The data are then processed to extract quantitative information, as proposed by Phelp and Tulsi (2006). A typical 3D image of a dolos breakwater is shown in Figure 1.2.

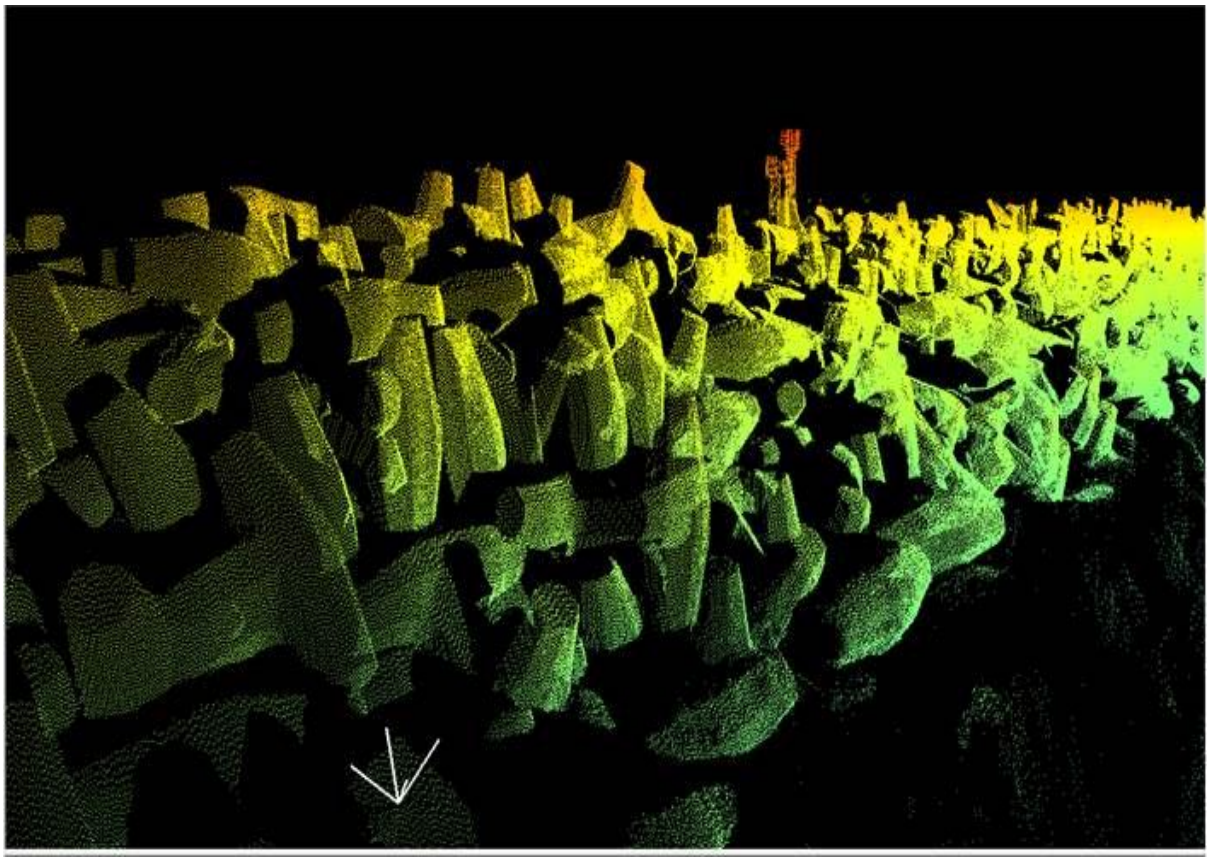

Figure 1.2: 3D image of Point data collected from scanning 20 tonne dolos units on a breakwater

This method of data capture provides an enhancement to breakwater monitoring by offering more quantitative information in a three dimensional (3D) form as opposed to photographic damage assessment or two dimensional (2D) cross-sectional assessment of deterioration of rubble mound breakwaters. The photographic method is presently the norm internationally for concrete armoured breakwaters. This is limited to the above water part of the breakwater only. Therefore an estimate of damage below the water is required. Using current LIDAR and multi-beam echo sounding methods underwater damage can now be determined.

The spur section of the Cape Town harbour main breakwater was used for this investigation as a typical dolos breakwater. Photographic assessments of the spur section of the

breakwater indicate the occurrence of damage which provides an ideal opportunity to test the 3D method using the two types of survey methods, i.e combining the above water and below water data in one survey.

The present difficulty is to collect data within the intertidal zone of the breakwater. However by combining the two methods of LIDAR and multi-beam echo-sounding at high and low tide, a seamless data set can be obtained for analysis. Further to the capture of the 3D data, a method to quantify the damage is needed and is described in this study.

1.1.1 Objective of the study

The objective of this study is to test the 3D method by evaluating the accuracy of using the LIDAR and multi-beam echo sounder data to quantify damage to dolos breakwaters above and below the water surface, including the intertidal zone. Thus, this comparison is aimed towards the development of the 3D method. The study comprised two main components:

1. Physical model application: To compare the results (including progressive damage) from the 3D scanning method with the photographic method. Note that in a physical model (controlled environment), the water can be drained and both LIDAR scanning and taking of photographs can be done accurately.
2. Prototype application: To compare the damage calculated using the 3D method with the damage found by the photographic method, thus confirming the reliability of the 3D method.

1.1.2 Methodology

This report consists of six chapters: Chapter 1, Introduction; Chapter 2, the literature review, discusses available research on breakwater investigations. The chapter also discusses damage quantification in small scale physical models and in reality (prototype); Chapter 3 investigates the accuracy of the 3D scanning methods on a dolos slope; Chapter 4 describes the Cape Town harbour spur breakwater case study and outlines the methodology followed to collect the data. A physical model is carried out to test the accuracy of quantifying progression of damage. Chapter 5 presents the results of the analysis using the known aerial photographic method including three dimensional data in prototype. Chapter 6 discusses these results and the accuracy of the 3D method in further detail. The report concludes with Chapter 7, which contains a summary of the study, the conclusions drawn, and recommendations for future research.

1.1.3 Schematic of methodology

The methodology is schematised in Figure 1.3 below.

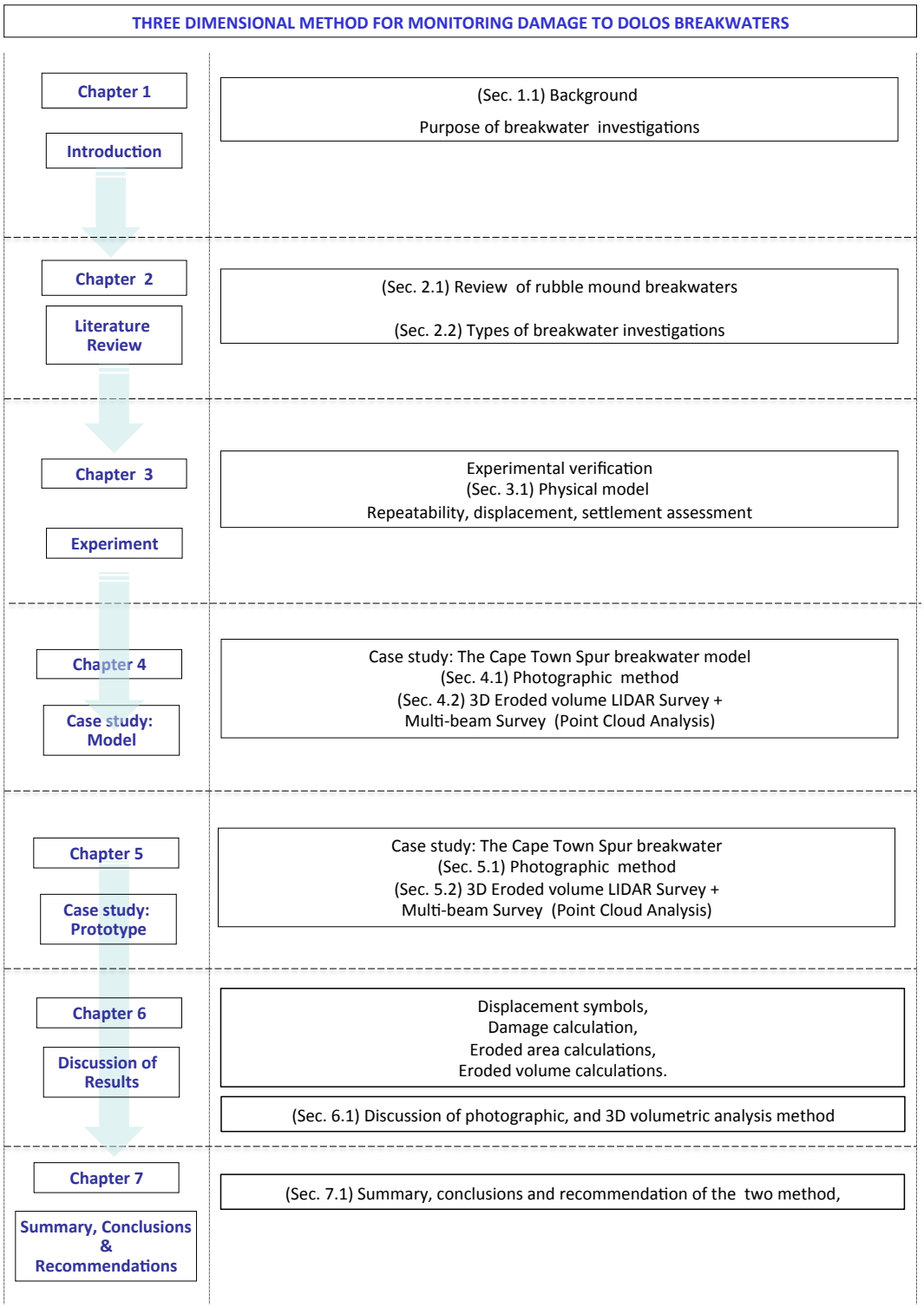

Figure 1.3: Schematic of methodology

Chapter 2

Literature review

2.1 Definitions of breakwaters and damage concepts

There are three common types of breakwaters although there are many variations in the basic designs. These are vertical caisson breakwaters, rubble mound breakwaters and berm breakwaters. The rubble mound breakwater being the focus of this study is further reviewed below.

2.1.1 Rubble mound breakwater

The primary function of a rubble mound breakwater is to protect coastal areas and infrastructure against wave action. A rubble mound breakwater dissipates wave energy mainly through absorption (between 60 to 70 percent) and reflection (between 30 to 40 percent) thereby differentiating this structure from other types of coastal structures. The term rubble refers to riprap and rock armour. Later developments include artificial concrete armour units.

Breakwaters are constructed in layers of different stone sizes from fine material in the centre progressing to larger material towards the outer layer Jenson (1984). They are generally constructed in the shape of a trapezoid. The finer material is contained underneath the adjacent outer layers.

The core is usually made up of quarry run. This fine material provides a semi-impermeable structure to reduce transmission of water through the breakwater. The core is protected by larger rock known as the underlayer or secondary armour layer. In certain circumstances the core may have an additional rock filter layer.

The toe armour is generally rock armour yet in some circumstances, eg. Xbase armour units may be used. The toe of the breakwater is the most important component providing support against sliding.

Rock armour or concrete armour units form the primary protection from wave attack

both during construction and throughout the breakwater design life. Rubble mound construction requires large volumes of rock of many sizes. When large rocks cannot be obtained for armouring, concrete armour units are used.

The crest of the structure is capped by a mass of reinforced concrete. This capping surface allows access for construction and maintenance when required. This splash wall is constructed of reinforced concrete, and limits overtopping by waves, thus limiting erosion on the lee side of the breakwater.

A sketch of a conventional rubble mound breakwater is provided in Figure 2.1. where, SWL is the still water level, h_t is the depth of the toe below SWL, h_c is the capping crest level relative to the seabed, R_c is the crest freeboard, relative to SWL, B is the structure width, G_c is width of armour berm at crest, t_a and t_u is the thickness of armour, and underlayer.

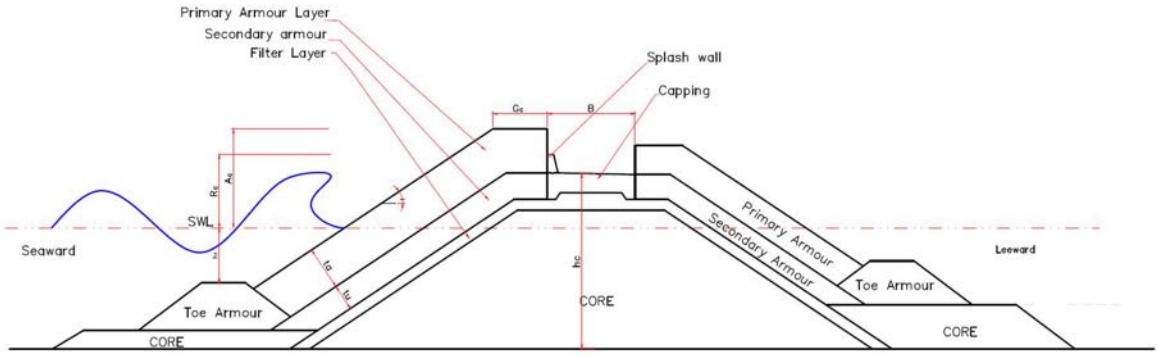

Figure 2.1: Typical cross-section of a breakwater

There are many parameters influencing armour layer stability. The parameters are sea state, structural components or combined. For armour units of complex shape and interlocking capability it is more difficult to make simple force balance models. It is advisable to carry out a three dimensional (3D) physical model test to verify the theoretical calculations of armour unit size and appropriateness USACE (2006).

The type and mass of material used to construct a breakwater is presented in Table 2.1. The material is given in terms of M, the mass of the primary armour unit. The mass of the primary armour unit may be determined using various stability methods. The Hudson stability equation (1958) and dolos stability formula (Holtzhausen, and Zwamborn, 1992) are documented below.

Table 2.1: Typical mass relation to primary armour for a breakwater

Type	Mass of Material
Primary Armour	M
Underlayer	M/10
Toe rock	M/10
Core	M/4000 to M/200

(M = mass of primary armour unit)

2.1.2 Armour stability

The Hudson stability formula, USACE (2006) recommends preliminary design calculations for the armour layer. This is based on the Hudson stability formula developed in 1959 following the work by Iribarren (1938) for a unit's stable weight given by equation (2.1)

$$W_a = \frac{\gamma_a {H_s}^3}{K_D(S_a - 1)^3 cot\theta} \tag{2.1}$$

Where: K_D = Hudson stability coefficient, H_s = design wave height, θ, angle of the structure slope measured from horizontal, W_a, weight of an individual armour unit, γ_a, specific weight of armour unit, S_a, specific gravity of armour unit relative to water (γ_a/γ_w), γ_w, specific weight of water.

The relationship between wave height and the weight of rock armour in rubble mound breakwaters is based on empirical or semi-empirical formulae compiled over many years from physical measurements. Considerable uncertainty exists about the ability of any of the formulae to cover all the effects of hydrodynamic structure interaction in an armour layer. Hudson's formula was developed for rock armour by undertaking extensive hydraulic model testing using regular waves.

The equation was derived for seaward armour stability under conditions when the crest of the structure is high enough to prevent major overtopping. The formula should not be used for a low crest breakwater. Cover layer slopes steeper than 1:1.5 are not recommended for rock armour, and the formula becomes unreliable as the natural angle of repose is approached (BS 6349-7:1991).

Hudson's formula has also been used for randomly placed concrete armour units in hydraulic model tests. This approach can be dangerous because many concrete units rely (for their stability) upon factors which are not included in Hudson's formula.

The USACE (2006) makes mention that the Hudson formula should be regarded as no more than a device for comparing the stability of different types of units, and K_D values

published from previous hydraulic model tests which should be used only as guidance for preliminary selection of armour sizes to be verified by hydraulic model testing. The Hudson formula is not applicable to armour units placed in a regular pattern.

2.1.3 Stability formula for dolosse

Holtzhausen, and Zwamborn (1992) investigated the stability of dolosse based on experimental test results and defined damage in relation to the number of units displaced more than one nominal diameter. Equation 2.2 expressed in terms of wave height and wave period Equation 2.3 is documented below.

$$N_{0.1} = 26700 N_{sm}^{5.26} S_{op}^{3} w_r^{20Sop^{0.45}} + E \tag{2.2}$$

$$N_{0.1} = 0.109 N_{sm}^{6.57} T_{np}^{0.33} w_r^{1.20Tnp^{0.55}} + E \tag{2.3}$$

$$N_{sm} = \frac{H_s}{\triangle^{0.74} Dn}$$

$$S_{op} = \frac{H_s}{L_{op}}$$

$$T_{np} = \sqrt{\frac{L_{op}}{Dn}}$$

$$L_{op} = \frac{T_p^2 g}{2\pi}$$

S_{op}, wave steepness with changes to wave height and period, T_{np} = peak wave period in terms of changes to wave period only for a constant D_n, w_r, dolos waist to height ratio, E , error term used to describe the random nature of dolos slope stability. By rewriting the equation with respect to the damage number N_{od}, the stability formula is rewritten as Equation 2.4

$$N_{od} = 6250[\frac{H_s}{\triangle^{0.74} Dn}]^{5.26} S_{op}^{3} w_r^{20Sop^{0.45}} + E \tag{2.4}$$

Dolos failures on rubble mound breakwaters have been found to be as a result of an inbalance in structural integrity and hydraulic stability which causes breakages of dolos units. Burcharth and Liu (1992), provide a damage formula for breaking and non breaking wave conditions for a two layer randomly placed dolos layer based on physical model tests. The equation is given below (Equation 2.5). The formula is suitable for trunk sections at a slope of 1:1.5 with dolos waist to height ratio of 0.33 to 0.40.

$$N_s = \frac{H_s}{\triangle D_n} = (47 - 72r)\varphi_{n=2} D^{\frac{1}{3}} N_z^{-0.1} \tag{2.5}$$

H_S, significant wave height in front of the breakwater, D damage number and N_z is the number of waves. For $N_z \geq 3000 N_z = 3000$.

2.1.4 Breakwater failure modes

The hydraulic stability of armour layers is decreased when armour units disintegrate because this reduces the stabilizing gravitational force acting on the unit, and possibly decreases interlocking effects USACE (2006),(Part VI-2-22).

Disintegrated pieces can act as projectiles transported by wave action thus accelerating breakage on armoured slopes. In order to prevent breakage it is necessary to ensure the structural integrity of armour units.

"Failure" usually implies a total or partial collapse of a structure. For this reason the partial collapse of a breakwater armour layer usually is classified as "damage" provided the structure still serves its original purpose. Figure 2.2 provides an overview of the failure modes relevant to rubble mound breakwaters (USACE, 2006).

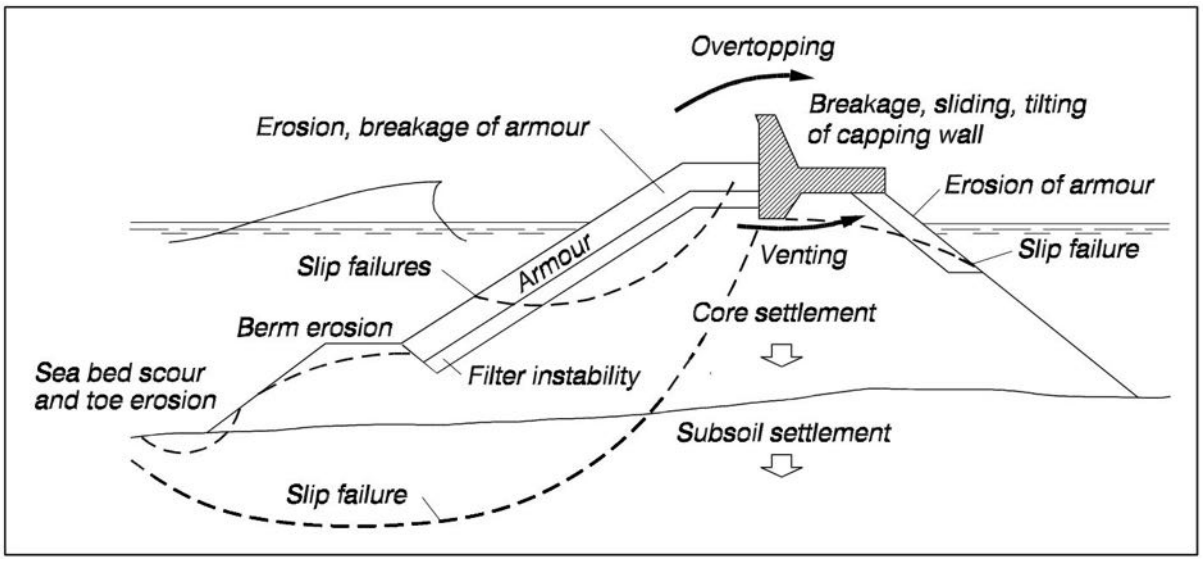

Figure 2.2: Typical breakwater failure modes (USACE (2006);(Part VI-2-22))

2.1.5 Damage index

CIRIA et al. (2007), including USACE (2006) provide information on several parameters to quantify rubble mound breakwater damage. The parameters are dimensionless to make them applicable to rock and concrete armour, Hughes (1993). It is used to quantify and track the damage to breakwaters in small scale physical model studies during design phase and in prototype when quantifying damage before storm events and before maintenance of breakwaters. The damage index is therefore used as a measure of damage and is discussed further in this section.

The most widely used parameters are N_d, N_{od} and S. The N_d from equation 2.6 is the amount of damage as a percentage of all armour in the active zone.

Relative displacement within an active area is given by Equation 2.6

$$N_d = \frac{number\ of\ displaced\ units}{Total\ number\ of\ units\ within\ reference\ area} \tag{2.6}$$

N_{od} in Equation 2.7 is the number of armour units eroded per D_{n50} width along the breakwater. These parameters have been used extensively to assess damage during laboratory experiments and prototype assessment and are used in this study to quantify damage to breakwaters.

Number of displaced units within a strip with width D_n, Van der Meer (1988) is given by Equation 2.7

$$N_{od} = \frac{Number\ of\ units\ displaced\ out\ of\ the\ armour\ layer}{Width\ of\ tested\ section/D_n} \tag{2.7}$$

The counting method is based on classifying the armour movements, as either no movement, single armour units rocking or single armour units displaced from their original position by a certain minimum distance, for example the nominal diameter, D_n or h_a, where h_a is the length (height) of the unit, USACE (2006).

Relative number of displaced units within total height of armour layer (Van der Meer, 1988) is given by Equation 2.8 and Equation 2.9.

$$\frac{N_{od}}{N_a} \tag{2.8}$$

where N_a is the total number of units within a strip of horizontal width D_n

$$\frac{N_{od}}{N_a} = D \tag{2.9}$$

if in D the total height of the armour layer is considered, and no sliding D_n of units parallel to the slope surface takes place given by equation 2.10

Percentage erosion of original volume, Hudson (1958) is given by:

$$D\% = \frac{Average\ eroded\ area\ from\ profile}{Area\ of\ average\ original\ profile} \times 100 \tag{2.10}$$

Various authors provide methods to determine the damage index. The methods are reviewed here. Broderick (1982) introduced S in equation 2.11, a damage parameter based on the averaged cross-sectional erosion area divided by the nominal diameter squared. Van der Meer (1988) used this damage parameter to quantify erosion/damage and defined three degrees of damage. Dependent on the slope, design values could be used, together with his stability formula, to determine the required armour size.

Relative eroded area (Equation 2.11) described by (Broderick, 1982), is still commonly used today

$$S = \frac{A_e}{D_n^2} \tag{2.11}$$

Where A_e refers to the average cross-sectional eroded area and D_n the nominal armour unit diameter.

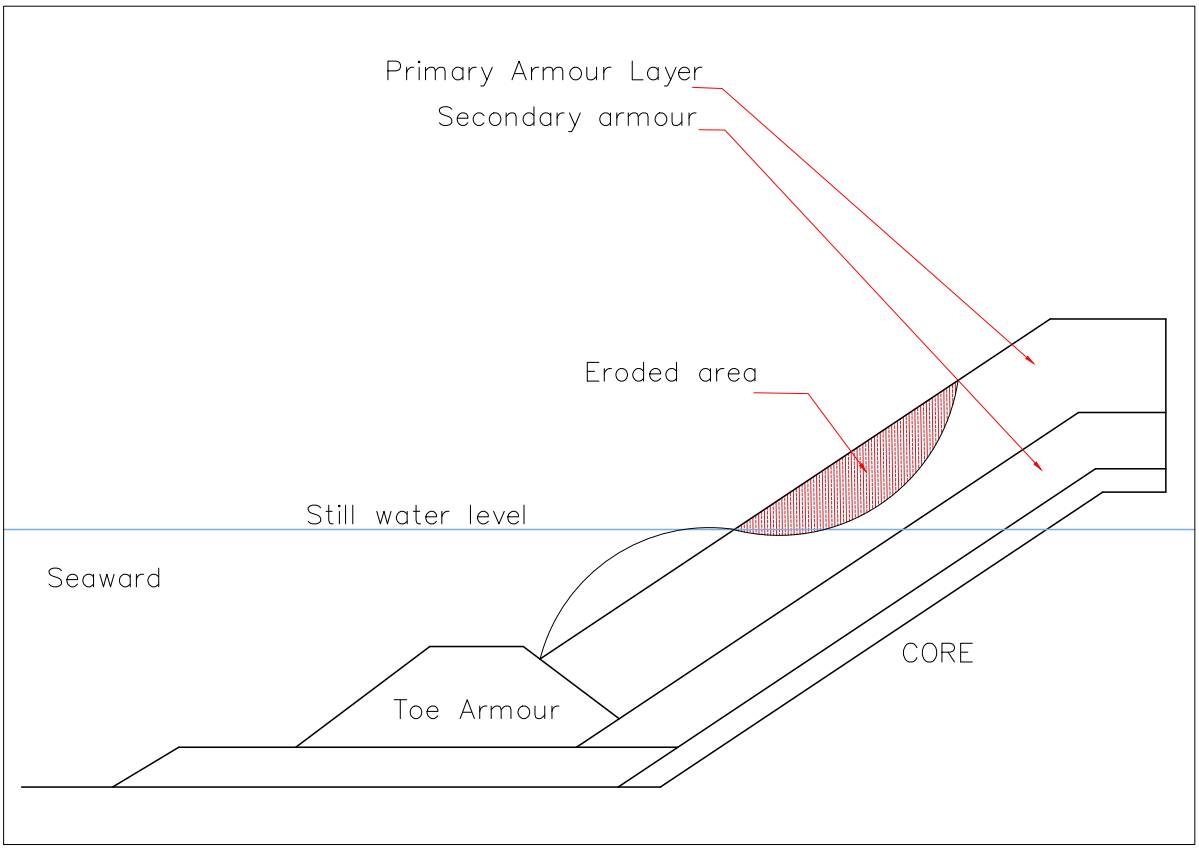

Figure 2.3: Profile of a rubble mound revetment showing eroded area (USACE (2006))

- Damage is related to a specified sea state and duration.
- Damage to armour layers is characterized either by visually counting the number of dislodged units or
- Damage is assessed by quantifying the average eroded surface area of the armour slope cross-sectional profile (see Figure 2.3, above).

Displacements are defined as units being removed from the layer or units sliding along the slope to fill in a gap. In case of steep slopes, displacements could also be caused by the sliding of the armour layer due to compaction or loss of support.

Damage in terms of displaced units is generally given as the relative displacement. Nd, defined as the proportion of displaced units relative to the total number of units, or preferably, to the number of units within a specific zone around still water level (SWL). The height where the erosion can be expected is around the SWL. Vidal et al (1991) found that the height of the damage location relates to the significant wave height H_s, namely between SWL-H_s and SWL+$2H_s$.

Damage D can be related to any definition of movement including rocking. The relative number of moving units can also be related to the total number of units within a vertical

strip of width D_n stretching from the bottom to the top of the armour layer. For this strip displacement definition, Van der Meer (1988) used the term N_{od} for units displaced from the armour layer and N_{or} for rocking units. The disadvantage of N_{od} and N_{or} is the dependence on the slope (strip) length D_n along the length of a breakwater.

Damage classification for concrete armour units can be defined in various ways. The most preferred means is by percentage of damage to the slope by a certain number of units. Since the total number of units differs in each design, percentages can vary between investigations, therefore another definition in terms of the damage number N_o is described by Van der Meer (1988).

The damage number is defined as the actual number of units displaced (moving, or rocking) in a width of one nominal diameter D_n. This damage number can be used on various slopes and lengths of breakwater and is easily transformed to percentage damage. The damage number accommodates for units displaced, and units rocking.

N_{od} = number of units displaced out of the layer (at least more than $2D_n$
$N_{o_{>0.5}}$ = number of units displaced more than $0.5D_n$
$N_{o_{<l0.5}}$ = number of units displaced less than $0.5D_n$

The damage number can be further categorised in terms of failure of the breakwater slope as listed in Table 2.2.

Table 2.2: Damage level by N_{od} for two layer armour Van der Meer (1988)

Unit	Slope	initial damage	intermediate damage	Failure
Cube	1:1.5	0		2
Dolosse	1:1.5	0		1.5
Accropode	1:1.33	0		0.5

Damage characterization based on the eroded cross-section area A_e around SWL was used by Iribarren (1938) and Hudson (1958). Hudson defined D as the percent erosion of original volume. Iribarren (1938) defined the limit of severe damage as occuring when the erosion depth in the main armour layer reached D_n. Torum, A. Mathiesen, B. Escutia (1979) and Davies and Cornett (1994) characterised damage in relation to the minimum depth of cover, d_c, which represents the profile shape in a single parameter, Figure 2.4

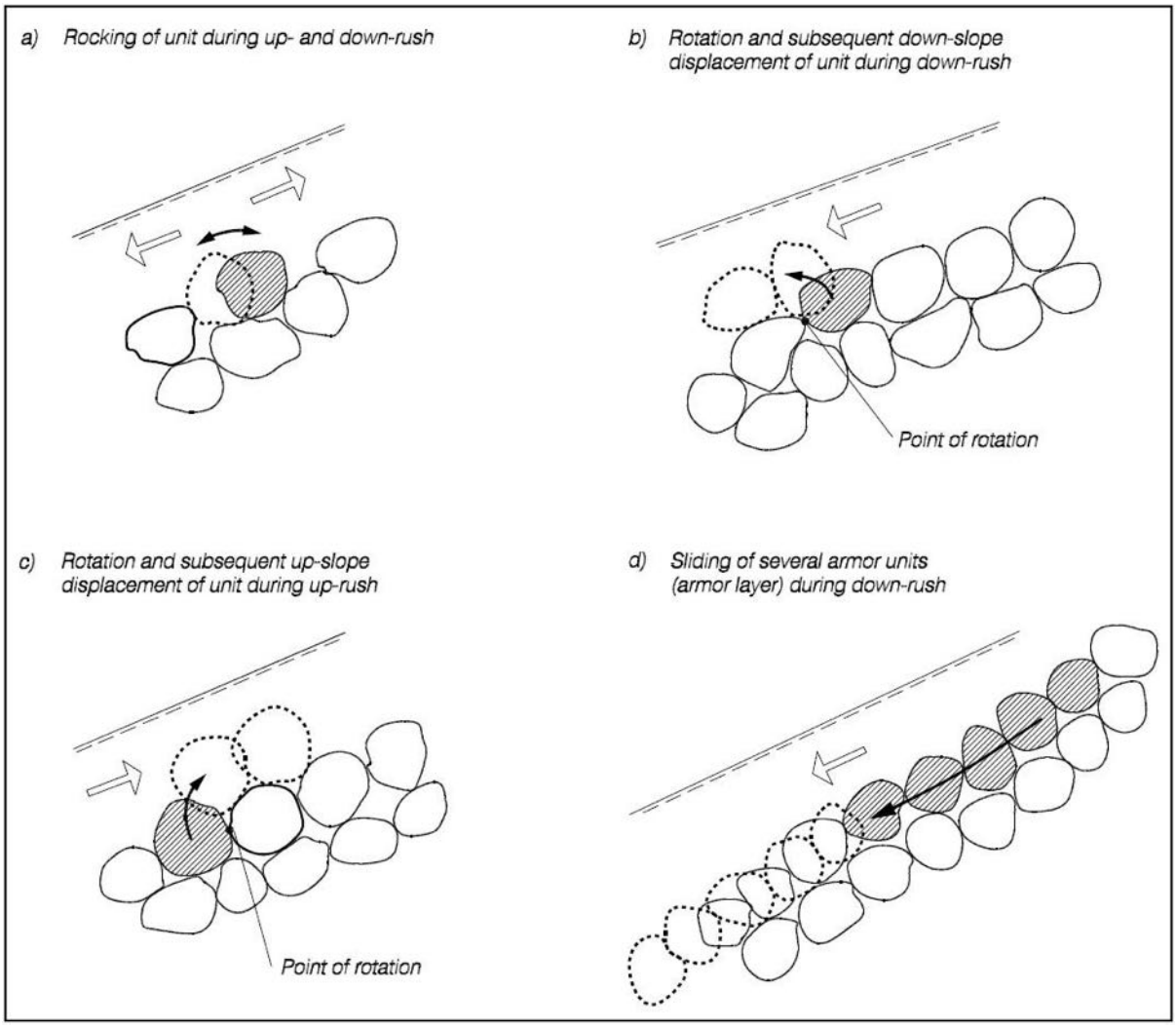

Figure 2.4: Typical armour layer failure modes, Burcharth (1993)

Displacement has to be defined, e.g. as position shifted more than distance Dn, or displacements out of the armour layer. The reference area has to be defined, e.g., as the complete armour area, or as the area between two levels, e.g. SWL $\pm$ H_s, where H_s corresponds to a certain damage for a given wave height, or SWL $\pm$ nD_n, where $\pm$ nD_n indicates the boundaries of armour displacements.

Broderick (1982) and Van der Meer (1988) defined a dimensionless damage index for rock armour which is independent of the length of the slope and takes into account vertical settlements but not settlements and sliding parallel to the slope. S can be interpreted as the number of squares with side length D_{n50} which fit into the eroded area, or as the number of cubes with side length D_{n50} eroded within a strip width D_{n50} of the armour layer. The damage parameter S is less suitable in the case of complex types of armour like dolosse due to the difficulty in defining surface profile. (USACE, 2006)

Melby and Kobayashi (1998) noted that average damage was related to the armour layer

for trunk cross-sections with reference to eroded depth, d_e , cover depth, d_c, and the slope eroded length, l_e. These parameters are all made dimensionless by dividing by D_{n50} depicted in Figure 2.5.

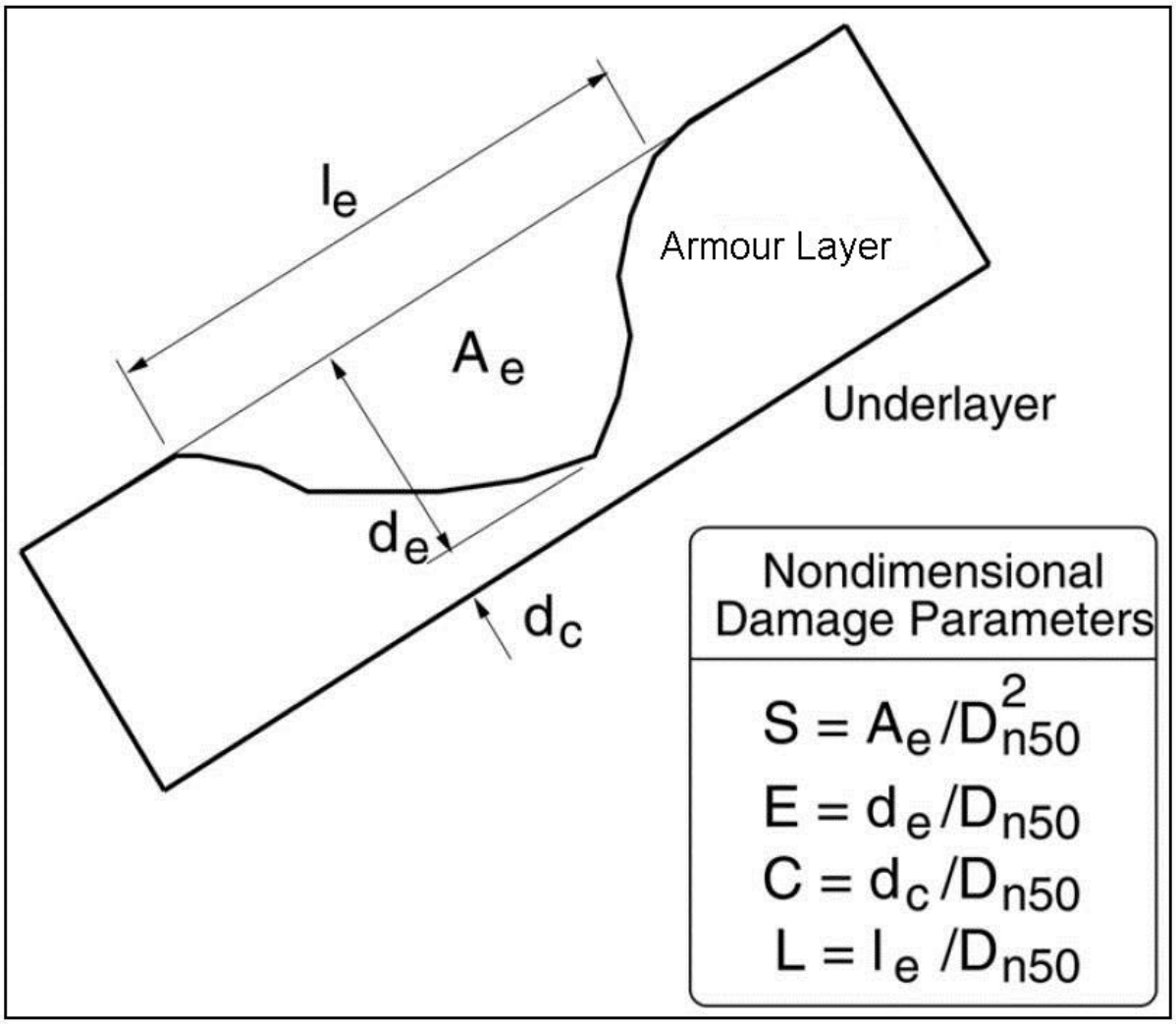

Figure 2.5: Damage parameters for structure armour layer, (Melby and Kobayashi, 1998)

Cornett (1995) computed the damage index ratio over the entire structure rather than the active region and presents it by Equation 2.12:

$$\frac{S}{D\%} = \frac{t_a(\frac{w_c}{2} + \frac{h_c - h_t + H}{\sin\theta})}{100 D_{n50}^2}, H < h_t \tag{2.12}$$

t_a, referring to armour layer thickness, w_c, the crest width, h_c, the breakwater crest elevation above the bottom, h_t, water depth at toe, H, design wave height, θ seaside angle of armour slope relative to horizontal.

The range for the damage index ratio is between 0.6 to 1.25 for typical rubble mounds(Cornett,

1995). For $\frac{S}{D\%} = 0.8$, the zero-damage criteria of $D = 5\%$ corresponds to $0 < S < 4$. For the same zero-damage criteria by Broderick (1982) and Van der Meer (1988) it is given by $S = 2$.

Breakwaters are three dimensional structures therefore erosion is a three dimensional phenomenon. Thompson and Shuttler (1976) derived a volume method to quantify damage(Equation 2.13). They computed the eroded volume V_e using the trapezoidal rule with a profiler which had a foot diameter of $\frac{D_{n50}}{2}$ with sounding spaces of D_{n50} (Equation 2.14). Their test section was represented by a $9D_{n50}$ wide section and damage number N_Δ was calculated assuming armour with a sphere shape. The equation being:

$$N_\Delta = \frac{\rho_a^B V_e}{\rho_a \frac{\pi}{6} D_{n50}^3} \tag{2.13}$$

Which is equivalent to:

$$N_\Delta = \frac{54\rho_a^B}{\pi\rho_a} \frac{A_e}{D_{n50}^2} \tag{2.14}$$

for a $9D_{n50}$ width of structure, where ρ_a^B is the armour bulk density, V_e is the average eroded volume and ρ_a, is the actual armour density. For Thompson and Shuttler (1976) defined failure as the point at which an area of exposed underlayer was equal to D_{n50}.

Wallingford, H. R. Ltd. (1990) used the eroded volume method where an average profile is used to determine the average eroded area as described by Hudson (1959), this is described in detail in Melby (1999). The results of Wallingford, H. R. Ltd. (1990) showed that depending on the method used to compute the average eroded area the results would differ. They proposed an alternative method which was to sum the eroded area from all profiles in order to compute an average eroded area. The difference ranged between 2 to 82 percent for the two methods. The difference decreased as the damage level increased.

It should be noted that the damage methods discussed above have been based on the tools available to produce a profile shape, or the maximum depth of erosion. Nowadays three dimensional data are available and methods to compute damage to structures should be investigated using the new techniques. The information is used to compute the average damage, which may be concentrated in one sector of the breakwater or spread out over several sections. The method to determine damage is generally unclear to readers as most authors do not describe the method they use to compute damage.

Hedar (1960), Owen and Allsop (1983), (CSIR,1989), Vidal et al (1991) Holtzhausen, and Zwamborn (1992), Hughes (1993), Davies and Cornett (1994), Phelp and Zwamborn (2000), and Phelp and Tulsi (2006), describe breakwater damage measurements through counting displacements. Besides visual counting during the test, photo overlays and digital image processing, known as the flicker technique and software such as armour track can be used to determine movements as small displacements. The armour tracking

software (Holtzhausen et al., 2000) provides a semi-automated process in determining the displacement and percentage damage. Lomónaco et al. (2009) mentions, The flickering technique Hough, G. and Phelp (1999) can be used for the tracing of displacements and settlement of units up to a 20% damage level. Accurate profiling would describe in detail the deformation of the structure, able to assess any damage larger than 3% to 5%. Lomónaco et al. (2009) also mentions a virtual net technique similar to the flickering technique, which is particularly suitable to assess changes in porosity and settling.

These methods are relatively complex and time consuming. Unit count methods are useful for determining very low damage values but become inaccurate if more than a few stones or concrete units begin to move and if movement is due to sliding rather than dislodgement of individual units. Unit count suffers from the same weaknesses as the eroded volume method, namely that the spatial concentration of damage is generally not specified and the maximum depth of erosion is not computed as discussed by many authors. Visual counting is generally used to determine the initial damage level as defined by Vidal et al (1991). Unit count is also subjective to the visual ability of the operator to have an eye for spotting movement.

2.1.6 Digital dolos movement analysis for model tests

The analysis of dolos movement is presently done by flashing digital images of the breakwater slope before and after a specific wave condition on a computer program. Software such as Armour Tracking is used to identify dolos movement in a graphical drawing environment Holtzhausen et al. (2000). An image of the output of the Armour Track package is shown in Figure 2.6.

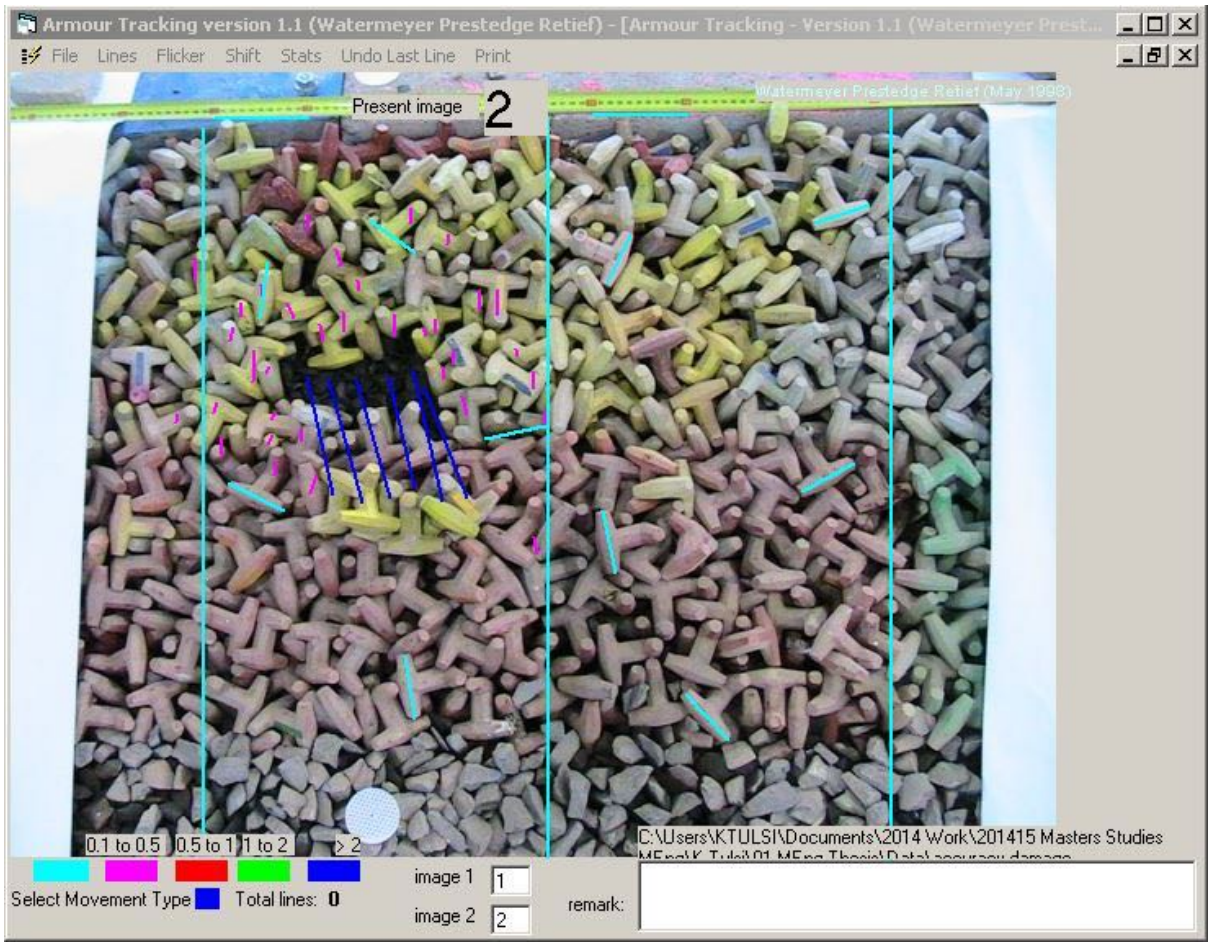

Figure 2.6: Recorded displacement using the Armour Tracking software

It was found that the Armour Track method is not practical in capturing and analysing rocking motions during tests as this would increase the number of images a thousand fold, therefore only dolos displacements are recorded with reference to the height of a dolos unit using two images (Holtzhausen et al. (2000)). The nature of flashing images is that any movement on screen will appear rocking if it is not completely displaced from its original positions ie. less than one dolos height may appear to be rocking. Rocking analysis is done by video recording an entire test to quantify the rocking duration before the unit is finally displaced representing damage.

2.1.7 Correlation between prototype and model damage

Correlating damage of concrete armour units in small scale physical models is done by counting the number of units displaced, and recording the duration and number of units that were rocking during model studies. This is done by visually comparing photographs. It is therefore essential to calibrate model displacement and rocking with prototype damage due to the model units not breaking during model tests Holtzhausen et al. (2000). A

means of quantifying this is expressed in the equations for movement (see below), and in this study based on dolos units.

The damage formula (Equation 2.15) used to track movement is given by:

$$D_T = d_H + 0.5d_{0.5H} \tag{2.15}$$

D_T, refer to the estimated total damage (including breakage), H, the dolos height d_H, the dolos displacements larger than the dolos height, H, $d_{0.5H}$, dolos displacements smaller than H and larger than H/2.

The validation of this equation is based on prototype aerial photography of breakwater stations along the Richards Bay south breakwater and a physical model study using the digital image technique (Phelp and Zwamborn, 2000). However, in prototype this is limited to the above water section which is visible from photographs and damage is recorded visually. Quantifying very small displacements in prototype such as rocking and movement smaller than the dolos height are difficult to identify and are only noticed if breakages or large movements have occurred.

Dolos are slender armour units in comparison with bulkier units like Accropode, CoreLoc and Xbloc. Thereby making the dolos unit susceptible to rocking as documented with the historic failure of Sines (Portugal) breakwater in 1978. Rocking of units occurs during design storm conditions and is difficult and dangerous to monitor in prototype, however in small scale models, the duration of rocking can be observed during a test and recorded. Holtzhausen et al. (2000) provide an equation for rocking to be recorded during model tests (Equation 2.16).

$$Rocking = r_1 + 2/3r_2 + 1/3r_3 \tag{2.16}$$

r_1, refer to continuous rocking, r_2, rocking about two thirds of the time, $r3$, rocking about one third of the time. Holtzhausen et al. (2000) describe an empirical equation to represent damage by evaluating displacement and rocking (Equation 2.17).

$$D_T = d_H + 0.15L_n d_H + 0.55 \tag{2.17}$$

It was found that although displacement and rocking were useful for design purposes given by Equation 2.17 the use of Equation 2.15 consistently produced higher damage numbers and was conservative for damage estimations including rocking. Rocking of dolos units can result in settlement or breakage and eventually loss of armour units from the slope. However, units in prototype may still contribute to the breakwater cover layer

if settlement or breakage has occurred. An example of dolos units which have broken during settlement or rocking but are contributing to slope stability is shown in Figure 2.7. This figure shows the eastern breakwater at the Port of Ngqura at spring low tide from the 2015 aerial photographic investigation. Some dolos units within the tidal zone have broken, but still are providing cover by interlocking with other units. The correlation of these breakages is estimated at 67 percent related to small movements ($d_{0.5H}$) and 33 percent related to larger movement (d_H) in prototype. This is a complex problem for smaller movements relating to damage Holtzhausen et al. (2000).

Figure 2.7: Broken dolos units at the Port of Ngqura contributing to slope cover, Photo: K. Tulsi

Based on field monitoring of other concrete armour units and small scale model tests, damage formulae have been suggested for Toskane, Core-loc units, XBloc and Stabit units as recorded in Phelp and Tulsi (2006).

2.1.8 Damage classification related to damage parameters D, N_{od} and S

The criteria for damage classification (USACE (2006)) used are listed below:

- **No damage** - No unit displacement. Note that S might not be equal to zero due to settlement.

- **Initial damage** - Few units are displaced (ranging from moderate to severe damage). This damage level corresponds to the no damage level used in the Shore Protection manual 1977 and 1984 in relation to the Hudson equation stability coefficient. In the equation the no damage level is defined as 0-0.5% displaced units within the active zone.
- **Intermediate damage** - Units are displaced but without causing exposure of the under or filter layer to direct wave attack.
- **Failure** - The under layer or filter layer is exposed to direct wave attack

The criteria for damage to concrete armour layers are presented in Table 2.3.

Table 2.3: Damage level by D for two-layer armour

Unit	Slope	initial damage	intermediate damage	Failure	Reference
Rock[1]	1:2-1:3	0-5%	5-10%	$\geq$ 20%	Jackson(1968)
Cube[2]	1:1.5-1.2		4%		Brorsen et al. (1974)
Dolosse[2]	1:1.5	0-2%		$\geq$ 15%	Burcharth and Liu (1992)
Accropode[2,3]	1:1.33	0%	1-5%	$\geq$ 10%	Burcharth et al. (1998)

[1] D is defined as percentage of eroded volume
[2] D is defined as percentage of units moved more than D_n within the following level restricted areas: Rock see definition under initial damage, Cube SWL $\pm 6D_n$, Dolosse SWL $\pm 6D_n$, Accropodes between levels SWL $+5D_n$ and $-9D_n$
[3] One-layer armour cover layer

2.2 Review of literature on breakwater investigations

Infrastructure monitoring is a vital part of any successful maintenance programme. For rubble mound breakwaters the complexity and scope of a monitoring effort can vary widely from simple periodic on-site visual inspections at the low end of the scale to elaborate and expensive long-term measurement programmes at the other extreme USACE (2006);(Part VI-8-2). The most important aspect in any monitoring and inspection programme is to determine carefully the purpose of the monitoring. Some of the breakwater monitoring techniques used internationally are discussed in this section.

2.2.1 Visual inspection

A visual inspection is accomplished by walking on the concrete capping of the breakwater while inspecting the above water section of the breakwater armoured slope. Figure 2.8

depicts a typical visual inspection of a breakwater. Phelp (1995) discusses the advantages of visual surveys as a means of gaining experience on the type and nature of breakages of armour units and information on structural analysis. It has been found to reveal more breakages to armour units than can be easily seen by a photographic inspection. The visual inspections are important in a monitoring programme to form the base-line for ongoing monitoring combined with other techniques.

The limitation of the visual surveys is that there is no reference point to work from when evaluating displacement of units. It is however useful to obtain a preliminary qualitative indication of the condition of a breakwater. Field notes, sketches and pictures and GPS co-ordinates of photographs are valuable for future reference and should be documented during the inspection for comparison with future inspections USACE (2006);(Part VI-8-2).

Figure 2.8: Visual inspection of rock armoured breakwater, Photo: K. Tulsi

Pope (1992) mentions that should there be a need to quantify structure changes, a few simple, inexpensive techniques can be used during the onsite inspection. These measures include:

- counting broken armour units,
- paint markings around cracks or suspected displacements,
- measure and mark distances between established points on the structure.

While this method is not suitable to obtain a detailed quantification of breakwater damage, it plays a vital role in the monitoring process.

2.2.2 Photographic survey from a boat

Kluger (1982) discusses photographic surveying of the above-water part of the breakwater for detecting the displacement of individual armour units on a breakwater slope by taking

photographs from a boat. This method is described as simple and inexpensive, involving a few people with cameras and a boat. This method is often used to do rapid checks for damage after significant storm events. Phelp (1995) explains the procedures of the method which requires relatively calm seas and is carried out at spring low tide. A stable boat is required with sufficient space for the photographer to stand near the bow. The boat should also be reasonably manoeuvrable and can range in size from a 4 m ski boat with outboard engines to a 10 m launch.

A typical survey boat and images of a survey are presented in Figure 2.9.

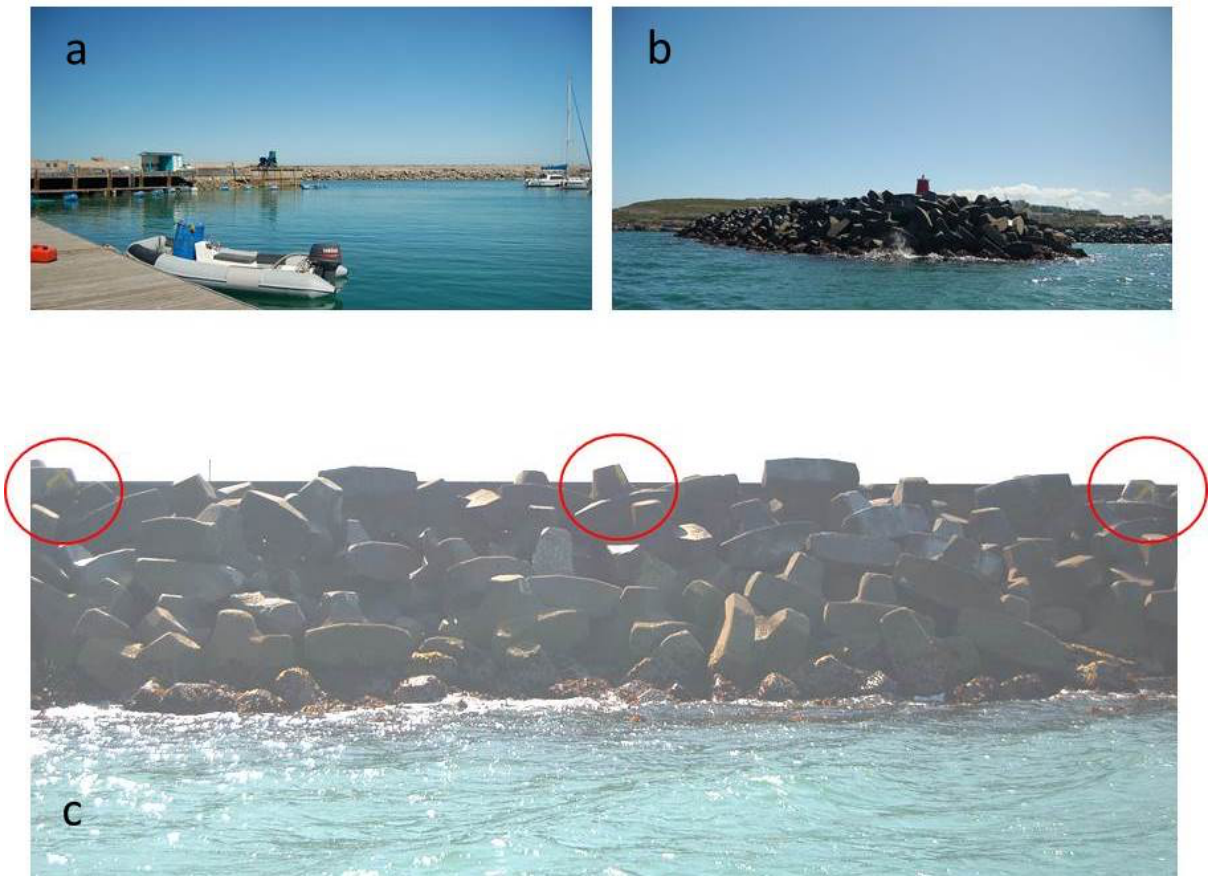

Figure 2.9: Photographic survey from a boat (a) equipment, (b) breakwater, (c) station view, Photo: R. Vonk

The exact positioning of the boat is attained by sighting two yellow crosses or two beacons on the breakwater and judging the distance from the breakwater by means of an electronic distance measuring device. At the center of each station, which has already been marked on the capping slab, two reference marks are made, one on either side of the breakwater capping exactly perpendicular to the breakwater slope, Kluger (1982).

The greatest advantage of the boat survey method is that it gives the best perspective to measure vertical movement of armour units; however, it is rather difficult in rough sea conditions.

2.2.3 Close-up photography

Close-up photography usually documents the results from the visual inspection. It is also useful for checking the detailed progress of localized damage such as cracks in the concrete capping. Aerial and boat inspections are not possible during storm events so close-up photography may be the only survey method available. Valuable information can be obtained during extreme storms, in the form of identifying focused wave action, which often relates to damage on the breakwater. A telephoto lens is normally needed in this type of photography because the photographer will be standing some distance away, i.e at a safe vantage point. A benefit of close-up photography is presented in Figure 2.10 taken during stormy conditions at Mykonos harbour in Saldanha Bay, South Africa. The figure shows wave overtopping, and the severity of a typical storm.

Figure 2.10: Close-up photography in a storm, Mykonos breakwater, Saldanha, September 2008, Photo: R Vonk

2.2.4 Crane and Ball survey method

This method of survey is carried out along profiles normal to the armour slope at intervals of 10 m to 20 m, described in USACE (2006). Its intention is to record an average profile of the surface of the armour unit or rock layer. However, the method is very time consuming, taking between two to three days to complete a 600 m -long breakwater and does not always provide very accurate information. This type of survey is normally carried out during construction of breakwaters and after severe storm damage has occurred.

Surveys using the Crane and Ball method monitor the breakwater profile at predefined intervals. The probe sounding technique was originally developed by the US Army Waterways Experimental Station for small scale model application in the 1950s. This

method involved the use of a sounding disk which was later replaced by a ball for the prototype Dolos measurements. A mobile crane is usually used to position the ball and the level of the ball is measured from a theodolite or total station on the breakwater or using a GPS (Phelp (1995)). The size of the ball to be used for the survey of a concrete armour unit breakwater profile (which should be kept constant from one survey to the next) is determined using Equation 2.18 :

Ball diameter for concrete armour units:

$$D_{ball} = \frac{1.14 D_n}{\sin 45 \deg} \tag{2.18}$$

D_{ball} is the diameter of the ball and D_n being the cube root of the armour unit volume. The size of the ball for survey rock armour on a breakwater slope is given by equation 2.19.

Ball diameter for rock armour units:

$$D_{rock} = 0.5 D_{n50} \tag{2.19}$$

2.2.5 Aerial, LIDAR and sonar monitoring

Aerial photographic monitoring is described by many authors, Cialone (1984), Kendall (1989), Hughes (1993), Phelp (1995); Phelp and Zwamborn (2000) and Tulsi and Phelp (2009). Aerial photographic monitoring is undertaken using differential global positioning system (DGPS) to match images to produce overlapping photographs covering the entire above-water section of the breakwater. Viewed at low spring tide, this is a most useful and cost effective method of breakwater monitoring. The helicopter was found to be the most suitable platform, in that it can hover (wait for wave draw-down) and move quickly between monitoring stations. Positioning of the helicopter is normally done by the use of differential GPS, which is accurate to within 1m. However, the ability of the pilot to hover at that position is variable. A typical image from the aerial monitoring investigation for this study using this method is shown in Figure 2.11. The photographic station is identified by crosses at the boundaries (highlighted by the red line) and a line in the centre with a station reference number on the concrete capping. The staining on the dolos units indicate the tidal fluctuations. The units can be counted and tracked visually for movement and breakages.

Figure 2.11: Image from the 2014 aerial photographic investigation undertaken at spring low tide. Photo: K Tulsi

Weymouth and Magoon (1968) and Bradbury and Allsop (1989) discuss making spot height surveys of breakwaters to generate contoured plans and profile lines of the structure. Prickett (1996), Phelp and Tulsi (2006), Lomónaco et al. (2009) cited in (Lemos and Santos,2007), USACE (2006),CIRIA et al. (2007),Marujo et al. (2013) and Tulsi and Phelp (2009) mention the advantages of new inspection techniques including 3D topographic LIDAR scanning, multi-beam sonar, combined and integrated into a larger asset management framework to assess the structure and to manage the structure more efficiently as more data is captured.

Laser scanning is based on LIDAR technology, which is an active remote sensing technology measuring the return properties of scattered light to determine range and 3D coordinates of the objects reflecting the laser beam to illuminate an object and then a photo-diode to register the backscatter radiation of the beam, Wehr and Lohr (1999).

Tomlinson et al (2001) explain that randomly orientated units are more difficult to assess. However, LIDAR has the potential to identify armour movements and breakage, and is of value in identifying scour, sedimentation and settlement. The time-of-flight (ToF) and phase shift (PS) methods are the two common techniques used for range measurement in current laser scanning systems. The ToF ranging uses precise timing to determine the range from the pulse time of flight based on the speed of light travelling in air. Phase

shift ranging uses continuous laser illumination and amplitude modulation of the beam to derive the range at high frequencies, Kukko (2013).

Although topographic LIDAR and airborne LIDAR bathymetry (ALB) operate in a similar configuration (i.e., a pulsed laser system transmitting from an airborne platform), their capabilities are different due to the wavelengths at which they operate (i.e., eye-safety regulations and water-penetration characteristics) (Guenther, 2007; Fowler et al., 2007). Peeri et al. (2011) provide a review of the available Airborne LIDAR Bathymetry(ALB) land-water interface algorithms (green, red, and IR channel waveforms) and present newly developed algorithm's. They provide a quantitative evaluation of the algorithm's performance based on both individual laser measurement products and the resulting shoreline vector features. An image of an Airborne LIDAR application for topographic surveys is shown in Figure 2.12.

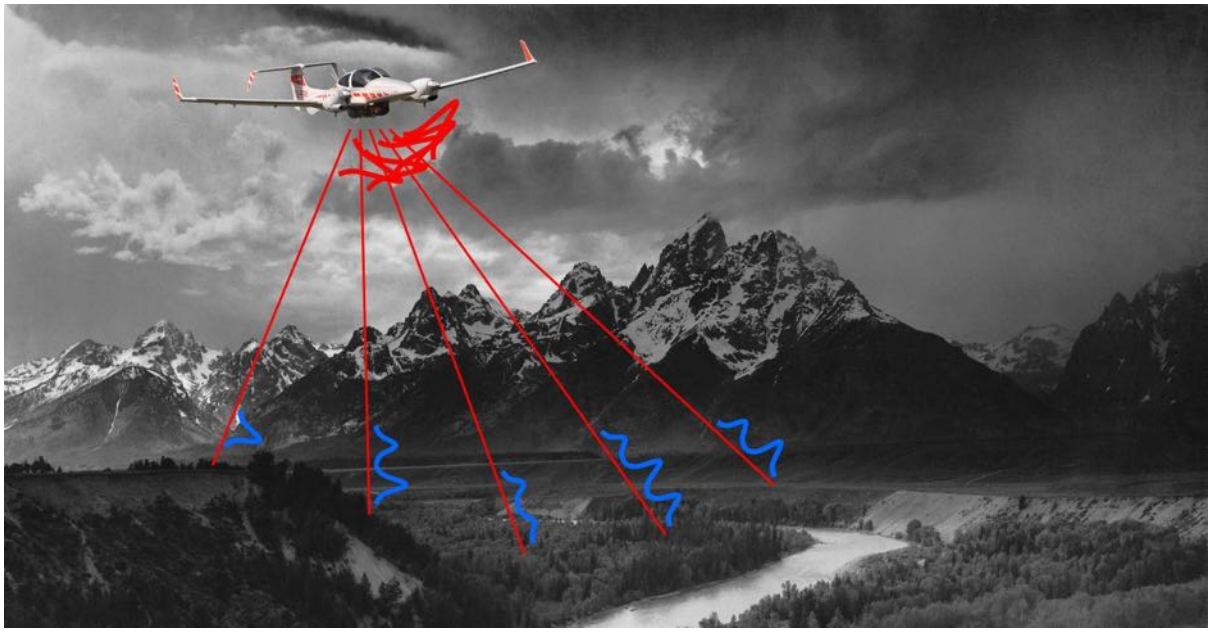

Figure 2.12: Airborne LIDAR for topography and bathymetry (RIEGL, 2012)

Topographic LIDAR shown in Figure 2.12 typically operates at an infrared (IR) wavelength (700nm to 1mm), whereas ALB operates at a green wavelength (520 nm to 570 nm). Modern commercial topographic LIDAR systems operate at a pulse repetition frequency of at least 20000 Hz, with a footprint diameter of 15 to 20 cm. A topographic LIDAR can record the water surface, but it cannot penetrate it. However the ALB system, operates at a lower pulse repetition frequency than topographic LIDAR (up to 3000 Hz), with a footprint diameter of 2 m. The laser measurements from the ALB system can penetrate water to measure the seafloor depth up to two to three Secchi depths, depending on the application. A Secchi depth is measured using a Secchi disk: a circular plate divided into quarters painted alternately black and white. The disk is attached to a rope and lowered into the water until it is no longer visible. The depth is then recorded. For this procedure to work well it requires clear water. Therefore turbidity and wave turbulence around the

South African coast line may create inaccuracies during measurements.

Coveney and Monteys (2011) and Pastol (2011) compare the data sets obtained from two LIDAR systems deployed over different coastal environments. Based on the results from the studies, the authors suggest merging the two data sets to achieve higher resolution. Pastol (2011) provides an example of an integration between data sets from ALB multibeam echosounder surveys with historical data sets.

Side-scan sonar records are obtained by towing an instrument from a vessel running parallel to the structure. Additional information and operating methods are discussed by Kucharski and Clausner (1989), and Morang, Larson and Gorman (1997).

Airborne LIDAR can be employed on both the underwater and above-water portions of sloping structures as carried out by Parsons, L.E. and Lilycrop (1988). They mention that the spatial distribution of data is insufficient to recognise small irregularities; however, large problems and scour holes are easily identifiable. Collin et al. (2011) explore the potential use of airborne LIDAR for coastal mapping and discuss the technology further and suggest merging data between airborne LIDAR and multi-beam echo soundings to produce a high definition digital elevation model (DEM).

Collin et al. (2011) investigate land monitoring after a coastal flooding disaster. Their study presents a three-year monitoring programme of land cover, elevation, and volume changes subsequent to a hurricane disaster over the south shore of Lake Pontchartrain, Louisiana. They present digital elevation models using ALB and land-cover classifications from hyperspectral imagery. Reif et al. (2011) utilize remote-sensing capabilities to enhance the understanding of coastal processes. They make mention that ALB performance over the surf zone is limited, and reliable bottom detection is not always possible. As a consequence, the elevation model produced from the ALB measurements contains gaps. Reif et al. (2011) present an assimilation method using aerial video imagery with dissipation profiles produced by a wave energy transformation model. The result is a seamless elevation model of the seabed across the surf zone. Measurements and profiles can be extracted from the dataset.

2.2.6 Summary

Breakwater design is usually based on the Hudson and van der Meer stability equations. Various safety factors have been introduced into the design formulae to stay within a conservative design. Breakwater designs are presently based on the designer testing the design using physical models. Damage assessment methods discussed are based on technologies of the past and require an update, using new technologies to better assess engineering structures in the attempt to provide more detail to interpret structure deterioration.

The information computed by photographic, LIDAR and sonar techniques to provide the condition of breakwaters with reference to damage is investigated further. Field monitoring provides its own challenges as to which are the best monitoring approaches and assessment methods. However, there are advantages in using combined methods of analysis being either counting the number of displacements or degree of damage and measurement of profiles along the structure.

The present way of conducting breakwater assessments is the photographic method. However, it is limited to the above water section and does not cover the underwater portion of the dolos slope. This has been compensated by quantifying the damage above water and multiplying it by a damage factor of 1.5 to accommodate the one third portion underwater but still within the active zone (Phelp and Zwamborn (2000)). This is a major limitation of the photographic method and alternatives are needed to assess dolos breakwaters. Nowadays, equipment such as multi-beam echo sounders and 3D Laser scanners are available to visualise underwater surfaces below and above water. Before this equipment can be used in reality a method should be developed to analyse the dolos slope accurately, cost effectively and efficiently.

Therefore an attempt is made to quantify the percentage damage using a 3D Laser scanner in the laboratory for physical model tests of the complex randomly placed units like dolos and then apply it to field measurements. Chapter 3 experimentally verifies the accuracy of a scanned slope focussing on repeatability of measurement followed by quantitative progression of damage in a small scale physical model. This is continued in Chapter 4 by testing the photographic and 3D method in a physical model study for the Table Bay spur breakwater. The method is then applied in prototype which is described in Chapter 5 providing the output of a prototype breakwater scan to determine the percentage damage to the spur breakwater slope in reality.

Chapter 3

Experimental verification

3.1 General

The main objective of the study is to test the accuracy of a method using high density point data to assess damage progression on a breakwater slope. To achieve this objective, the accuracy of using the three dimensional (3D) data was tested by conducting physical model experiments comparing the photographic and three dimensional method of analysis. The method is then tested in reality by comparing an aerial photographic survey with a multi-beam and laser scan survey (3D method) of the breakwater from a boat. The collection of data is discussed in subsequent chapters for both methods relating to equipment used, set-up procedures for the equipment and considerations during collection of the data.

Data collection comprised:

3.1) A physical model study comparing the accuracy of the two methods followed by a physical model study of the Cape Town spur breakwater comparing damage to dolos armour units.

3.2) Obtaining an extensive dataset from 1991 to 2013 from the CSIR. This consisted of aerial photographic data of the Port of Cape Town. The author carried out the 2014 aerial survey to bring the data collection up to date;

3.3) Acquiring the bathymetric multi-beam and LIDAR breakwater survey data. These data sets were collected and processed during the course of this study.

3.2 Accuracy test

The ability of the 3D scanner to capture minor, moderate and large movement on a dolos protected slope is investigated in this chapter. To achieve this, damage will be created manually by individually moving dolos units. The experiment was set-up in the CSIR Coastal and Hydraulics Laboratory, Stellenbosch.

The dolos units scanned represent 30 tonne dolos with a station width of 27 m prototype scaled at 1:75. Two stations are monitored of width 11Dn each, namely station 1 and station 2. Station 1 was manipulated by creating damage by hand and station 2 was the control where no damage occurs. Dn of the model dolos represents 3.28 cm, and each station represents 11 Dn = 36.16 cm (model). Station 1 has a total of 190 dolos units and station 2 has 178 dolos units.

A fixed digital camera (Cannon DV-MV830i) was set-up on a tripod and focussed perpendicular towards the slope. The camera was remotely controlled to limit any unnecessary movement or editing of the captured image to compare with other Test images. This is followed by the 3D laser scanner which was also set-up perpendicular to the slope with the same view as the fixed camera, as shown in Figure 3.1. The scanner was remotely controlled using a laptop computer.

3.2.1 3D Laser scanner

The Riegl VZ-400 3D laser scanner was used for the experiment. The 3D laser scanner emits a laser pulse which is deflected by a polygonal mirror to its surroundings. The laser beam may hit one or many targets over the range of 600 m causing several echo pluses. These reflected optical echo signals are recorded by the instrument's receiver. The receiver converts the optical returns into electronic signals which are digitized for waveform processing. The waveform analysis calculates the optical echo signals by multiplying it with the known speed of light (299 792 458 m/s) leading to a point at a distance away from the scanner. The manufacturer's specification indicates the scan data acquisition produces 5 mm accuracy with 3 mm precision and repeatability within a range of 600 m RIEGL (2012). Table 3.1 provide further scanner specifications.

Table 3.1: Riegl VZ-400 Laser scanner specification

Laser Pulse Repetition Rate PRR (Peak) [1])	100 kHz	300 kHz
Effective Measurement Rate[1])	42 000 meas./s	122 000 meas./s
Max. Measurement Range[2])for natural targets,0%	Long Range Mode 600 m 280 m	High Speed Mode 350m 160 m
Max. Number of Targets per Pulse	up to 15	up to 5
Accuracy [3,5])	5 mm	5 mm
Precision 4, 5)	3 mm	3 mm
Minimum Range with Near Range Activation	1.5 m 0.5 m[6]	
Laser Wavelength	near infrared	
Beam Divergence [7])	0.3 mrad	

[1] Rounded values.

[2] Typical values for average conditions. Maximum range is specified for flat targets with size in excess of the laser beam diameter, perpendicular angle of incidence, and for atmospheric visibility in excess of 23 km. In bright sunlight the operational range is considerably shorter than under an overcast sky.

[3] Accuracy is the degree of conformity of a measured quantity to its actual (true) value.

[4] Precision, also called reproducibility or repeatability, is the degree to which further

measurements show the same result.

[5] One sigma @ 100 m range under RIEGL test conditions.

[6] Reduced accuracy within a 1.5 m range

[7] 0.3 mrad corresponds to a 30 mm increase of beam width per 100 m of range.

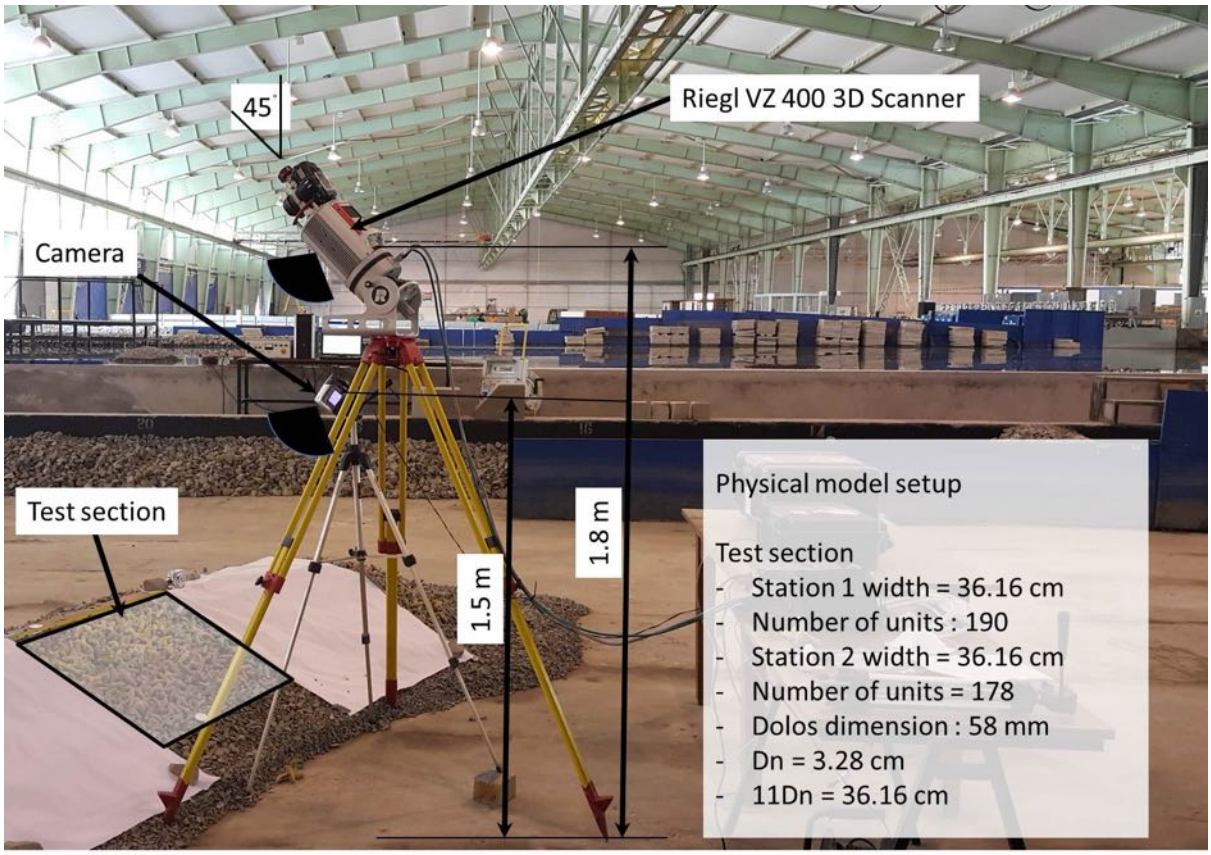

Figure 3.1: Laser scanner and fixed camera positioned over test section

The digital image captured by the fixed camera is presented in Figure 3.2. It is used as a reference and analysed visually by blinking two images and tracking displacements. This is explained in the previous section, Section 2.1.6.

The data captured from the laser scanner are meshed using 3DReshaper program to view and mesh the point data and project colour onto the surface (Figure 3.3). The laser scan image is created from a data set of x,y,z points and colour returns captured by the scanner which are meshed to provide a quantifiable image in 3D. Both images are of the same slope using different technologies. The image taken by the camera is clear whereas the scanned image is dark yet picks up the entire slope of dolos units.

Figure 3.2: Camera image of slope as reference

Figure 3.3: 3D laser scanner image

3.2.2 Repeatability

The reliability of the scan results is dependent on producing the same result for every identical scan. To assess the repeatability, the scanner was set-up to scan a dolos slope repeatedly. The assumptions is that the scanner is always placed on the same position therefore, for the purpose of this experiment it is fixed similar to the photographic method. The scanner is also orientatedperpendicular to the slope. The scanner is switched off and on, and then programmed to scan the test section. This is repeated ten (10) times. No displacement is created for these tests. The results of the test are presented in Table 3.2 below.

When carring out the repeatability tests it was not known that the spacing of $1D_n$ apart as opposed to 0.25 D_n apart would have made any difference since movement was minute and no movement was created. Only during minor movement and settlement tests it could be seen that the underbreak (erosion) values differed when the mesh was improved to 0.25 D_n as opposed to 1 D_n apart for the volume calculation. A confirmation Test was carried out between Test 1 and Test 3 and Test 9 using the 0.25 D_n spacing which produced a volume difference of 0.001 cm^3.

Each scan was processed by importing the point data into the 3D reshaper CAD software to mesh the point data. The volume of the voids of the surface is then computed by creating a water level above the surface shown in Figure 3.4. The volume under the waterlevel is computed by summation of the voids between the meshed surface and the water level. The void volume is then compared with the other nine scans. The standard deviation calculated is in the order of 0.001 with the scanner set-up in this manner.

Table 3.2: Repeatability deviation error results of scans in laboratory

Test number	Volume (m^3)
Test 1	0.030
Test 2	0.030
Test 3	0.031
Test 4	0.031
Test 5	0.031
Test 6	0.029
Test 7	0.030
Test 8	0.030
Test 9	0.029
Test 10	0.029
Mean	0.030
STDev	0.001

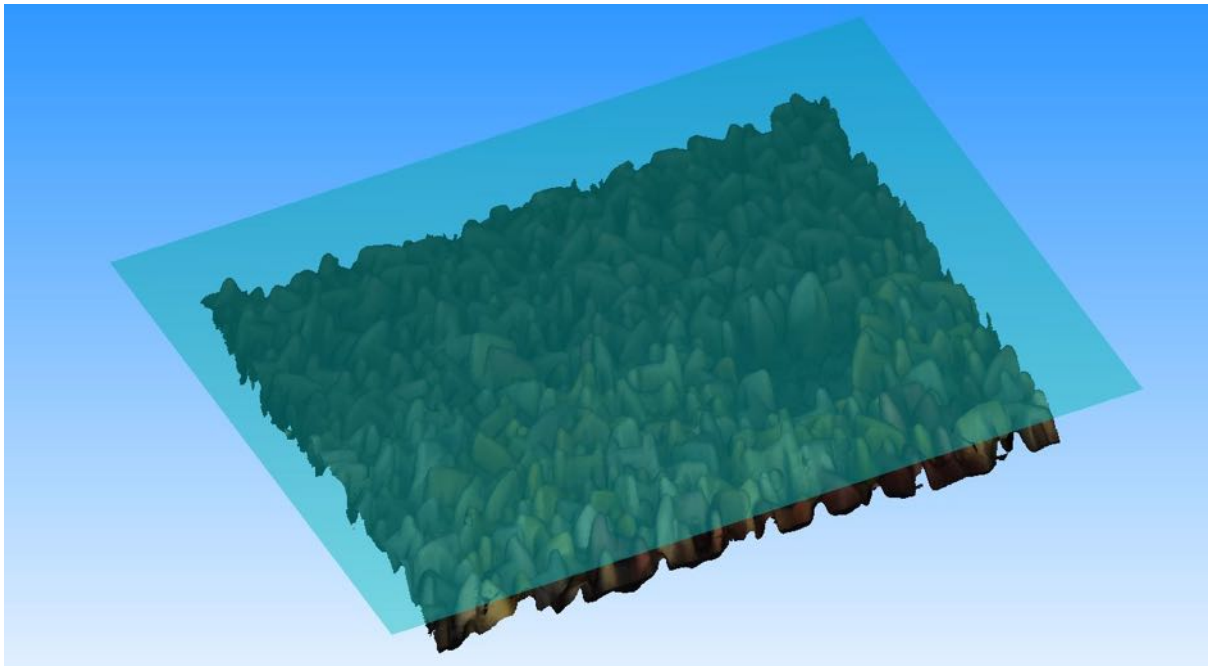

Figure 3.4: Volume calculation by filling the meshed surface voids beneath the artificial water surface.

Profiles of the surface were compared. A total of 22 cross-sections were created over the two stations. Each station having 11 cross-sections extracted every 3.29 cm equal to 1 D_n apart. An image showing the section lines comparing scan 1 and scan 3, is shown in Figure 3.5. The profiles can be seen to follow the dolos meshed surface adequately.

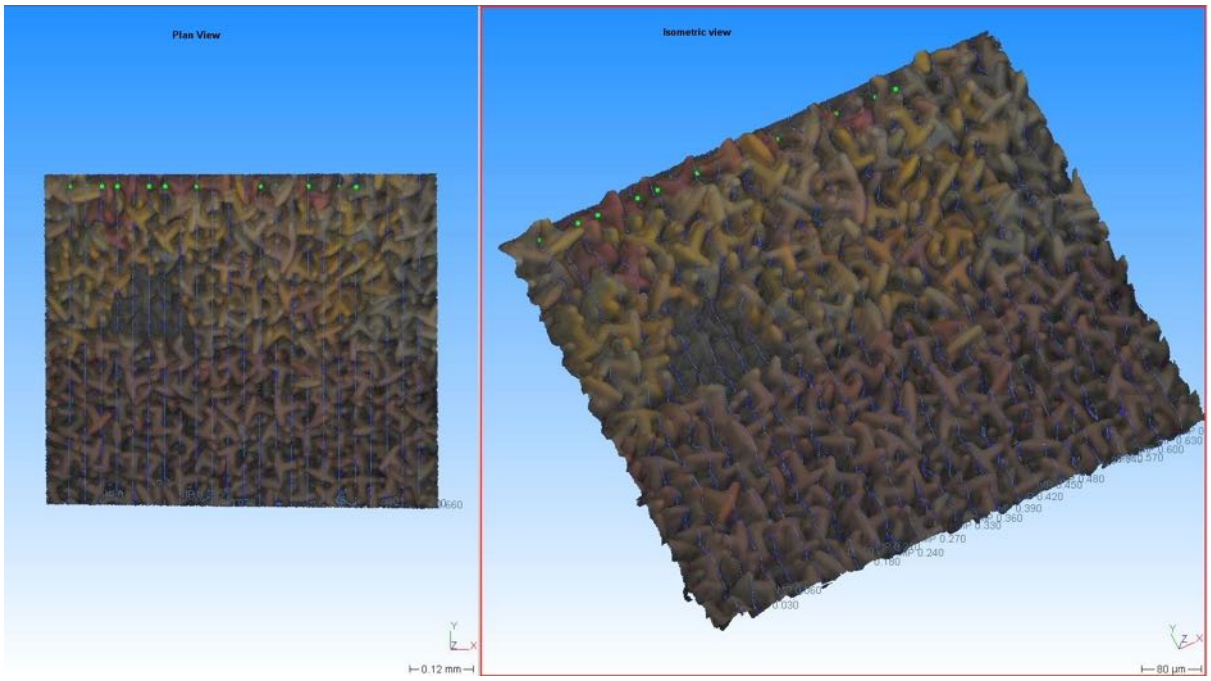

Figure 3.5: Image showing lines spaced equally (1 D_n) apart on the meshed surface for scan 1 and scan 3

3.2.3 Cross-sectional analysis

The cross-section view shown in Figure 3.6 illustrate the profile track line spaced 1 D_n apart. Due to the random placement of dolos and its complex shape cross-sections can be missinterpreted as being irregular especially at a spacing of 1 D_n apart. However with a 3D surface meshed overlay, the profiles are more easily recognised and can be interpreted as shown in Figure 3.6. The same profile view is presented in Figure 3.7 without the 3D image making it difficult to visualise the surface and less representative. The maximum deviation recorded on the slope between the ten repeated profiles was 6 mm. This was recorded near the edge of the profile. It should be noted that care should be taken when creating a mesh and it is advised to scan an area equal to 1.5 times the area of interest thereafter the focus area is cut out to improve the meshing of the data points along the boundary.

The cross-sections are used for volume calculations by interpolating between the parts between cross-sections. One surface is used as a reference and the others compared over or under the reference surface. Therefore, the closer the spacing between profiles the better the accuracy. However, this may be difficult to achieve as it will require excessive computing time. The spacing between profiles was therefore evaluated at 1 D_n, 0.5 D_n, 0.25 D_n, 0.125 D_n, 0.0625 D_n, and 0.03125 D_n to determine the most suitable in terms of processing time and accuracy. The finding of this investigation indicates there can be up to 19% improvement in calculating the volume difference by reducing the spacing to 0.25

D_n between profiles. The results for volume calculations become similar at 0.25 D_n, and 0.125 D_n. The computations become impractical and time consuming when processing profiles are less than 0.0625 D_n apart. It should be noted that due to the limitations in computing equipment the smaller D_n spacing was not possible. The selection of the spacing refines the 3D Reshaper software by forcing the volume calculation to be done at equal 0.25 D_n by 0.25 D_n intervals over the two meshes to calculate the overbreak (accretion) or underbreak (erosion).

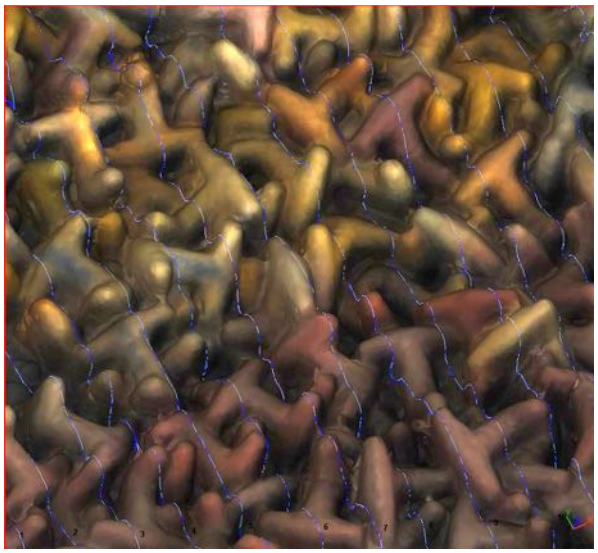

Figure 3.6: Image of mesh and profile at 1Dn spacing of scan 1 and scan 3

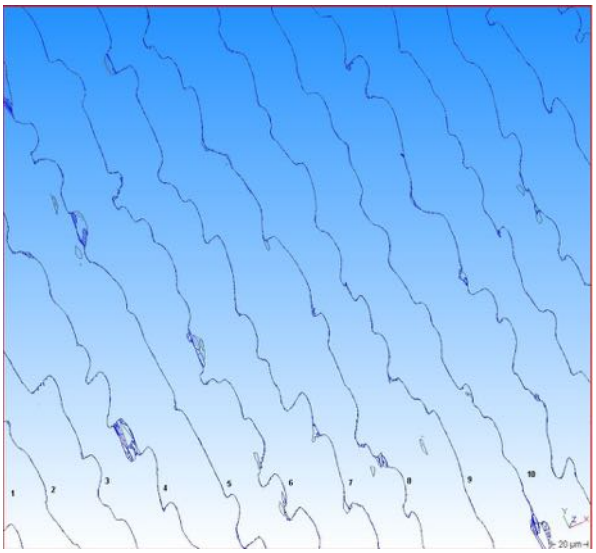

Figure 3.7: Image of profiles from Scan 1 and scan 3 excluding mesh

A closer inspection of the profiles is shown in Figure 3.8. This shows minimal deviations between scan 1 and scan 3. The profiles captured are easily produced for small scale physical model tests and spacing can be predetermined. Spacing of 1 D_n apart provides a suitable average profile of the surface, however spacing of 0.5 D_n, 0.25 D_n and 0.0125 D_n were compared in Table 3.3 to calculate the volume eroded between scan Test 1 and scan Test 3. The image of the void and representation of the spacing between profiles for 0.25 D_n and 0.125 D_n are shown in Figure 3.9 and Figure 3.10. The volume computed for the cross-sections taken at 1 D_n apart deviated by 19%. This was the most extreme for this case. The most similar results were between 0.5 D_n, 0.25 D_n and 0.125 D_n with a deviation of 10%, and 9% respectively with reference to 0.125 D_n. The processing time was however the fastest for 1 D_n spaced cross-sections to determine the eroded volume. An attempt was made at reducing the gap between the cross-section to 0.0625 D_n and 0.03125 D_n however, processing times were in excess of 80 mins and computing power was limited.

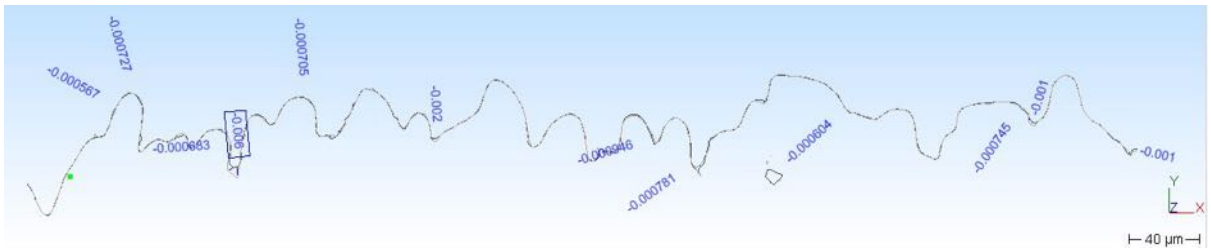

Figure 3.8: Profile of scan 1 and scan 3 showing no significant deviation

Table 3.3: Comparison of cross-sectional spacing and volume calculation

Spacing	Spacing	Profiles	Volume Eroded	Absolute Average Percentage deviation	Processing time
D_n	mm	unit	m^3	%	minutes
1 D_n	32.8	11	8.99	19	15 min
0.5 D_n	16.4	22	12.131	10	20 min
0.25 D_n	8.2	44	12.059	9	35 min
0.125 D_n	4.1	88	11.024	0	55 min
0.0625 D_n	2.05	176			>80 min impractical to process
0.03125 D_n	1.025	352			>80 min impractical to process

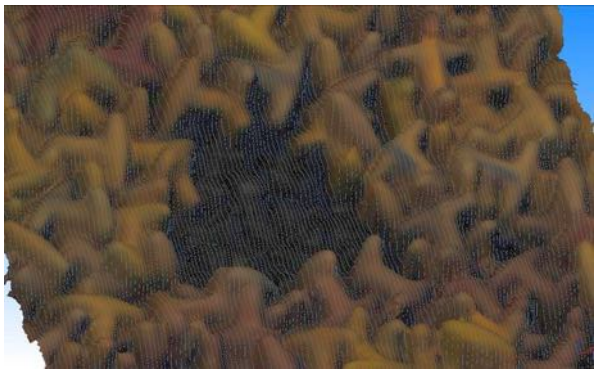

Figure 3.9: Image of slope with profiles taken every 0.25Dn

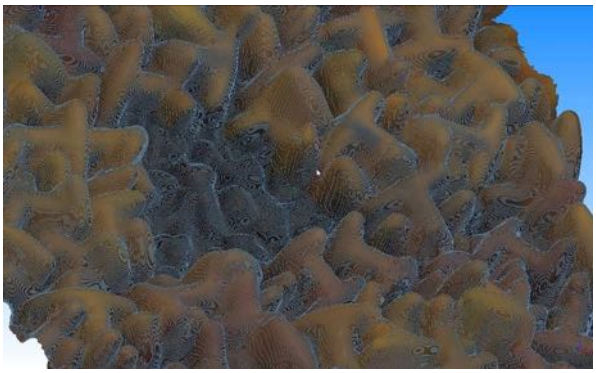

Figure 3.10: Image of slope with profiles taken every 0.125Dn

3.2.4 Displacement, rotation and settlement quantification

The experimental verification of the 3D method included tests ranging from minor movement to major displacement. The displacements were carried out by hand to control small movements, rotations, settlement and complete exposure down to the underlayer. The test data were recorded using the fixed camera and the 3D Laser scanner as shown in Figure 3.1. The camera and 3D Laser scanner provide visuals therefore both are processed using the Armour Track software.

Damage classification by visually counting displacements can be done according to the method described in Section 2.1.5. To date, methods have been developed to quantify damage to rock armoured breakwaters using the average eroded area approach. Presently

there is no information on classifying dolos armour unit damage using eroded volumes therefore a new method is described.

The analysis using this method quantified the displacement in terms of 0 to 0.5 Dn displacement for minor settlement and movement, 0.5 to 1 Dn displacements for intermediate movement and large displacements in terms of 1 Dn to 2 Dn and greater than 2 Dn. The 24 Tests with reference to damage levels are listed in Table 3.5.

Table 3.4: Visual displacement criteria used to categorise H and Dn for the armour track software at model scale 1:75

Category	mm	mm	Category	mm	mm
H	60	mm	Dn	33	mm
0.125H to 0.25 H	8	15	0Dn to 0.5Dn	0	16
0.25H to 0.5H	15	30	0.5Dn to 1Dn	16	33
0.5H to 1H	30	60	1Dn to 2Dn	33	66
>H	60		>2Dn	66	

The analysis results of the 24 tests are tabulated in Table 3.6 and Table 3.7. The analysis of the data in these tables was done visually using the method described by Holtzhausen et al. (2000) for the recording of displacement and Van der Meer (1988) and Burcharth and Liu (1992) for the damage level. Table 3.8 presents the results in terms of eroded volume.

Table 3.5: Damage Level assumption and Test conditions for 3D method

Dolos displacement Test	Initial	Intermediate	Failure
Damage Level criteria	0-2%	3-14%	≥15%
Test Description	Test 1 to 6	Test 7 to Test 19	Test 20 to Test 24

Damage classification using the eroded volume method

In order to classify damage using the 3D eroded volume method some assumptions and recommendations were made with reference to the width of the test section and volume of the primary armour layer are presented in this section to be able to compare visual quantification of damage to CAD volumetric quantification.

By adapting the relative eroded area method described by (Broderick, 1982), the 3D eroded volume method is defined to analyse the design station. The average eroded area of each cross-sections taken every Dn apart is used to determine the eroded area (Equation 3.1). The equation being

$$S = \frac{A_e}{D_n^2} \tag{3.1}$$

Where A_e refers to the average cross-sectional eroded area and D_n the nominal armour unit diameter.

The 3D eroded volume method (Equation 3.2) uses the station width i.e, one station can be the sum of $11D_n = 36.26cm \approx 27m$ in the case of the test station Figure 3.1. Depending on the size of unit the stations will vary. It is recommended using 11Dn width as a station for ease of processing the data. This makes it possible to compare the photographic station damage with the multi-beam and laser scanning. The eroded volume is calculated using the 3D Reshaper CAD software to compute the eroded volume difference between the two profiles. This is computed at intervals of 0.25 D_n across the width of the station.

By including the station width, the equation is:

$$S_{3D}D\% = \frac{V_{station\ erosion}}{V_{station\ design}} \times 100 \tag{3.2}$$

Where $V_{station\ erosion}$ refers to only the sum of the eroded volume of the station armour layer and $V_{station\ design}$ the volume of the station armour layer including voids. The equation does not account for any accretion above the design surface.

Therefore S_{3D} can be expressed as a percentage of the slope that is damaged and $V_{station\ erosion}$ is computed from the comparison of the two scanned datasets to extract the volume eroded. The $V_{station\ design}$ is the as-built volume created by a 3D shape of the slope. It is assumed for the investigation that $S_{3D}\%$ can be related directly to the damage level D % for two-layer armour given in Table 2.3.

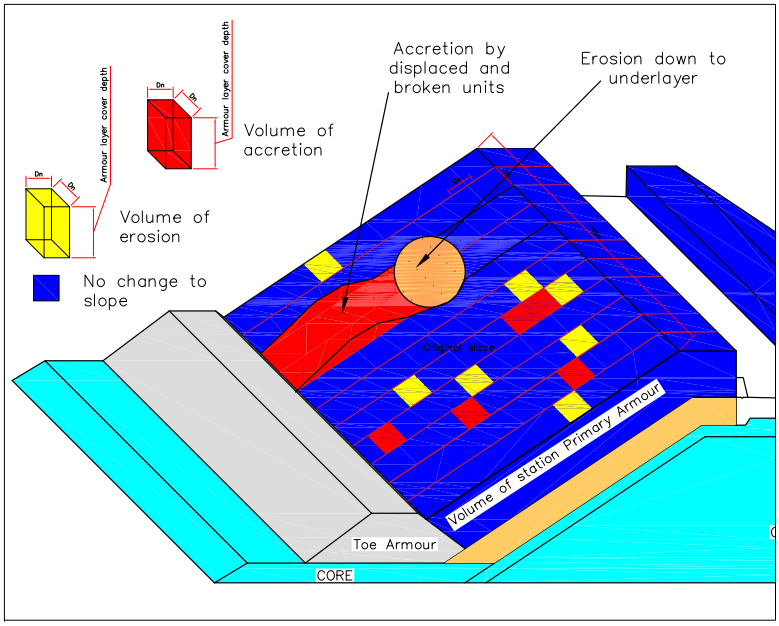

Figure 3.11: Definition of 3D eroded volume method

3.2.5 Erosion quantification comparison using visual analysis and 3D laser scanning technique

The 3D laser scanning technique using eroded volumes to measure damage to dolos breakwaters was compared with the traditional visual analysis method. The test programme was carried out in stages:

1. Test 1 to Test 6: Minor movement less than 0.5 D_n (Figure 3.12 and 3.13)
2. Test 7 to Test 16: Rotations of an individual unit until displacement out of the slope (Figure 3.14 and Figure 3.15)
3. Test 17 to Test 19: Settlement tests (Figure 3.16 and Figure 3.17)
4. Test 20 to Test 24: Major changes to the slope with units displaced to expose the underlayer (Figure 3.18 and 3.19).

The Figures shown below are images of the meshed point data.

Figure 3.12: Visual image from scaned method T1.1

Figure 3.13: Visual image from scaned method T1.6

Figure 3.14: Visual image from scaned method T2.1

Figure 3.15: Visual image from scaned method T2.9

The results of the displacement, rotation and settlement tests using the photographic method are presented below in Table 3.6 and Table 3.7. The 3D scanned eroded volume method is also shown in Table 3.8.

The results of the 24 tests are presented in Figure 3.20. The model displacement is presented as cumulative damage percentage in relation to the changes based on the first image and/or the data from the scanner. The percentage damage is calculated in two ways for the two data sets. The digital camera analysis which uses the Armour Track programme and the second the 3D method which uses the 3D Reshaper software. The digital camera photograph is calculated by counting the number of displacements using Equation 2.15 and Equation 2.10 for the damage total for the entire slope. The second method uses Equation 3.2 to calculate the cumulative damage percentage by the 3D scanned eroded volume method.

Figure 3.16: Visual image from scaned method T3.1

Figure 3.17: Visual image from scaned method T3.3

Figure 3.18: Visual image from scaned method T4.1

Figure 3.19: Visual image from scaned method T4.5

The S_{3D} results after computing the eroded volume using a 0.25 Dn spacing across the width of the station is presented in Table 3.8. The volume of the station $V_{station\ design}$ was 0.375 m x 0.65 m 0.065 m = 0.01584 m^3. The method computed a no percentage damage for the first four Tests. The results of the initial damage movement of less than 0.5 Dn (Test 1 to Test 6) was similar to those of the visual method with no change until Test (6)1.6 with a result of 2.1 % for the minor displacement.

Test (7)2.1 to Test (16)2.10 focused on individual units rotating and recording the comparative damage value. For this verification experiment only one unit was rotated until it was completely out of its original position and then removed from the slope. The movement can easily be seen when flickered and recorded within the categories of 0 D_n to 0.5 D_n, 0.5 D_n to 1 D_n and 1D_n to 2D_n and greater than 2 D_n yet when inserted into the damage formula D_T, N_d, N_{od} and D%, the damage differs. D_T sums up 50% of dolos displacement larger than 0.5 D_n to 1D_n and all displacements larger than 1D_n. The N_{od}

Table 3.6: Damage calculation by *camera* images using visual assessment

Test Description	Displacement	0-0.5Dn	0.5Dn-1Dn	1Dn-2Dn	$2Dn$	D_T	Nd(%)	Nod(%)	D(%)
initial damage	(1)T1.1	0				0.0	0.0	0.0	0.0
initial damage	(2)T1.2	0				0.0	0.0	0.0	0.0
initial damage	(3)T1.3	1				0.5	0.0	0.0	0.0
initial damage	(4)T1.4	0				0.0	0.0	0.0	0.0
initial damage	(5)T1.5	1				0.5	0.0	0.0	0.0
initial damage	(6)T1.6	1				0.5	0.0	0.0	0.0
intermediate	(7)T2.1		1			1.0	0.0	0.0	0.0
intermediate	(8)T2.2		1			1.0	0.0	0.0	0.0
intermediate	(9)T2.3		1			1.0	0.0	0.0	0.0
intermediate	(10)T2.4			1		1.0	0.5	0.8	2.8
intermediate	(11)T2.5			1		1.0	0.5	0.8	2.8
intermediate	(12)T2.6			1		1.0	0.5	0.8	2.8
intermediate	(13)T2.7			1		1.0	0.5	0.8	2.8
intermediate	(14)T2.8				1	1.0	0.5	0.8	2.8
intermediate	(15)T2.9				1	1.0	0.5	0.8	2.8
intermediate	(16)T2.10				1	1.0	0.5	0.8	2.8
intermediate (Settlement minor)	(17)T3.1	25			1	13.5	0.5	0.8	2.8
intermediate (Settlement moderate)	(18)T3.2	34			1	18.0	0.5	0.8	2.8
intermediate (Settlement major)	(19)T3.3	37			1	19.5	0.5	0.8	2.8
Failure	(20)T4.1	37			7	25.5	3.7	5.9	19.7
Failure	(21)T4.2	37			7	25.5	3.7	5.9	19.7
Failure	(22)T4.3	39			7	26.5	3.7	5.9	19.7
Failure	(23)T4.4	39			11	30.5	5.8	9.3	30.9
Failure	(24)T4.5	40			11	31.0	5.8	9.3	30.9

Table 3.7: Damage calculation by *scanned* images using visual assessment

Test Description	Displacement	0-0.5Dn	0.5Dn-1Dn	1Dn-2Dn	$2Dn$	D_T	Nd	Nod	D(%)
initial damage	(1)T1.1	0				0.0	0.0	0	0.0
initial damage	(2)T1.2	0				0.0	0.0	0.0	0.0
initial damage	(3)T1.3	1				0.5	0.0	0.0	0.0
initial damage	(4)T1.4	0				0.0	0.0	0.0	0.0
initial damage	(5)T1.5	1				0.5	0.0	0.0	0.0
initial damage	(6)T1.6	1				0.5	0.0	0.0	0.0
intermediate	(7)T2.1		1			1.0	0.0	0.0	0.0
intermediate	(8)T2.2		1			1.0	0.0	0.0	0.0
intermediate	(9)T2.3		1			1.0	0.0	0.0	0.0
intermediate	(10)T2.4			1		1.0	0.5	0.8	2.8
intermediate	(11)T2.5			1		1.0	0.5	0.8	2.8
intermediate	(12)T2.6			1		1.0	0.5	0.8	2.8
intermediate	(13)T2.7			1		1.0	0.5	0.8	2.8
intermediate	(14)T2.8				1	1.0	0.5	0.8	2.8
intermediate	(15)T2.9				1	1.0	0.5	0.8	2.8
intermediate	(16)T2.10				1	1.0	0.5	0.8	2.8
intermediate (Settlement minor)	(17)T3.1	22			1	12.0	0.5	0.8	2.8
intermediate (Settlement moderate)	(18)T3.2	36			1	19.0	0.5	0.8	2.8
intermediate (Settlement major)	(19)T3.3	35			1	18.5	0.5	0.8	2.8
Failure	(20)T4.1	38			7	26.0	3.7	5.9	19.7
Failure	(21)T4.2	38			7	26.0	3.7	5.9	19.7
Failure	(22)T4.3	39			7	26.5	3.7	5.9	19.7
Failure	(23)T4.4	39			11	30.5	5.8	9.3	30.9
Failure	(24)T4.5	40			11	31.0	5.8	9.3	30.9

Table 3.8: Damage calculation by 3D eroded volume

Test Description		Displacement	Overbreak (accreation)(cm^3)	Underbreak (erosion) (cm^3)	Volume (cm^3)	S_{3D} D(%)
initial damage	1	(1)T1.1				0.0
initial damage	2	(2)T1.2				0.0
initial damage	3	(3)T1.3				0.0
initial damage	4	(4)T1.4				0.0
initial damage	5	(5)T1.5	7.113	2.462	2.46E-02	1.6
initial damage	6	(6)T1.6	2.435	3.254	3.25E-02	2.1
intermediate	7	(7)T2.1	4.054	1.162	1.16E-02	0.7
intermediate	8	(8)T2.2	3.83	3.51	3.51E-02	2.2
intermediate	9	(9)T2.3	8.816	5.492	5.49E-02	3.5
intermediate	10	(10)T2.4	1.49	5.006	5.01E-02	3.2
intermediate	11	(11)T2.5	1.905	7.756	7.76E-02	4.9
intermediate	12	(12)T2.6	4.659	2.808	2.81E-02	1.8
intermediate	13	(13)T2.7	4.855	4.716	4.72E-02	3.0
intermediate	14	(14)T2.8	2.339	4.643	4.64E-02	2.9
intermediate	15	(15)T2.9	17.93	9.725	9.73E-02	6.1
intermediate	16	(16)T2.10	1.931	3.081	3.08E-02	1.9
intermediate (Settlement minor)	17	(17)T3.1	4.529	7.037	7.04E-02	4.4
intermediate (Settlement moderate)	18	(18)T3.2	9.988	9.722	9.72E-02	6.1
intermediate (Settlement major)	19	(19)T3.3	9.069	15.459	1.55E-01	9.8
Failure	20	(20)T4.1	12.547	23.164	2.32E-01	14.6
Failure	21	(21)T4.2	6.795	28.748	2.87E-01	18.1
Failure	22	(22)T4.3	16.611	38.358	3.84E-01	24.2
Failure	23	(23)T4.4	14.211	33.945	3.39E-01	21.4
Failure	24	(24)T4.5	5.026	35.332	3.53E-01	22.3

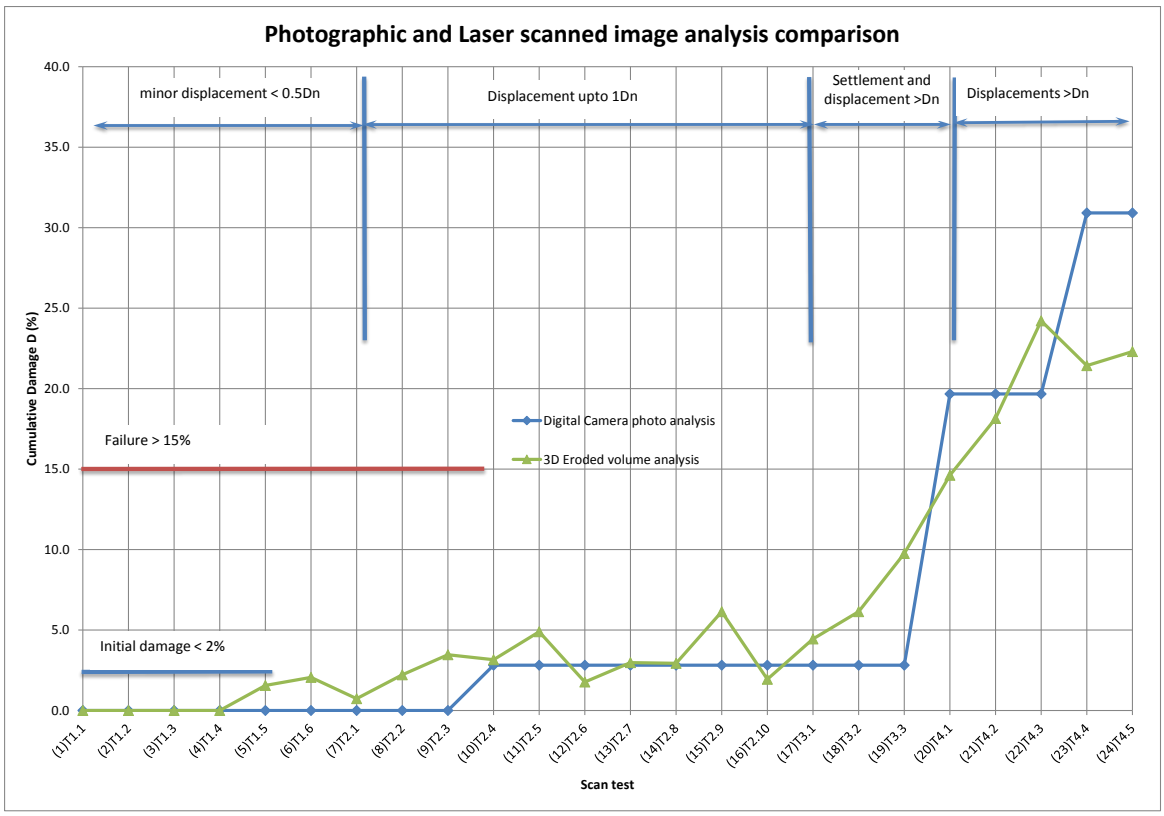

Figure 3.20: Comparison of damage percentage determined using photographic and scanned data

formula records movement greater than $2D_n$ as damage. N_d formula records displacement larger than $1D_n$ divided by the total number of units within the reference area.

Test (17)3.1 to Test (19)3.3 compared the recording of settlement progression from minor

to major in terms of damage percentage. The visual analysis picks up settlement, however it is not recorded as it falls outside of the damage criteria which only addresses movement greater than 1 Dn. The 3D method recognises the settlement as a void between the two surfaces therefore, as the settlement and voids increase, the damage percentage increases. The 3D method recorded a damage percentage of 9.8% and the visual method 2.8% for this experimental case. This is more than a factor three diference between individual measurements. This is due to the $D(\%)$ formula recording only movements larger than 2Dn. However, if the method developed by Holtzhausen et al. (2000) is used the Damage result for $D_T(\%)$ would be 19.5 divided by 190 (dolos units) = 10.26%, which is in accordance with the results from the 3D method.

Test (20)4.1 to Test (24)4.5 looked at major changes to the slope with units displaced to expose the underlayer. Both methods recorded values in excess of 15% indicating failure. The results from the visual method were initially lower than those from the 3D method but since the void size did not change much the volumetric method recorded only 22.3 %. The visual method recorded individual units being displaced of 30.9 %, which is 27.8% higher than the volumetric mentod.

Both methods provide a reasonable track of damage progression from minor movement, to rotational displacements and major movement. The settlement using the visual method does not include settlement less than 1 Dn therefore an alternative criterion should be adopted using (Phelp and Zwamborn, 2000) or Holtzhausen et al. (2000), which would increase the damage percentage and follow a similar trend as the 3D method in this case. This is calculated using Equation 2.15.

3.2.6 Measurement Accuracy

The measurements accuracy check was carried out by scanning five (5) dolos units and a set of callipers. The five units were scanned using the LIDAR scanner and measured using the 3D Reshaper CAD programme. Figure 3.21 shows an image of the five dolos units that were scanned and the calibration box used for the accuracy measurements. The results from the actual measurements are presented in Table 3.9. The accuracy check was done by measuring the height and waist of the dolos units. The average dolos height measurement was 73.9 mm while the waist measurement was 24.46 mm using the caliper. The mean absolute error between the five units was ± 0.22 mm for the Height and ± 0.12 mm for their waist. The units were then scanned and measurements done using the CAD software package. The measurements are presented in Table 3.10.

Figure 3.21: Model dolos units used for the mean absolute error measurements

The average dolos height was measured at 74.00 mm and waist at 24.60 mm. The mean absolute error was zero for the height measurement and ± 0.48 mm for the waist measurement when comparing the physical error in Table 3.11 and scanned error in Table 3.12

Table 3.9: Absolute error of model dolos units

Model	1	2	3	4	5	Average
Dolos Height (H) mm	74.00	73.62	74.14	73.62	74.10	73.90
Dolos Waist (W) mm	24.36	24.66	24.42	24.56	24.32	24.46
W/H (-)	0.33	0.33	0.33	0.33	0.33	0.33
Absolute error (H) mm	0.10	0.28	0.24	0.28	0.20	0.22
Absolute error (W) mm	0.10	0.20	0.04	0.10	0.14	0.12

Table 3.10: Absolute error of LIDAR scanned model dolos units

LIDAR Scan	1	2	3	4	5	Average
Dolos Height (H) mm	74.00	74.00	74.00	74.00	74.00	74.00
Dolos Waist (W) mm	24.00	25.00	25.00	25.00	24.00	24.60
W/H (-)	0.32	0.34	0.34	0.34	0.32	0.33
Absolute error (H) mm	0.00	0.00	0.00	0.00	0.00	0.00
Absolute error (W) mm	0.60	0.40	0.40	0.40	0.60	0.48

Table 3.11: Mean absolute error of model dolos units

Mean Absolute error (H) (mm)	0.2208		
Mean Absolute error (W) (mm)	0.1168		
Max H (mm)	74.12	Min H (mm)	73.68
Max W (mm)	24.58	Min W (mm)	24.35
Max W/H (-)	0.33	Min W/H	0.33

Table 3.12: Mean absolute error of LIDAR scanned model units

Mean Absolute error (H) (mm)	0		
Mean Absolute error (W) (mm)	0.48		
Max H (mm)	74.00	Min H (mm)	74.00
Max W (mm)	25.08	Min W (mm)	24.12
Max W/H (-)	0.34	Min W/H	0.33

3.3 Summary

Prior to this study a comparison between visual quantification, 2D cross-sectional eroded areas and 3D eroded volumes were evaluated for rock slopes Drake (2007), Risser (2011). Concrete armour units namely Antifer cubes, Core-Loc and dolos units were evaluated further by Wüst (2012). The comparisons were accomplished by simulating typical damage levels of initial, intermediate and failure conditions to quantifying damage levels.

The outcome of the investigations indicated the accuracy of the measurements depended on the ability to process and create a mesh of the scanned data, therefore previously photographic and manual methods proved to provide more accurate results in the past. Nowadays, mesh generation has improved and individual armour units can be recognised in mesh form similar to photographs.

In this experimental verification the 3D scanned data were dense with limited shadows and coverage problems were reduced by the angle of the scanner and height above the dolos slope which made data capture suitable for analysis. This is also the case for the photographs taken in this experiment using the traditional methods. The repeatability tests provided information on the reliability of repeated scans in this controlled environment which gives confidence when comparing identical scans. The repeatability test were carried out by comparing 10 consecutive scans with the first scan. The standard deviation was 0.001 cm^3. A cross-sectional analysis was also carried out as part of the repeatability tests in tracking the variation in extracting cross-sections. The difference between scans was negligible with the maximum being 6 mm found at the edges of the cross-section.

The process of extracting the eroded volumes requires a minimum of two cross-sections on either end of the station. This can be improved by creating more cross-sections. The ability to track the intricate shape of the dolos unit was tested and cross-sections were taken at intervals of 1Dn, 0.5 Dn, 0.25 Dn, 0.125 Dn, 0.0625 Dn and 0.03125 Dn. Cross-sections between 1 Dn to 0.125 Dn were possible with the optimal cross-section being limited to 0.25 Dn due to limitations in computing power. This is important for the volume calculations as the closer the cross-section interval the more accurate the volume calculation. The most similar results were found between 0.5 Dn, 0.25 Dn. The method can be made more accurate in future depending on the processing speed and memory of the computer, therefore smaller spacing can be used. However, for this application 0.25 Dn was used in the computations.

Twenty four (24) tests were carried out to quantify the expected damage percentage that can be associated with displacement, rotation and settlement using the eroded volume method. This was compared with the visual method. Damage percentages for both methods are plotted in Figure 3.11. The damage classification used was Van der Meer (1988) for the damage parameter $D\%$, Equation 2.9. The method indicates there are variations by a factor of three times between the two methods for some individual

results however the results have a similar trend when comparing all twenty four tests. Both methods are able to track differences in the slope if there is settlement, minor displacements and rotations and provide a damage percentage in relation to the first scan or first image. The 3D eroded volume method can be further refined by improving the mesh triangulation grid spacing and edge detection to improve intricate surfaces for eroded volume calculations.

Chapter 4

3D Physical model of the Cape Town Spur breakwater

4.1 Background

This section explains the 3D physical model set-up for the Cape Town spur breakwater. The model study was conducted at the CSIR Coastal and Hydraulics Laboratory. Chapter 3 demonstrates the 3D method is able to track displacements representing damage progression in a physical model. In this phase of the study the 3D method is tested in a physical model study were displacement occurs by wave interaction.

4.2 3D Physical model facility and equipment

This section provides details of the 3D wave basin, wavemakers, wave probes, cameras, and 3D laser scanner used to conduct the study. The physical model was conducted at a scale of 1:54 using the Froude Law of Similitude. Inertia and gravity are the dominating criteria and the model is geometrically undistorted in length scale while effects of viscosity and surface tension are neglected. It is recognised for most physical models, the Froude and Reynolds scaling laws cannot be met simultaneously.

4.3 Basin boundaries and absorbing beach

The 3D wave basin (SB2) was used for the study with dimensions 40 m wide x 32 m long x 1.2 m deep. Figure: 4.1 provides a sketch of the basin in plan view indicating location of wavemakers, wave guides, rock absorption beach and location of the spur structure. Figure: 4.2 shows an image of the completed model set-up in the 3D wave basin.

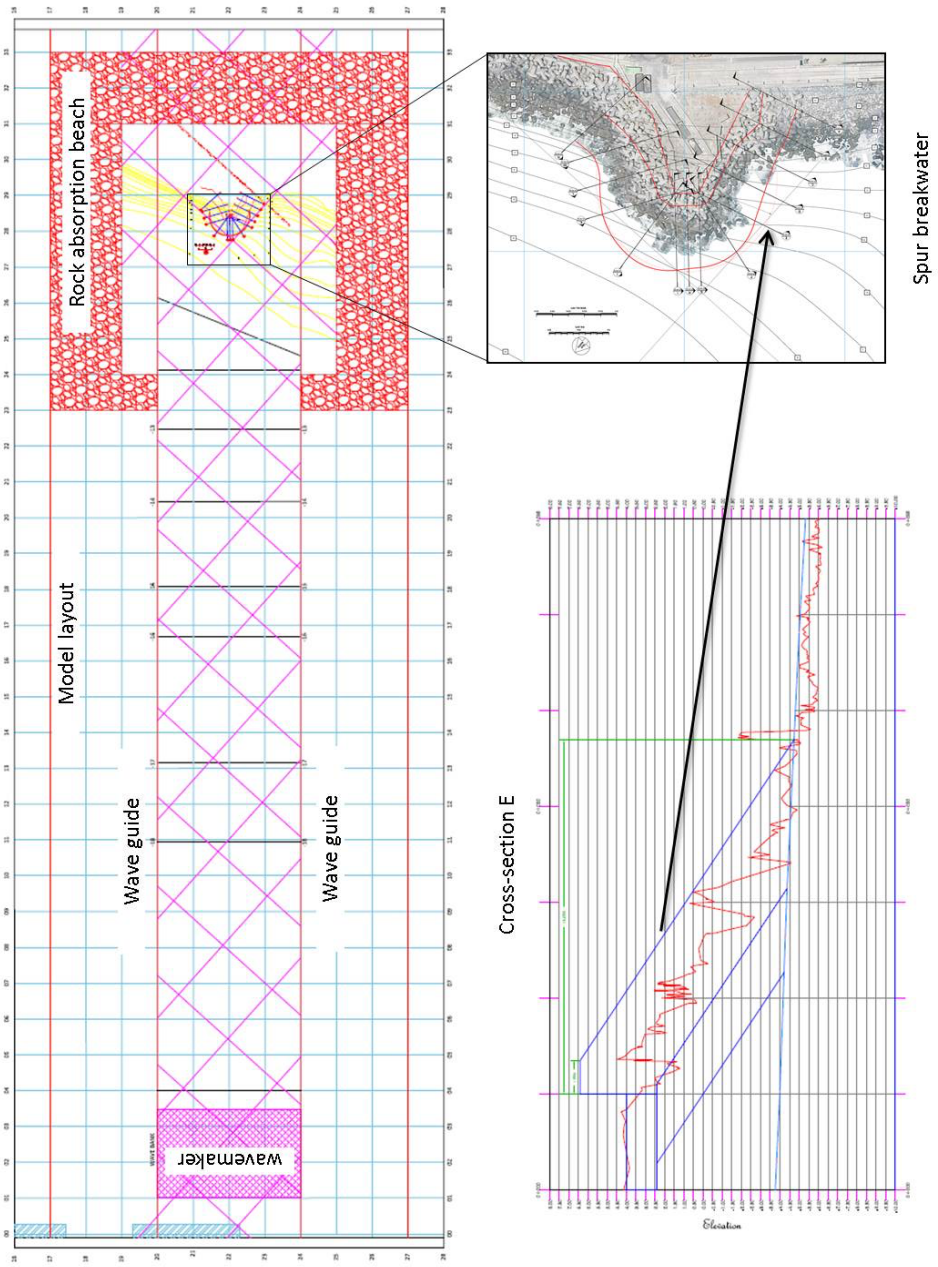

Figure 4.1: 3D Wave basin, spur model structure, profle of the test section and wavemaker position

The most important constraint to any physical model is the basin boundary wall. These are always either too close to the structure or too low for the proposed scale therefore the 40 m basin was selected. The area of interest was 4 m in length. Breakwater structures being tested should not be affected by the waves travelling towards side walls or have absorbing beaches reflecting waves towards the breakwater structure being tested. In order to dampen the reflection originating from the boundary walls, a sloping layer of coarse rubble was placed with reeled wire mesh placed at the waterline. The coarse rock beach and reeled wire mesh of diameter 200 mm was placed on the sides and behind the tested structure to minimize the reflection back towards the breakwater from the walls.

The influence of the reflected waves on the propagating incident wave climate is also minimized.

Figure 4.2: The model with scanner (left) and calibration box (foreground)

4.4 Wave generation

The waves were generated by a 4 m bank of multi-element wavemakers. The wavemakers consisted of 8 individual paddles of width 0.50 m. The wavemaker was set-up parallel to the model boundary wall. The wavemakers are capable of generating irregular waves either long crested or short crested with a maximum stroke of 0.50 m. Figure: 4.2 shows the 4m bank of wavemakers in the background used for the model study.

The dynamic wave absorption feature was turned off for the model study due to the large 3D area. This was done since the absorption function would introduce spurious waves instead of reducing the reflected wave components in the large basin. The formation of spurious reflected waves was suppressed by constructing coarse rock berms and rolled wire reels for absorbing and reducing the effect of reflecting waves around the model perimeter. However, there is always some reflection which may involve several risks eg. cross-waves in the basin.

The incident wave climate arriving at the breakwater may have a higher wave height than accounted for as the re-reflected wave of the wavemaker can be sent back to the

breakwater. This can also result in waves breaking before reaching the breakwater due to the depth limitation when combining a re-reflected wave and incident wave.

Standing waves should also be considered as this phenomenon is a result of resonance in the basin causing reflection from vertical faces and overlapping of waves without breaking. To limit these effects, the wavemaker bank to structure distance chosen was three times the maximum wavelength to allow sufficient space for wave energy to form and disperse. Rock absorption beaches were placed such that waves were not trapped between vertical faces within the test area.

All wave conditions were generated with the standard wave spectral function, namely the JONSWAP spectrum. A peak-enhancement factor (gamma) of 3.3 was applied. During the calibration process, the uniform gain factor of the wave generator was adjusted to control the output wave height at the control point. This iterative calibration procedure allowed for a variety of wave conditions that could be used for a specific wave spectrum and water level during testing.

4.5 Wave climate

The two common wave spectra to represent a sea state is JONSWAP (JOint North Sea WAve Project) representing a wave climate with limited fetch and storm duration given by Equation 4.1 and the other a Pierson-Moskowitz spectrum which describes the sea state for fully developed seas. The variance density spectrum generating the waves are as follows Holthuijsen (2007) :

$$E_{JONSWAP}(f) = \alpha g^2 (2\pi)^{-4} f^{-5} \exp\left[\frac{-5}{4}\left(\frac{f}{f_{peak}}\right)^{-4}\right] \gamma^{\exp\left[-\frac{1}{2}\left(\frac{f/f_{peak}-1}{\sigma}\right)\right]} \tag{4.1}$$

where:

$$\sigma = \begin{cases} 0.07 \ if \ f \leq f_{peak} \\ 0.09 \ if \ f > f_{peak} \end{cases}$$

In which $E_{JONSWAP}(f)$ is the variance density with unit (m^2/s). f and f_{peak} recorded in (Hz), are the frequency and peak frequency parameters respectively, while g the gravitational acceleration. α represents an energy scale parameter, γ is a peak enhancement factor ranging from 1.0 to 3.3, (3.3 is more commonly used creating a very steep wave spectrum) and σ is a peak width parameter. A conventional JONSWAP energy spectrum compared with the Pierson-Moskowitz spectrum is provided in Figure 4.3 .

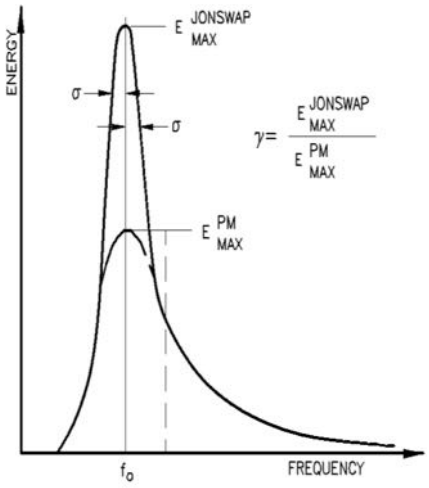

Figure 4.3: The PM and JONSWAP spectra source: (USACE, 2006)

The test condition was initially based on extreme value analysis for the design condition and MIKE 21 SW modelling is tabulated in Table 4.1. The water level for the high water design condition was determined by the summation of MHWS, sea level rise and storm surges. This was applied as well for the low water design condition (MLWS). Table 4.2 presents the results for the water level calculations. When determining the best way to test the accuracy of the two damage analysis methods the tracking damage progression for minor movement, intermediate movement and extreme movement until exposure of the underlayer by failure of the toe was chosen. This was achievable by using the MSL water level. The higher water level would have resulted in wave impact loss on the structure as waves overtopping with have been predominant. The lower water level resulted in the majority of waves breaking before the structure and being depth limited.

Table 4.1: Test condition selected for damage assessment

Test ID	Objective	WL [m MSL]	Hm0_I -10.8 [m]	Tp_I [s]
1.1 (A)	Shake down at MSL	0	4.00	14
2.1 (B)	Design condition at MSL	0	4.60	14
3.1 (C)	Overload at MSL (120%)	0	5.50	18
4.1 (D)	Design condition at MSL	0	4.60	16

Table 4.2: Design water level for MHWS and MLWS

Astronomical tide	Unit	MHWS	MLWS
Astronomical tide	m MSL	0.92	-0.58
Sea Level Rise	m	0.3	0
Storm Surge	m	0.75	-0.75
Water Level (MSL)	m MSL	1.97	-1.33
Water level (Design)	m MSL	2	-1.3

Figure 4.4 depicts the wave direction, with wave height contours for the design condition. The dominant wave direction is from a refracted wave propagating from a westerly direction around Green Point. Figure 4.5 shows a Google Earth image of waves refracting around Green Point towards the breakwater.

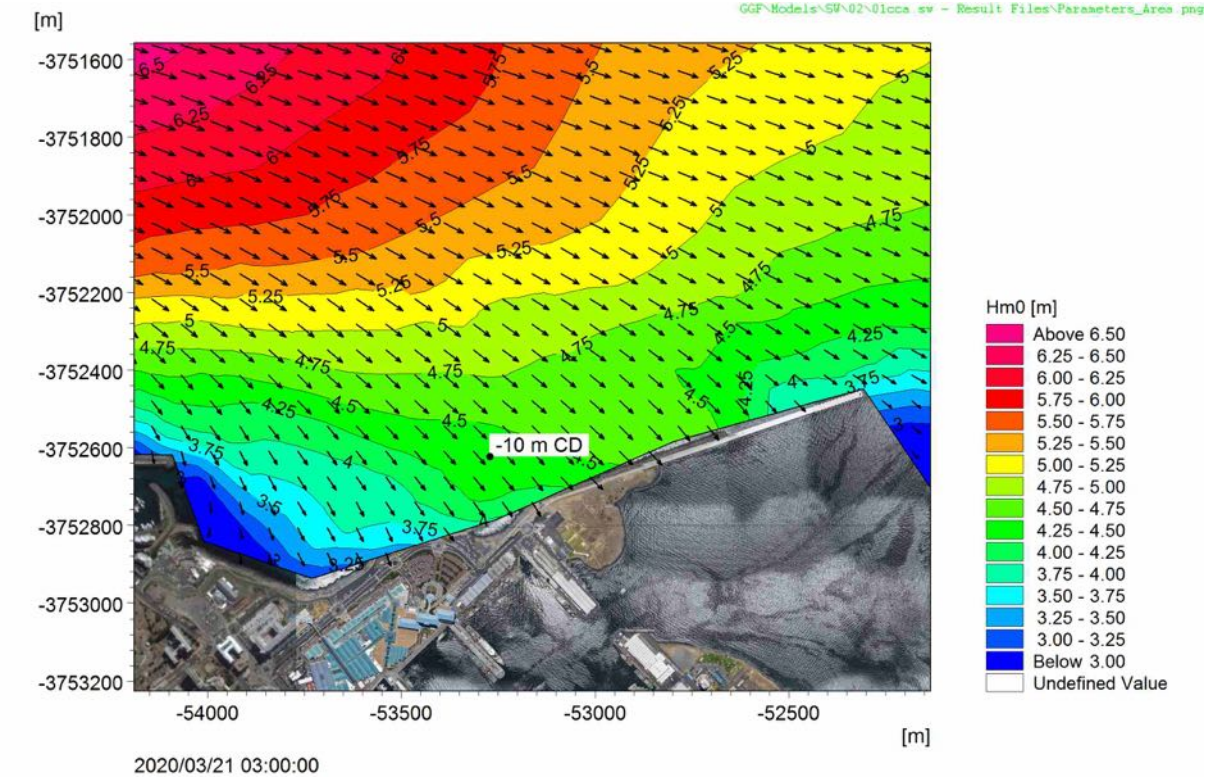

Figure 4.4: Model output showing wave height contour and direction (CSIR, 2015)

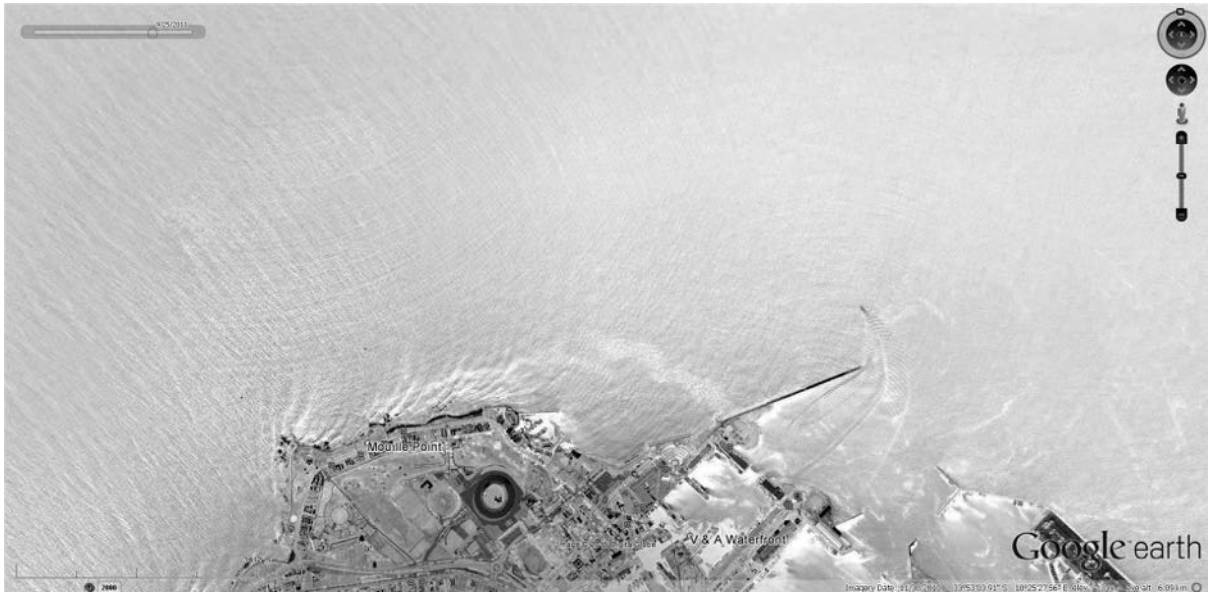

Figure 4.5: Wave refraction around Green Point, Cape Town (Google Earth image 2010)

4.5.1 Consideration for the physical model

Physical models are usually scaled in relation to certain parameters such as dimensions in prototype and model. Therefore, the following formula (Equation 4.2) is used to scale the parameter x:

$$n_x = \frac{x_p}{x_m} \tag{4.2}$$

where: "n_x" represents the prototype to model scale ratio, "x_p" refers to prototype and "x_m" refers to model. When scaling a physical model all physical processes should be scaled. This is not always possible for practical reasons and also not necessary in most occasions. In the physical model all lengths are scaled by a certain factor. Typically, scaled models are constructed to be as large as possible to diminish scale effects. The scaling effects occur because not all physical processes can be scaled down to the same extent. The scale used in the physical model study is 1 : 54.

According to Hughes (1993), scale effects occur in hydraulic models because the properties of water (such as density, viscosity and surface tension) can not be scaled. Viscosity does not play any significant role in rotational free gravity surface waves. The energy dissipation because of friction with the bottom is not significant for the small distance the waves travel in the model. Therefore the viscosity is neglected and the model is not scaled according to Reynolds Law. The surface tension of the air-water surface can play a role in the wave celerity for small waves. For depths over 2 centimetres and periods of over 0.35 s, this does not play a significant role.

In this model, gravity and inertia are the dominating forces that drive the waves. The set-up of the model was therefore chosen to ensure similitude with the Froude Law of Scaling (Equation 4.3). Thus

$$F_r \equiv \sqrt{\frac{inertial\ force}{gravity\ force}} = \frac{u}{\sqrt{gl}} \tag{4.3}$$

In which "l" is a certain length (in most cases the water depth) and u the flow velocity "m/s". An important requirement in physical modelling of coastal structures is that the ratio between the inertial force and gravity force is the same in the prototype and the model. i.e. the Froude number must be the same. This requirement results in (Equation 4.4) :

$$[\frac{u}{\sqrt{gl}}]_p = [\frac{u}{\sqrt{gl}}]_m \tag{4.4}$$

Re-arranging Equation 4.4 to an expression in terms of scales yields (Equation 4.5)

$$\frac{n_u}{\sqrt{n_g.n_l}} = n_{Fr} = 1 \tag{4.5}$$

Since gravity cannot be scaled, it follows that:

$$n_u = n_l$$

Reynolds scaling law with reference to the flow in the model must be turbulent. A widely used parameter used to indicate turbulence is the Reynolds Number (Equation 4.6), which is defined as:

$$R_e \equiv \sqrt{\frac{inertial\ force}{viscous\ force}} = \frac{u.l}{v} \tag{4.6}$$

In which "v" is the viscosity of water. The Reynolds Number is used to distinguish between laminar and turbulent flow. In order to achieve similitude, Reynolds number in prototype and model must be the same. The criterion for similitude (Equation 4.7) is:

$$\frac{n_u.n_l}{n_\mu} = n_{Re} = 1 \tag{4.7}$$

This criterion is impossible to meet, due to the fact that the viscosity of water "v" is the same in prototype and model. However, this is not a problem in physical models of coastal structures as long as the flow is turbulent in prototype, hence the ratio for the inertial force and viscous force is large. As long as this ratio is still large in the model, the flow is still turbulent and it is assumed and expected to behave the same as in prototype.

4.6 Model scale effects

Hughes (1993) explains that the properties of water which cannot be adjusted are viscosity, air content and surface tension. These properties will cause scale effects with wave and structure interaction and in general it is impossible to achieve complete similitude as not all processes can be modelled according to the scale laws.

4.7 Viscous flow effects

As discussed extensively in Hughes (1993) it is important that the flow in the model wave is turbulent for coastal structures when modelling flow over armour units. However, the flow in the under layer and core of the breakwater might be laminar in the model. As a result viscous scale effects occur due to a reduced permeability of core layers and this may lead to higher downrush pressures from inside the structure. It is therefore required that the flow in the armour layer of model is turbulent. The armour layer Reynolds Number is used to indicate the type of flow in the armour layer (Equation 4.8):

$$Re_{model} = \frac{\sqrt{gH_s}D_n}{\mu} > 30000 \tag{4.8}$$

In which Hs (m) is the significant wave height and D_n (m) is the nominal diameter of the armour unit. μ is the absolute viscosity of air being 1.8×10^{-5} N s $m^{-}2$. It was found that the minimum value of Re_{model} at a scale of 1:54 is in the order of 5×10^4 resulting in negligible scaled flow effects.

4.8 Friction effects

In physical models the contact friction between the armour units may differ from the prototype. Most model units are made of a polypropylene and barium sulphate mixture and prototype units out of concrete. For this reason, model units can have a slightly greater relative roughness than in prototype. By adding a light coat of paint to the armour units, this increases the friction between units. This additional friction needs to be considered as less conservative and minor movements considered with reference to damage. The different colours however helps to distinguish movement of individual units.

4.9 Aeration effects

Hughes (1993) performed experimental research on the entrainment and movement of air bubbles due to the water movement near breakwaters. He found that in small scale models the air bubbles are relatively large compared to the prototype. This results in more energy dissipation along the slope in model than in prototype. This phenomenon has an influence on the wave run-up. It is therefore considered that aeration scale effects may contribute to model effects as water and air are not scaled. However, the effect of overall energy dissipation is still in similitude between prototype and model. Thus, scale effects due to wave breaking in a scaled model can be neglected.

4.10 Set-up of the experiments

The model dolos represent a prototype mass of 25 tonnes. The specific weight of the dolos armour unit was 2400 kg/m^3. The corresponding $D_n = 2.183$ m with $V = 10.416$ m^3. At a scale of 1 : 54 the dolos mass in the model is 154.89 g. The corresponding $D_n = 0.0404$ m with $V = 66.478$ cm^3. The Reynold's Number is greater than 30000.

A plan image of the location of the cross-section templates used to build up the spur breakwater is shown in Figure 4.6. The templates were constructed from the laser scanning, multi-beam survey and as-built drawings. Figure 4.7 shows the placement of the dolos in a random orientation as a double layer arrangement. The rope line seen on the ground in the image provides for the horizontal axis placement which has the spacing intervals marked out. The placement grid used is tabulated in Table 4.3.

Table 4.3: Placement grid for model dolos units

Prototype		
Concrete density	2400	kg/m^3
Dolos	**25**	tonnes
Volume	10.417	m^3
Packing density	0.94	
Dn	2.184	m
n	0.197	units/m^2
1/n	5.074	
Unit cover	10.148	m^2
Distance between units	3.186	m
Model		
scale	**54**	
model distance	58.993	mm
Placement Grid		
Vertical (0.9)	53.094	mm
Horizontal (1.1)	64.892	mm

Figure 4.6: Construction of the Cape Town spur breakwater scale model

Figure 4.7: Placement of model dolos using the grid spacing

4.11 The 3D method and visual analysis method

The damage assessment is carried out according to the method described in Section 3.2.4. Damage measurement test conditions are summarised in Table 4.1. The tests selected were for the purpose of evaluating accuracy of measuring change to the slope and comparing two methods. However, it should be noted that the tests were not carried out to reproduce the same damage recorded in prototype. In order to do this a variety of water levels and extended wave conditions would be required.

A total of four tests provided data for a comparative assessment of different wave heights and periods. All tests were conducted with one water level. The purpose of this was to test the accuracy of recording damage progression rather than simulating damage recorded in prototype. The high water level would result in larger wave overtopping and run-up therefore channelling the wave above the dolos slope. The low water level would result in more wave breaking before reaching the slope therefore fewer waves plunging directly onto the dolos units. The water level at the MSL in this case was suitable as during the initial preparations wave plunging, surging and breaking occurred predominantly within the bottom and top of the dolos slope. This was suitable to initiate movement of the dolos units. The wave condition for Test 1, 2 and 3 were incrementally raised to simulate an increasing storm build up to Test 3, thereafter a drop in wave condition for Test 4 to test the reserve stability threshold after damage stabilised, and if it could be recorded using the 3D analysis method. The durations of each of the four storm events were 1500 waves, yielding a total storm duration of 6000 waves. An image of the waves breaking on the spur is shown in Figure 4.8 during Test 3.

Figure 4.8: View of breakwater stability test for damage accuracy assessment using the two methods

The images taken before and after each test were analysed using the Armour Track software described in Holtzhausen et al. (2000). The results of the analysis is graphically recorded in Appendix C and summarised in Table 4.5.

The damage formula used for the visual assessment is given by (Equation 4.9) :

$$D_T = d_H + 0.5d_{0.5H} \tag{4.9}$$

Dolos damage is the recorded damage, "H" is the height of a dolos fluke and 0.5H is half the height of a dolos fluke length. The summation of displacement is categorised into movement between 0.5H and <H and movement >H for dolos breakwater slopes. H in relation to D_n for the 25 tonne units is $H = 1.83D_n$. Table 4.4 presents the categories used for the visual recordings used in the armour track software. The tracking of displacement is depicted in Figure 4.9. The image shows coloured lines which can be used for visual identification however a line file is also produced ".lin" which is post processed using the start and end co-ordinates to determine the distance the unit is displaced. This is possible only after calibrating the image with a reference plate. Table 4.4 provides the displacement categories which are given as a distance in H (dolos height) and is converted

in terms of D_n.

Table 4.4: Visual displacement criteria used to categorise H and Dn for the armour track software

Category	mm	mm	Category	mm	mm
H	74	mm	Dn	40	mm
0.125H to 0.25 H	9	19	0Dn to 0.5Dn	0	20
0.25H to 0.5H	19	37	0.5Dn to 1Dn	20	40
0.5H to 1H	37	74	1Dn to 2Dn	40	81
>H	74		>2Dn	81	

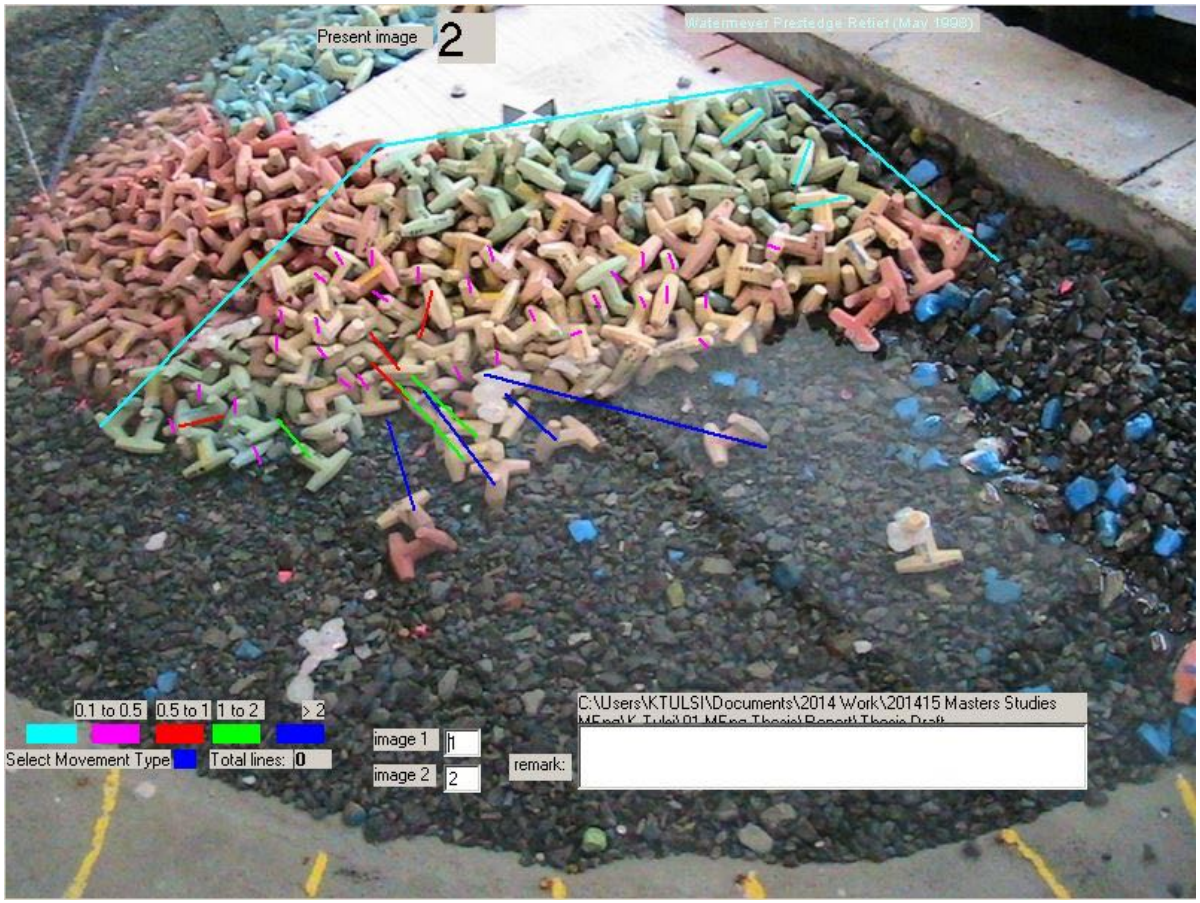

Figure 4.9: Recorded displacement for Test 3.1

After the images were taken the water level was drained to below the toe of the breakwater to scan changes before and after the tests. This allowed for a test by comparing the results obtained by the two damage assessment methods which includes the cumulative assessment.

The dolos armour unit dimensions are symmetrical and H, the height of the unit is used to classify displacement using the visual armour track method. The results of the analysis is presented in Table 4.5. Approximately 50 percent of small movements less than one dolos height, are considered lost; while displacements more than "H" or "$2D_n$" define the units that are displaced from their original position as lost.

Table 4.5: Damage table using visual analysis

Damage Table using visual analysis				
Movement criteria	**Test 1**	**Test 2**	**Test 3**	**Test 4**
0.125H to 0.25H ($0D_n$ to $0.5D_n$)	8	9	4	5
0.25H to 0.5H ($0.5D_n$ to $1D_n$)	14	10	26	17
0.5H to H ($1D_n$ to $2D_n$)	1	3	3	1
$>$ H ($> 2D_n$)	4	2	8	1
Total number of units considered as damage	4.5	3.5	9.5	1.5
Total Movement	27	24	41	24
Number of units Per Station	114	114	114	114
Percentage Damage (D%)	3.95	3.07	8.33	1.32
Cumulative Percentage Damage (CPD%)	**3.95**	**7.02**	**15.35**	**16.67**
Nod (%)	0.34	0.61	1.33	1.45

The volume of voids is calculated by the subtraction of two sequential surfaces before and after each test to determine the change in void volume. This increase in voids is taken as the cumulative damage. The result of this is summarised in Table 4.6.

An image of the scan that is analysed is presented in Figure 4.10.

Table 4.6: Damage table using 3D data eroded volume extraction

Damage Table using 3D data volume extraction				
Movement criteria	**Test 1.1**	**Test 2.1**	**Test 3.1**	**Test 4.1**
Cumulative Volume \ change to slope (m^3)	0.0001	0.0009	0.0013	0.0014
Cumulative Volume \ change to slope (m^3)	**0.0001**	**0.0009**	**0.0013**	**0.0014**
Total volume of theoretical design (m^3)	0.00754	0.007541	0.007541	0.007541
Cumulative Percentage Damage Change to slope	**1.33%**	**11.93%**	**17.24%**	**18.57%**

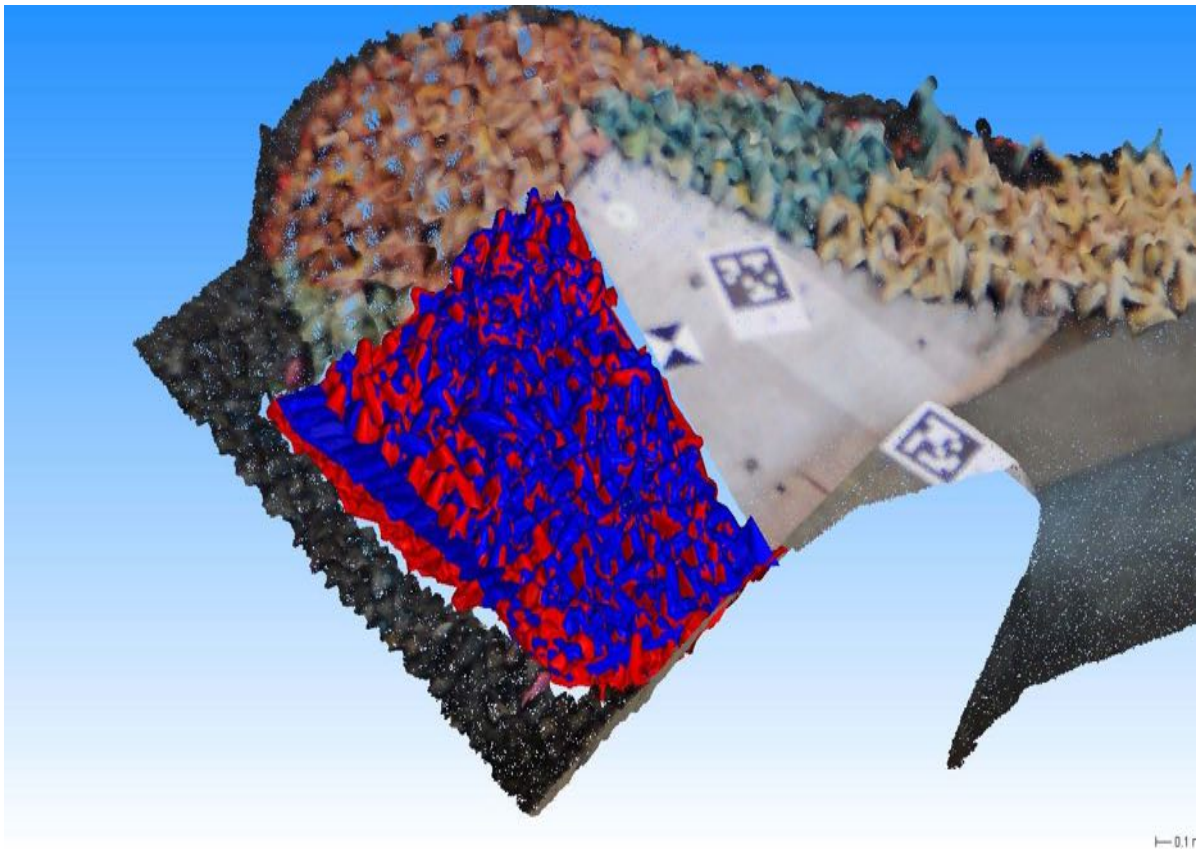

Figure 4.10: Scan of displacement for Test 3.1
The blue colour indicates no dolos movement and red the units that have been displaced.

4.12 Summary

Dolos armoured slopes are typically designed to have less than 2% displacement greater the H (height) per D_n width. However these tests are used to compare the two methods in quantifying damage in prototype. The estimate of damage error in Test 1 was 2.96 % (a factor of 3), Test 2 was 1.69 % (a factor of 2), Test 4, 1.12 % and Test 4, was 1.11 % respectively. The reason for this may be due to the nature of the measurement methods. The photographic method relies on the ability of the user to spot the movement while images flicker on the screen. The second method is dependent on the mesh that is generated and how well the control points are defined. The variation between the two analysis methods indicate approximately the error factor can be up to three times as recorded in Test 1.

Figure 4.10 shows displacement of the model units by the red colour occurring at the toe progressing up to the middle with a few red areas at the crest of the slope. The toe location shows a complete change from blue to red indicating a complete removal of dolos units. However, at the top of the slope the mix between blue and red color indicate a

subtle displacement between the two tests which is more easily seen from the laser scanned images than the photographs. The photographic flickering of images and manual marking show a similar cluster of displacement at the toe as shown in Figure 4.9 however not marked on the image as the displacement was less than the 0.5H (1Dn).

The result of the experiment comparing the two damage analysis methods are shown in Figure 4.11. The vertical axis on the graph represents cumulative percentage damage and horizontal axis, the test number. The blue line represents the visual photographic analysis method. The red line represents the volume extraction method using 3D Data.

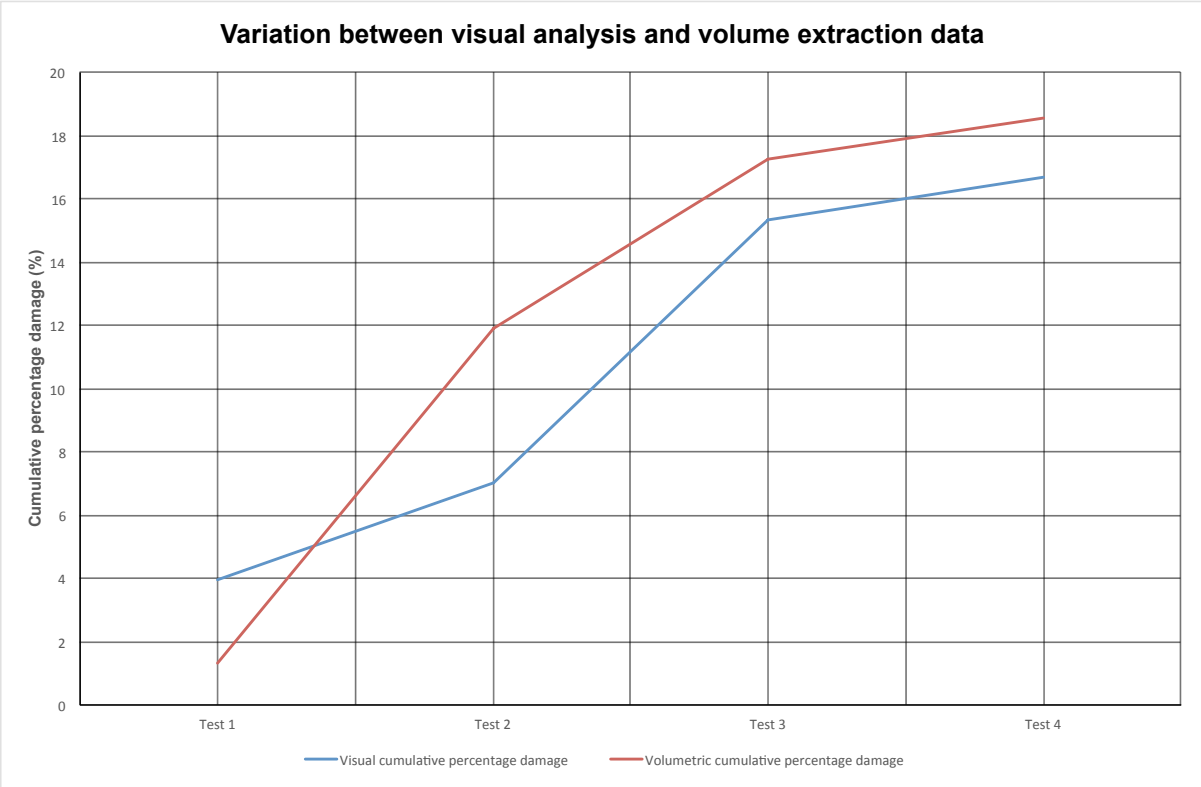

Figure 4.11: Comparison between visual analysis and 3D surface volume extraction

The results of the 3D method are a factor of 3 times that of the visual method. For new armoured breakwater designs a damage of more than 5 % would not be acceptable. For most model studies 0% to 5% is the important range to consider.

The damage is over-calculated in Test 2 and 3 indicating variability in the 3D method. This can be attributed to unit settlement and voids created by displacement which may be an overestimation of displacement. The damage recorded by the volumetric method is generally higher for this test set-up as seen in Figure 4.11 when comparing cumulative percentage damage on the slope using the two methods.

Chapter 5

Aerial photographic monitoring and three dimensional monitoring experiment

5.1 Aerial photographic data monitoring

5.1.1 Background

The Port of Cape Town is located in Table Bay, Western Cape, South Africa. The location is shown in Figure 5.1. The breakwater trunk spans 500 m south to north and is protected by 25 tonne dolosse.

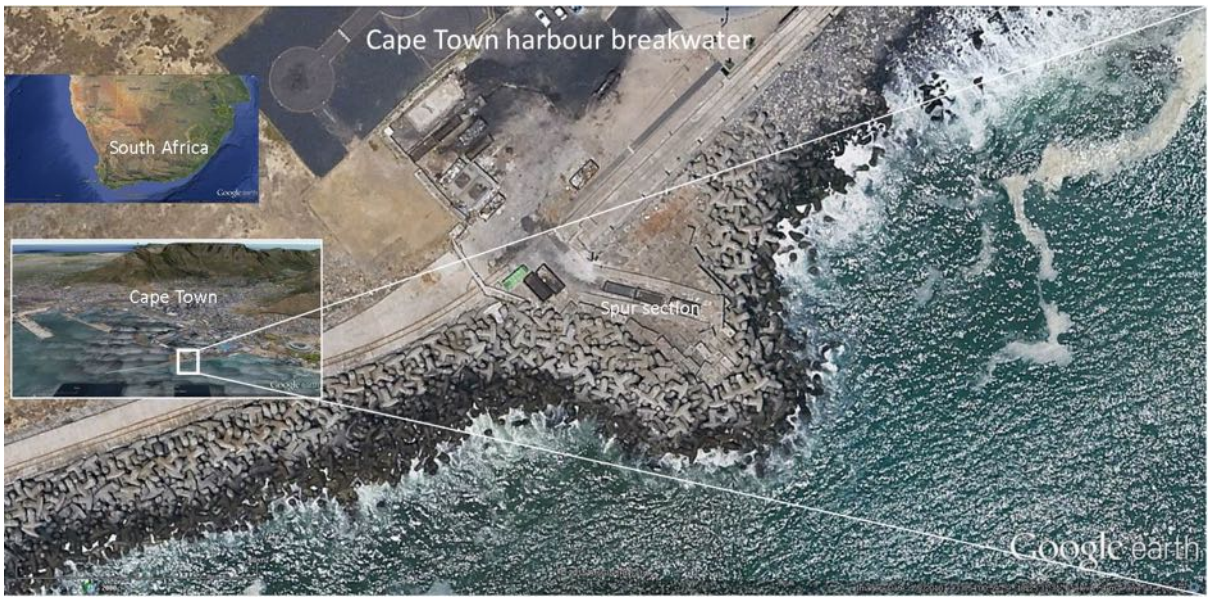

Figure 5.1: Location of the Cape Town breakwater protected with dolosse (Google Earth image 2010)

Aerial photographic monitoring of the Cape Town breakwater provided input on the condition of the roundhead (Spur) section protected with 25 tonne dolosse.

The western breakwater protecting the Port of Cape Town stretches from south to north for approximately 900 m and consists of three sections:

- the spur at the root of the breakwater in the south, protected by 25 tonne dolos units;
- the main original breakwater, 500 m long, also protected by 25 tonne dolos units; and
- the vertical breakwater stretching for a further 365 m northwards and consisting of block work and caissons.

The spur is constructed of rock and is capped by 30 tonne concrete blocks. The main breakwater consists mostly of block work capped by mass concrete. The construction of the 25 tonne dolos protection to the main breakwater was started at the end of 1986 and completed in 1988, and the spur, which was built to prevent the ingress of rubble into the dolos units of the main breakwater, was completed in December 1989, Phelp (1995). An aerial photograph showing the south spur section is presented in Figure 5.2.

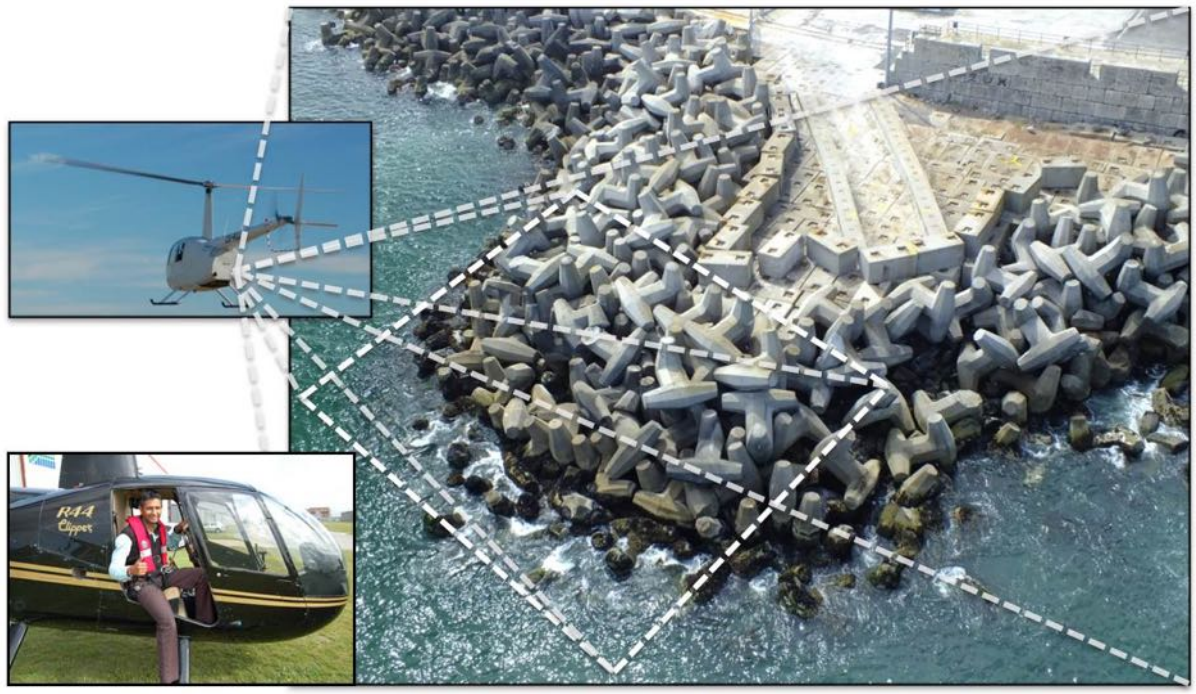

Figure 5.2: Image of helicopter over section of breakwater. The area of interest is indicated by the dashed lines

The original Chainage marking, with 0 m at the breakwater head, was used to identify the photo stations. The dolos protection starts at Chainage 365 m and the photographic monitoring covers the section of the breakwater between Chainages 365 m and 865 m including the spur. To ensure that adjacent photographs have atleast 40% overlap, the breakwater was divided into 21 equal sections of 25 m each (Figure 5.3). Because of its

shape, the spur section was divided into three stations namely, N. Spur, Mid. Spur and S. Spur. At the spur, one centre point PS, (at position Y 53 100,93 and X 52 434,80) was used to position the helicopter.

Since 1987 eight surveys have been carried out by using a boat to take photographs of the breakwater from a position seaward of each demarcated station. Vertical photographs were taken from a mobile crane, positioned on the mass-capping. Since 1990 a helicopter has been used as the platform to photograph the breakwater from a vertical position above each station.

5.1.2 Set-up of the photographic monitoring data gathering

A differential control point is set up at a coordinated benchmark at the root of the breakwater. The navigation and position fixing of the helicopter are controlled by a Trimble differential global positioning system (DGPS) using simultaneous measurements from a minimum of five satellites. The DGPS is attached to the helicopter directly above the door from which the photographs are taken. The survey navigator directs the helicopter pilot by using a laptop computer with the HydroPRO software package from Trimble. The PC, which is coupled to the DGPS for navigation data input, has the co-ordinates for the camera positions pre-programmed into the software, and displays the navigation data in animated graphical form.

At each station the helicopter is positioned perpendicularly above the breakwater slope as close as possible to the co-ordinated points, in line with the chainage mark on the breakwater. The altitude of the helicopter was kept at 65 m above mean sea level (MSL) and all photographs were taken normal to the breakwater slope. This ensured the least distortion and the largest area of the slope visible to the camera for accurate measurements (especially of horizontal movements of dolosse) on the photographs. Figure 5.2 shows a view of the helicopter cover area for a section of the breakwater indicating the area of interest. A Nikon D50 digital camera with 18 mm to 200 mm lens was used to record photographic stations along the breakwater. The lens is set to 50 mm. The photographer ensures that the photographs are taken at maximum wave draw down so that the maximum area of dolosse is exposed below the still water level. It takes approximately 30 seconds to capture a picture of a station before moving to the next station. The total flight time to carry out the Cape Town breakwater survey and back to the Cape Town airport was 60 minutes. The timing of the survey was carried out during mean low water spring tides(MLWS).

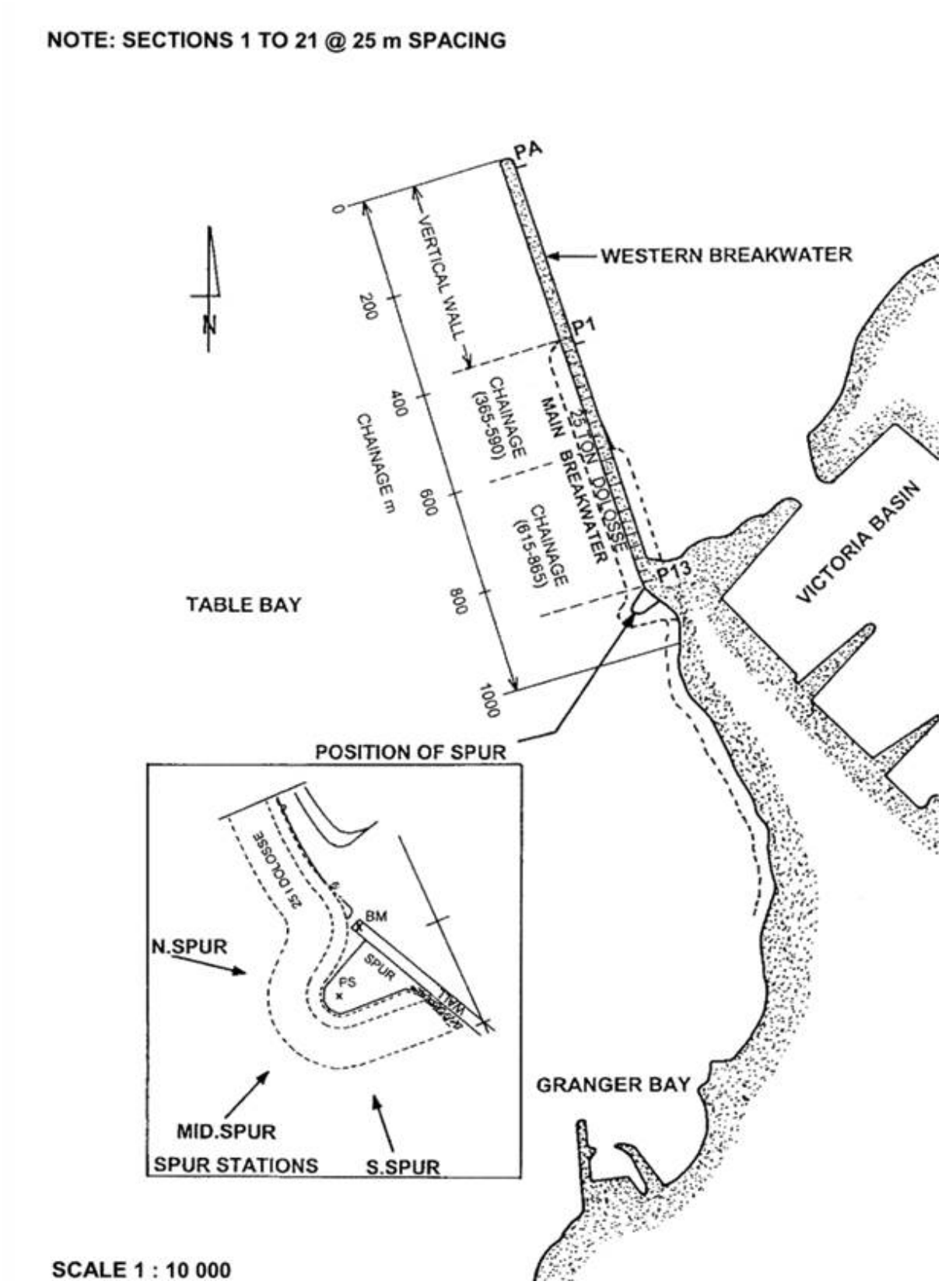

Figure 5.3: Aerial photographic stations at 25 m intervals starting at the breakwater head

The investigative team members who had to carry out the aerial and boat multibeam and laser scanning photographic monitoring are as follows:

1 Helicopter Pilot - Trevor Warner

2 Boat skipper - Hans Jelbert

3 Surveyor Navigator - Robert Vonk

4 Photographer - Kishan Tulsi

5 Data analysis - Kishan Tulsi

5.1.3 Data analysis

The damage to the breakwater is analysed per station by digitally comparing the images recorded during the two most recent photographic surveys. Those dolosse which have been displaced, broken or which had been lost from the visible slope since the previous survey, are highlighted (see Figure 5.4). The method is summarised from the method described by Phelp (1995):

- Photographs from two consecutive years are visually assessed.
- Damaged dolos units are marked with a square, triangle or circle respectively (see Figure 5.4).
- The dolos movements are further classified into A - movements less than 0,5 m, B - movements between 0,5 m and 1,5 m and C - movements greater than 1,5 m.
- These classifications are indicated on the photographs by the symbols
  □ - (displaced),
  △ - (broken) and
  ◯ - (lost) respectively.
  The letter P is used to indicate a "piece" of Dolos or rock which was previously broken.
  The letter N on the photograph indicates a new armour unit recently placed on the breakwater stations.

The new damage, previous damage and cumulative damage figures (PND, PPD and PCD respectively) are expressed as percentages where the sum of the damage per station is divided by the total number of armour units per station (N), both above and below water. The PND, PPD, PCD is used in Chapter 5, Table 5.1.

In the past in order to calculate the damage not visually detected a factor of 1.5 is applied to the PCD value resulting in the percentage adjusted cumulative damage (PACD). This factor is used in Phelp (1995) which incorporates possible damage to the below water slope and second layer of armour units not visible on the aerial photographic record. The concerns about not being able to quantify the damage underwater using the photographic method led to taking the multi-beam and LIDAR methods further to assess the breakwater slope in its entirety from crest to seabed.

The overlap between adjacent stations is indicated on the photographs by lines or points marked on those armour units, which are visible on both photographs. The number of dolos units attributed to each breakwater section, defined by the photographic survey stations, is calculated by using the "as-built" drawings of the breakwater, the historical records of the armour unit placing and the records of repair work undertaken. These numbers can vary from station to station depending on the actual prototype packing densities achieved, the irregular vertical boundaries chosen between stations (lines or points on the armour units in the photographs indicate these boundaries and overlapping of the photographs) and the amount of repair units placed.

The results of the photographic survey is presented in section 5.2. However with reference to the damage analysis method described above, the 2002 survey photograph of the south spur station is presented in Figure 5.4 indicating units that have moved, pieces that have moved, and broken units. This is recorded to determine the percentage damage to this section of the breakwater.

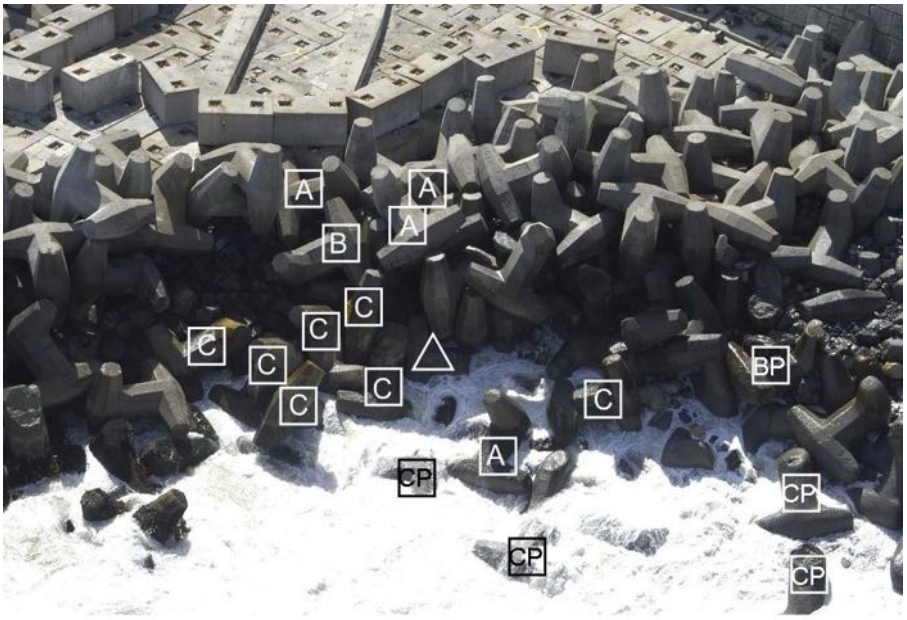

Figure 5.4: Analysed aerial photographic survey 2002 station South Spur (above)

The next section describes the set-up and analysis of the laser scanning and multi-beam data capture method.

5.2 Cape Town Breakwater aerial photographic data

A total of 24 years of photographic data was analysed along the length of the breakwater amounting to 576 photographs. The locations where the most movement occurred were at the south-spur. The 2014 Google Earth image of the spur is overlaid on the as-built plan view drawing indicating the location of the two layer dolos units on the slope by open and closed dots, shown in Figure 5.5. The bottom right has a red outline indicating where most of the damage has occurred.

The photograph in Figure 5.6 taken in 1991 identifies the start of movement of the dolos units at the toe, recorded as moving between 0 m to 0.5 m. The damage to the slope is calculated as described in section 5.1.3. The results of the photographic analysis of the south spur station is presented as the cumulative percentage damage with the maximum recorded wave height for that specific year presented in Table 5.1.

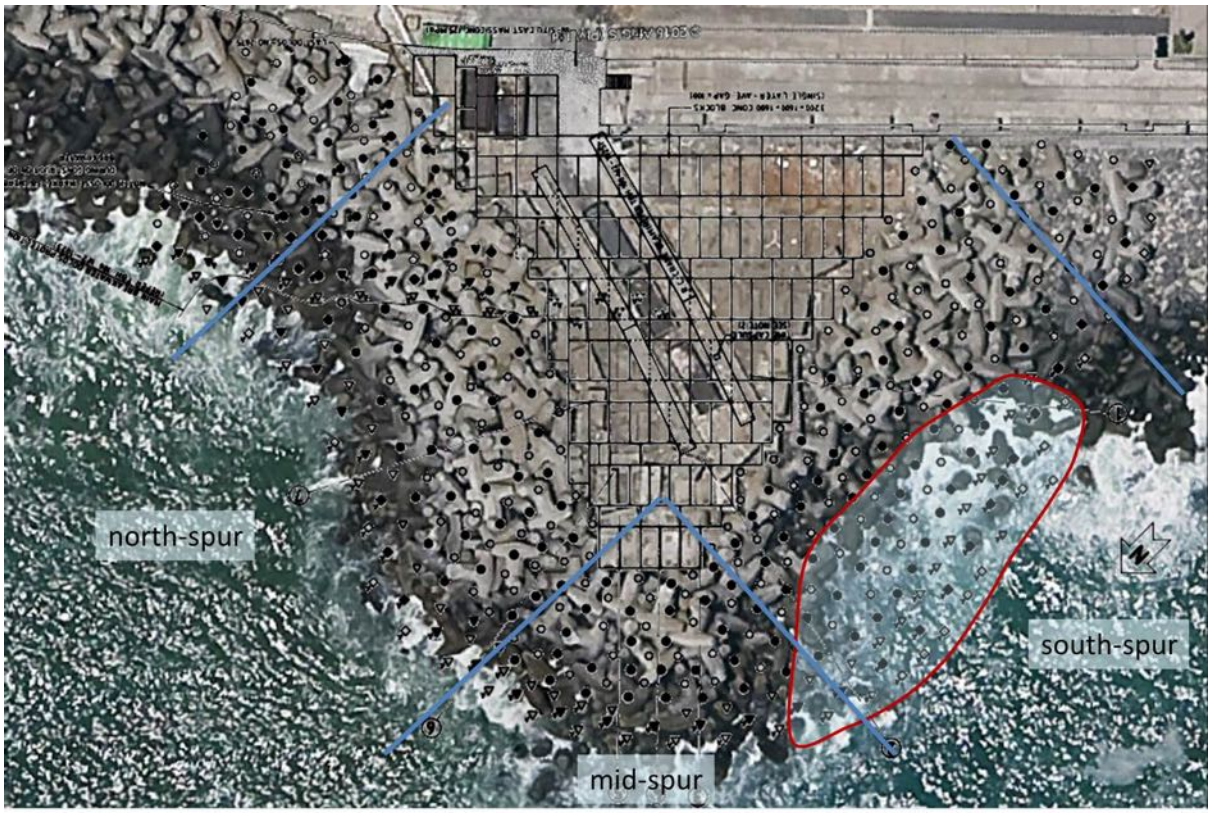

Figure 5.5: Dolos placement grid overlay on 2014 Google Earth image

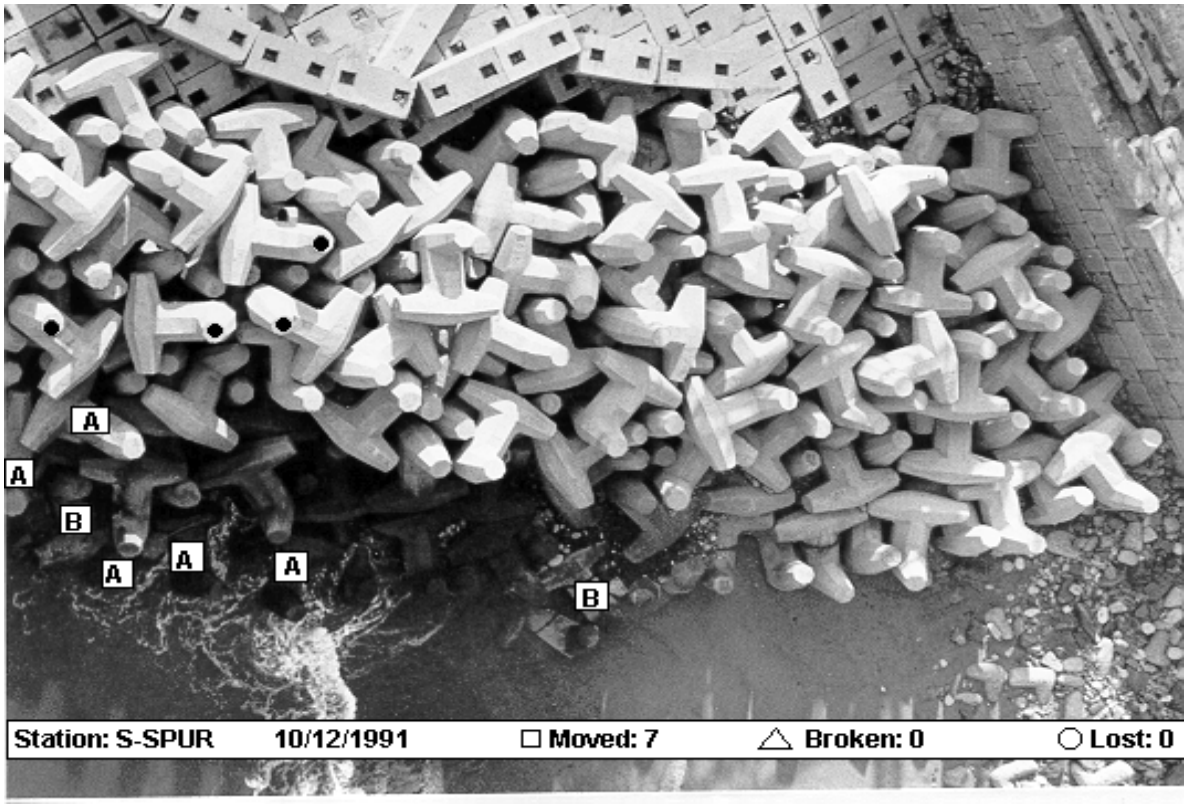

cpt10121991s-spur.bmp

Figure 5.6: Aerial photographic survey 1991 station south spur(above)

cpt09071997sts-spur.bmp

Figure 5.7: Aerial photographic survey 1997 station south spur(above)

Table 5.1: Cumulative percentage damage for the south spur station

Year	ND (No.)	CD (No.)	PCD (%)	Hmo (m)	delta (-)	Dn (-)	Ns (-)	Dolos D (%)
1991	0	0	0.0	5.60	1.4	2.18	1.83	0.0
1992	0	0	0.0	4.90	1.4	2.18	1.60	0.0
1993	0	0	0.0	4.50	1.4	2.18	1.47	0.0
1994	0	0	0.0	4.00	1.4	2.18	1.31	0.0
1995	1	1	0.9	4.10	1.4	2.18	1.34	0.9
1996	4	5	4.4	4.10	1.4	2.18	1.34	3.5
1997	27	32	28.1	6.30	1.4	2.18	2.06	23.7
1998	0	32	28.1	4.90	1.4	2.18	1.60	0.0
1999	0	32	28.1	6.62	1.4	2.18	2.17	0.0
2000	0	32	28.1	4.00	1.4	2.18	1.31	0.0
2001	17	49	43.0	4.90	1.4	2.18	1.60	14.9
2002	8	57	50.0	4.00	1.4	2.18	1.31	7.0
2003	5	62	54.4	4.00	1.4	2.18	1.31	4.4
2004	0	62	54.4	4.00	1.4	2.18	1.31	0.0
2005	0	62	54.4	4.00	1.4	2.18	1.31	0.0
2006	0	62	54.4	4.00	1.4	2.18	1.31	0.0
2007	0	62	54.4	4.00	1.4	2.18	1.31	0.0
2008	0	62	54.4	4.00	1.4	2.18	1.31	0.0
2009	6	68	59.6	4.00	1.4	2.18	1.31	5.3
2010	0	68	59.6	4.00	1.4	2.18	1.31	0.0
2011	3	71	62.3	4.00	1.4	2.18	1.31	2.6
2012	4	75	65.8	4.00	1.4	2.18	1.31	3.5
2013	0	75	65.8	4.00	1.4	2.18	1.31	0.0
2014	0	75	65.8	4.00	1.4	2.18	1.31	0.0

Damage to the breakwater section began in 1995 with the first dolos unit lost (Table 5.1). This progressed to 27% in 1997, visually represented by circles in Figure 5.7. From the wave climate information, the storm event that occurred in 1997 had a return period of 1:10 years.

The cumulative percentage damage progression as no repairs were done to the breakwater since 1997 is illustrated in Figure 5.8. Damage to the breakwater section progressed to 28%, 50% and 65.8% respectively in 1997, 2002, and 2012. This can be attributed to the toe dolos units being in the active zone. Consequently, the breakage of the fluke portion of the dolos is all that is required to destabilise the slope as can be seen from Figure 5.7. For the more recent years after 2002 damage was primarily as a result of the dolos on the upper slope sliding to fill the voids as can be seen in Appendix A . Figure 5.10 indicating mostly whole dolos unit movement.

This photographic record serves as reference for the comparison of the LIDAR and sonar technology to monitor breakwater stations. Figure 5.5 shows a top view overlay of the as-built positions of the dolos units indicated by the red outline. This clearly shows by counting the dots representing missing dolos units, 65% of the slope is recorded as lost. Therefore indicating the similar damage progression of 65.8% is agreeable in the 2D photographic record.

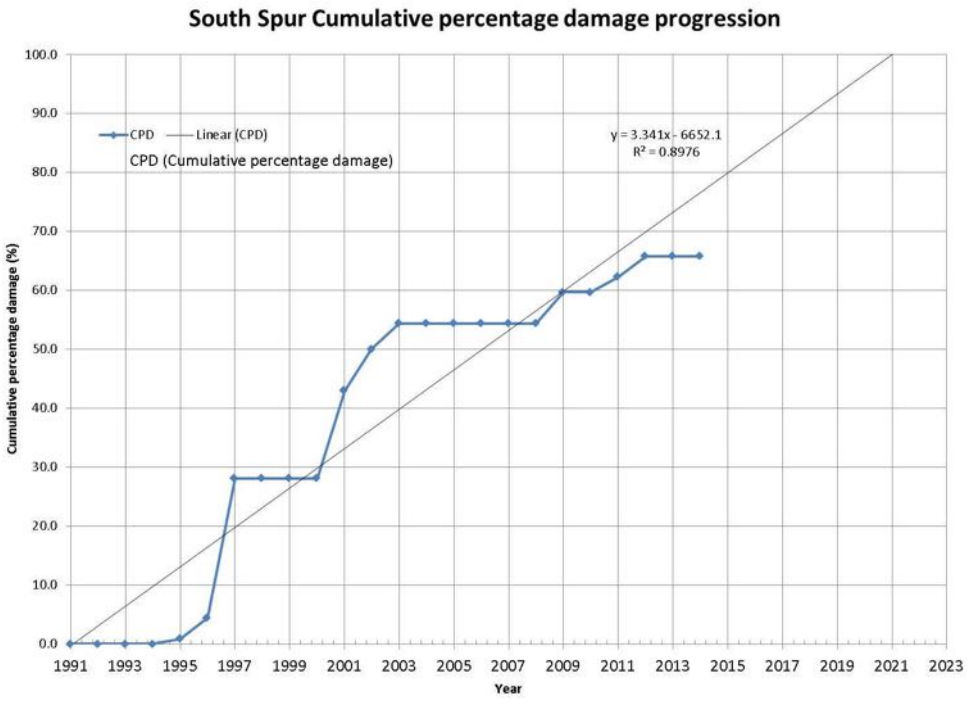

Figure 5.8: South spur damage progression according to photographic method

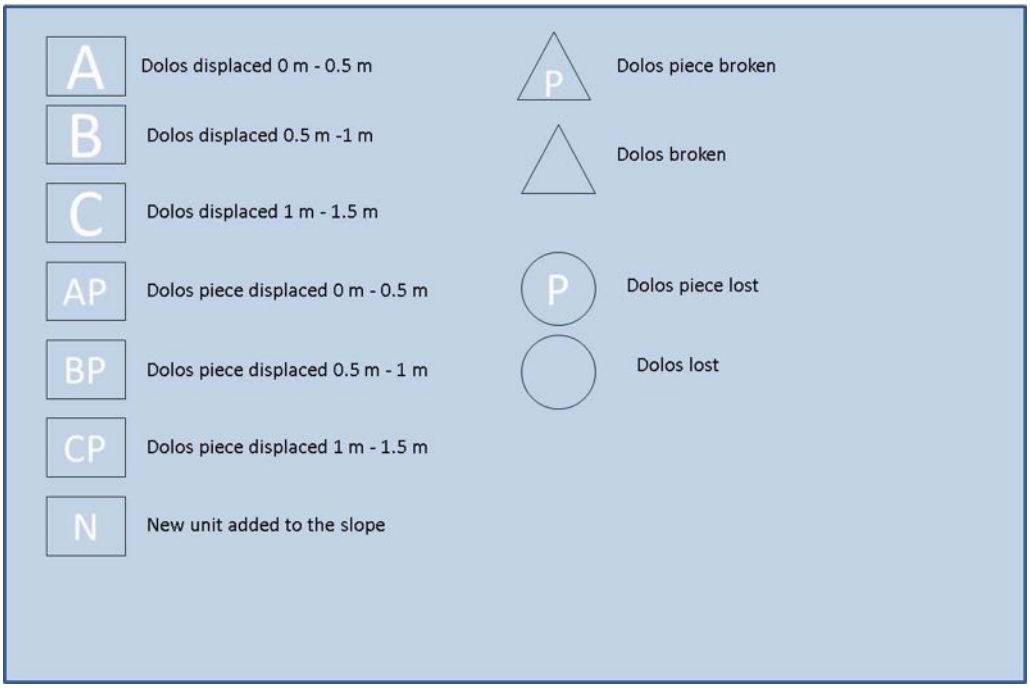

Figure 5.9: Legend used in identifying damage for Figure 5.10 and Figure 5.11

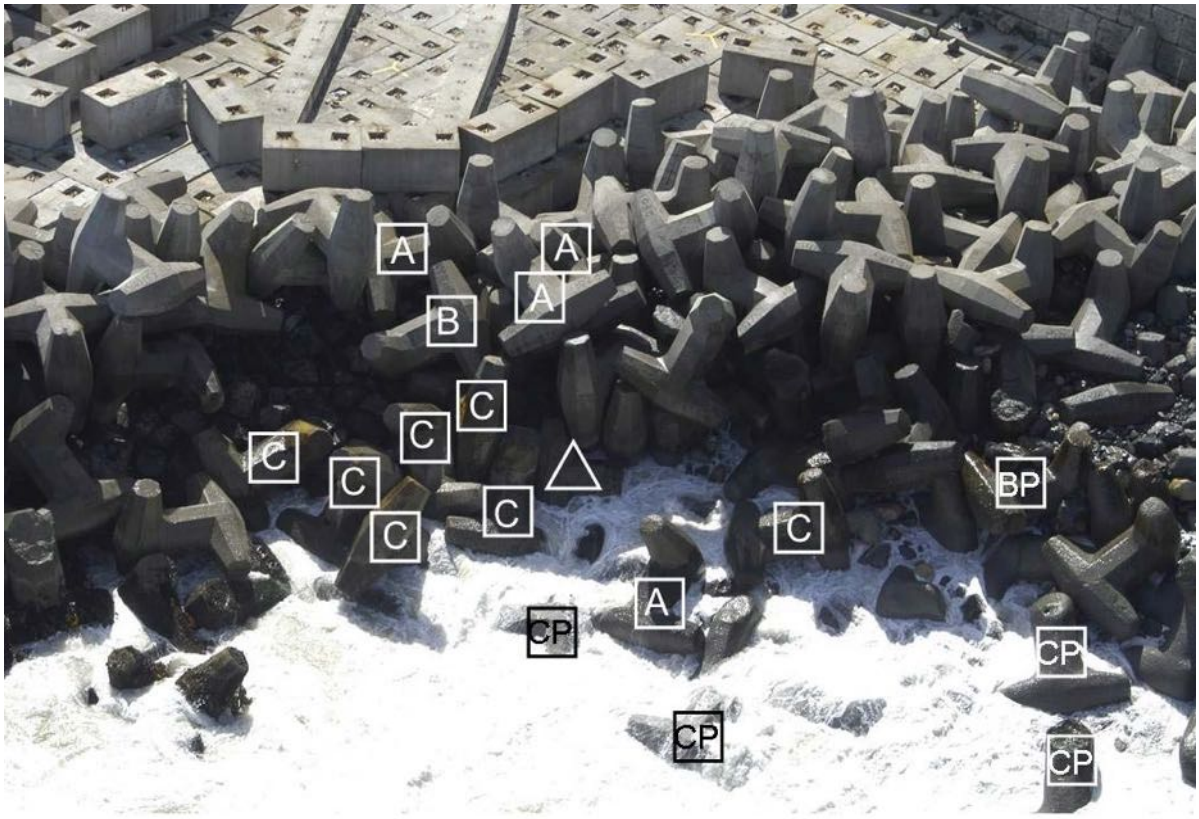

Figure 5.10: 2002 Aerial photographic survey station south spur

Figure 5.11: 2012 Aerial photographic survey station south spur

Table 5.2: South spur damage table according to photographic analysis method

Station		No.	N-SPUR	MID-SPUR	S-SPUR	Total
Displaced Dolosse	0 - 0.5m	(A)	0	0	0	0
	0.5 - 1.5m	(B)	0	0	1P	1P
	1.5m	(C)	0	0	0	0
Damaged Dolosse	Total	(D)	0	0	0	0
	Broken	(E)	0	0	0	0
	Lost	(F)	0	0	0	0
	New Damage	**ND (C+E+F)**	**0**	**0**	**0**	**0**
December 2012	Previous Damage	PD	11	26	75	112
November 2014	Cumulative Damage	CD (ND+PD)	11	26	75	112
	No of Dolosse	N	202	115	114	431
Percentage Damage	New	PND (ND/N*100)	0.00	0.00	0.00	0.00
	Previous	PPD (PD/N*100)	5.45	22.61	65.79	25.99
	Cumulative	PCD (PND + PPD)	5.45	22.61	65.79	25.99
	Adjusted Cumulative	PACD (PCD*1.5)	8.17	33.91	98.68	38.98
N_{od}		(9.9CD/N)	0.54	2.24	6.51	3.10
Cumulative	%	(CD/N*100)	5.45	22.61	65.79	25.99
Adjusted	Damage	(N_{od}*1.5)	**0.81**	**3.36**	**9.77**	**4.65**
		Intermediate damage - Needs Repair			$0.5 \leq$ Nod ≤ 1.5	
		Failure - Core Exposed			Nod ≥ 2	

The method described by Phelp (1995) was applied to the spur section of the breakwater to quantify the damage. With reference to Table 5.2, by differentiating between three categories of displacement (A,B and C) the method allows for the quantification of the initial shake-down displacement of whole units and pieces of units. The damage progression is based on the contribution of all the units interlocked together making up 100% of the main armour cover. This holds well for all visible parts of the analysis to determine the percentage cumulative damage (PCD). The percentage adjusted cumulative damage (PACD) can be considered extreme indicating almost 1.5 times more damage from the underwater portion of the section compared to the 3D method. This may be applicable only to sections were the slope extends further underwater. The damage parameter N_{od} calculated using the method described by USACE (2006) classifies the damage as failure once $N_{od} \geq 2$. Therefore failure would have occurred in 1997 which is also an extreme quantification.

Figure 5.12 is computed from prototype wave measurements against relative damage. This is depicted as a relationship of the stability number N_s and damage percentage $D\%$. It can be seen that with higher stability numbers, the measured damage increases. Coincidently the dolos which is a good interlocking unit should have a high stability number with a low damage percentage. Since the Dolos damage started at the toe (seabed settlement), unit to unit interlocking deteriorated. As a result, larger instabilities were introduced to these units leading to a higher damage percentage ie $D = 24\%$ with a corresponding $N_s = 2.06$ for this particular station.

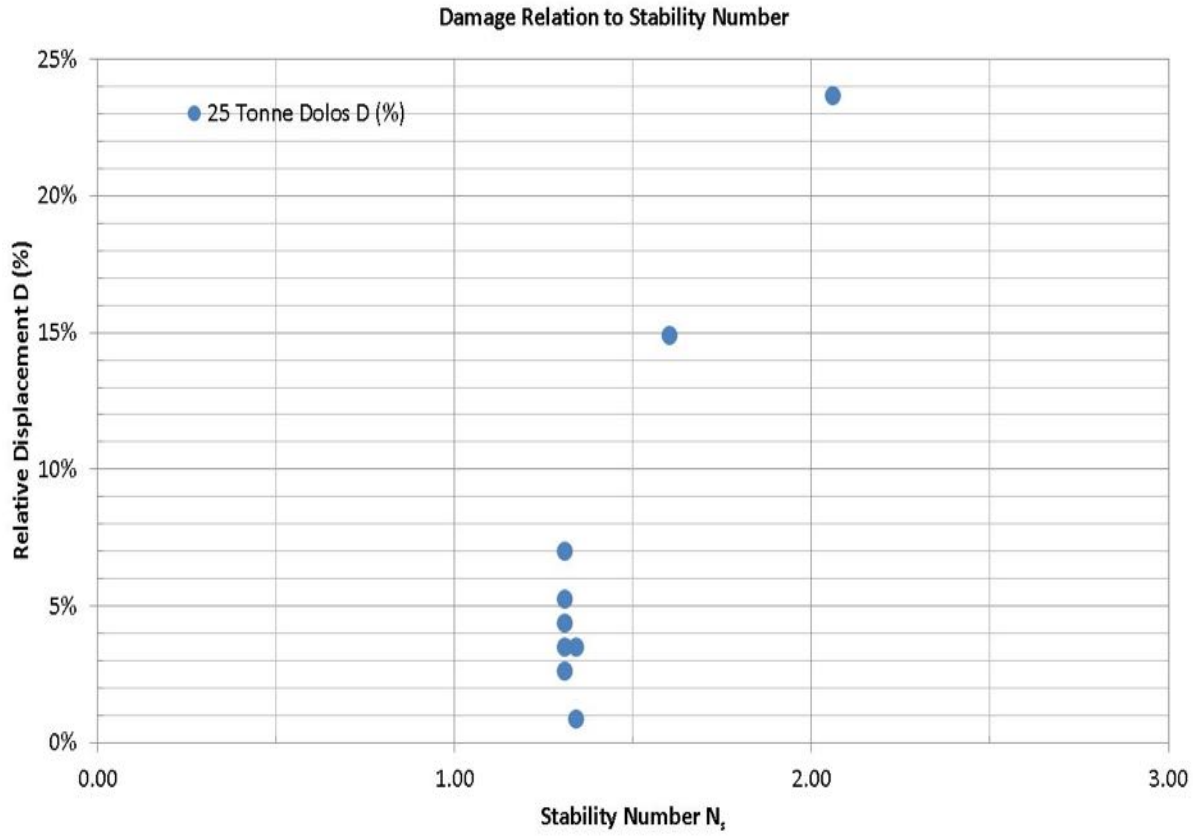

Figure 5.12: South spur damage relative displacement

5.3 Cape Town spur laser scanning and multi-beam sonar

This section presents the set-up of the data collection using the laser scanner and multi-beam sonar equipment.

The hydrographic survey (multi-beam and LIDAR Laser scan) was conducted from a 6 m long ski-boat which was very manoeuvrable in the surf-zone and close to the breakwater. The survey was done during calm sea (less than 1 m swell) conditions. The survey was conducted at low and high tide on the same day. The operating water depth was between 5 m and 20 m. During low tide, the laser scanning was carried out and during high tide the multi-beam soundings were done. The purpose of this is to ensure there is a seamless transition between the above water and below water data collection. This is a critical step in the data capture and should be ensured or the survey should be repeated if overlap is not achieved. Ideally both sets of equipment should be capturing data simultaneously throughout the day however this would require a duplication of the inertial moment unit.

The data from the multi-beam echo sounder provided the bathymetric information of the structure below the water surface. The laser scanner provided the topographic levels of

the breakwater above the water line. Figure 5.13 below shows how the multi-beam and laser scanner cover the survey area from the survey boat. A list of equipment used to conduct the survey is provided below.

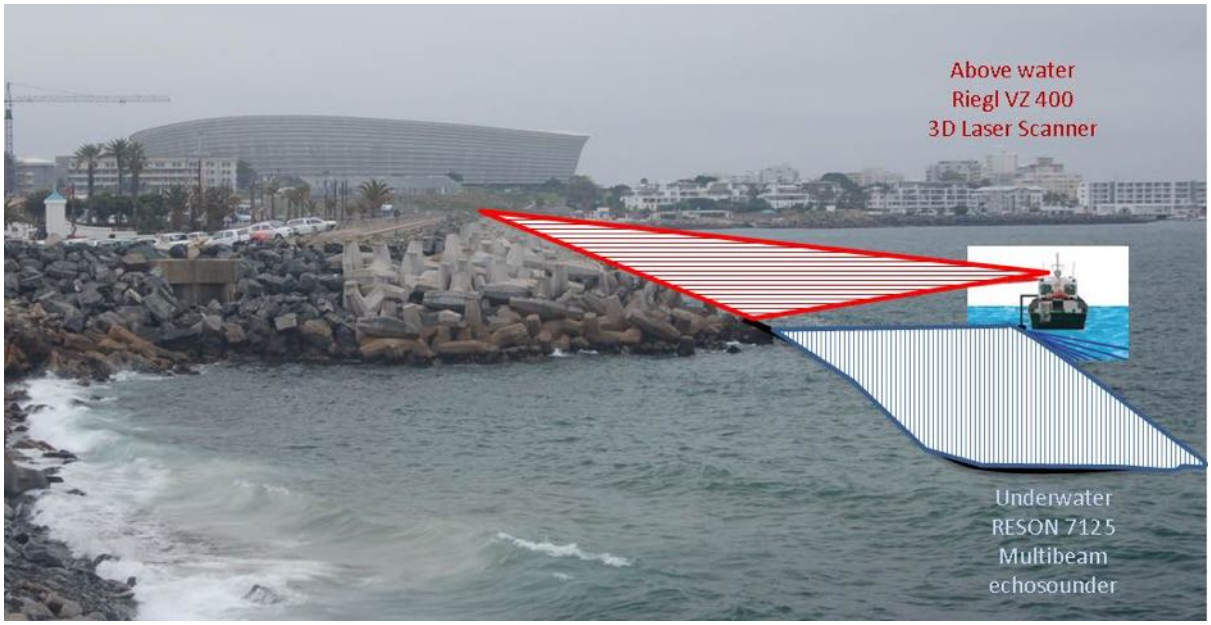

Figure 5.13: Multibeam and mobile laser scanner capture area

The equipment used for the survey:
Hardware:

- Riegl VZ400 scanner for ubove water 3D data capture
- Reson Seabat 7125 multi-beam echosounder - for underwater capturing of 3D data
- Applanix POS MV 320 position, heading and motion sensor for attitude and heading correction
- Reson SVP-70 sound velocity probe for underwater sound velocity correction
- Leica GX1230 GNSS RTK DGPS positioning system for water to land positioning

Software:

- QPS QINSy V.8.1 - for data capture
- QPS Qloud V2.2 - for data capture
- Autodesk Civil 3D 2015 - for data processing
- 3D Reshaper 2015 - for data processing
- Cloud Compare - for data processing

5.3.1 Set-up to gather hydrographic and topographic data

Hydrographic survey

For the survey, the Reson SeaBat 7125 multi-beam echo sounder was attached to the side of the boat and used to scan the underwater area of the breakwater. This system has an operating frequency of 400 kHz. The scanner is tilted at 45 deg to the vertical to capture the breakwater slope detail. It has a wide sector, wide-band, multi-beam sonar utilising 512 dynamically-focused receive beams at 0.5 degree across-track. The system measures a 128 degree swath coverage, at a depth resolution of 6 mm at 50 times per second. The manufacturers resolution specifications are presented in Table 5.3.

Table 5.3: Manufacturers Specifications for the Reson SeaBat 7125 multi-beam echo sounder

Parameters	SeaBat 7125
Sonar operating frequency	400kHz
Across-track beam width (nominal values)	Transmit: 145 Receive: 0.54 0.03 (center)
Along-track beam width (nominal values18)	Transmit: 1.1 0.2 Receive: 31 3.5
Across-track beams	240, 512, or 511
Swath coverage	140 (165)
Depth, typical19	0.5-150 meters
Depth, max.20	175 meters
Ping rate (range dependent)	Up to 50 pings/s
Pulse length	33-300s (CW)
Depth resolution	6mm

The instrument is calibrated with a Valeport underwater sound velocity meter, before and after each survey. This is to ensure proper beam steering to the measured surface in the water medium. The sound velocity probe is used to report the value to the transceiver. In the 0 to 50 m water depth in which the survey was conducted in the manufacturers accuracy rating is ± 0.05 m/s. Table 5.4 provides further specification information on the sound velocity meter.

Table 5.4: Manufacturers specification for the Valeport Sound velocity probe (SVP 70)

Specification	**Value**
Type	SVP 70
Sound velocity	Range: 1350-1800m/s Resolution: 0.01m/s Accuracy: 0.05m/s (0-50m) Accuracy: 0.25m/s (0-6000m)
Sampling rate	20Hz and lower, programmable
Depth	6000m
Baud rate	2400-115200
Supply	9-55VDC
Power	2W
Housing	Titanium

Navigational positioning

A Leica GX1230 GNSS RTK DGPS system was used for position fixing, and tidal and heave reduction. The system utilises its horizontal and vertical accuracy of 2 and 3 centimetres at 20 times per second and 0.01 second latency to remove the heave and tidal influences from the depth data in real time.

Topographic survey

The laser scanner LIDAR used for the survey was a Reigl VZ-400 fitted with a Nikon D700 digital camera. The laser scanner is mounted on the vessel as shown in Figure 5.14. The basic principle of topographic LIDAR operation involves transmitting light in the form of a laser onto a mirror that is rotated at a high rate of speed. The rotating mirror projects the laser as a series of pulses onto the surface. Light is reflected back to the instrument, and with known vessel position, two-way time travel is used to ultimately compute the positional measurement of the reflecting objects. The line orientation for capturing data for the multi-beam bathymetric and laser scanner topographic survey is carried out parallel to the breakwater. The vessel has a heading along the breakwater at a distance between 50 m and 100 m away from the breakwater to stay within the accuracy band of the VZ400. The accuracy of this particular scanner decreases over distance and can be noted as 0.2 mm/m, i.e (20 mm over 100 m).

Navigation and logging of data is then performed on a personal computer using QPS Qincy software which logged data continuously and produced the fix (position) information at 10 m intervals. The results are analyzed using the QPS software and corrected for tide and heave variations using the Applanix POS MV 320 inertial measurement unit (IMU). The IMU provides attitude, heading, heave, position and velocity data which is geo-referenced using the DGPS equipment on land. The IMU compensates for the the six degrees of freedom of the vessel to assist in correcting and align the data as it is captured. The manufactures specifications of the equipment is presented in Table 5.5.

Table 5.5: Manufactures specifications of the Applanix POS MV 320 inertial mesurement unit

POS MV 320	DGPS	IA RTK
Position	0.5 - 2 m^2	Horizontal: ± (8 mm) Vertical: ± (15 mm)
Roll and Pitch	0.02deg	0.01deg
Heading	0.01deg (4 m baseline) 0.02deg (2 m baseline)	0.01deg (4 m baseline) 0.02deg (2 m baseline)
Heave TrueHeave	5 cm or 5% 2 cm or 2%	5 cm or 5% 2 cm or 2%

The data are then exported to a digital terrain model where a topo-bathymetric chart is produced in Civil 3D AutoCad 2015 format as well as in ASCII xyz format.

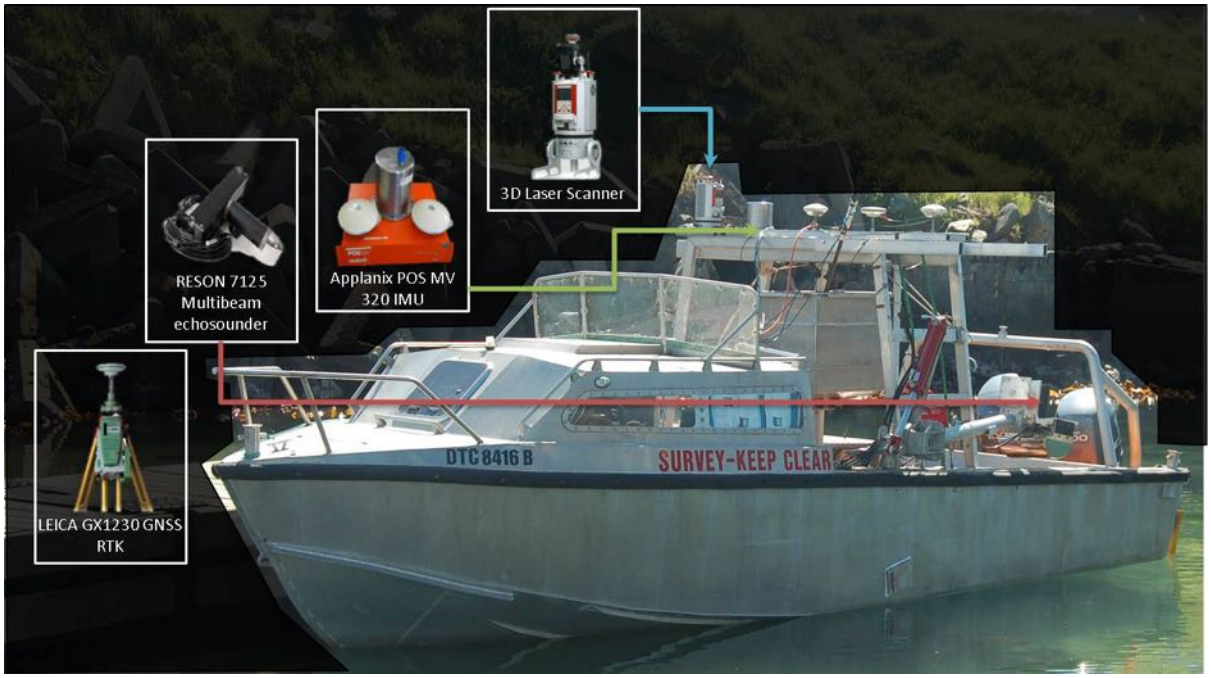

Figure 5.14: Multibeam and mobile laser scanner on boat set-up for the breakwater survey

5.4 Multi-beam and LIDAR prototype survey data

The scanned spur section is presented in ASCI format as collected from the survey and overlaid on a three dimensional representation of the as-built 2D cross-sections from 1989 which is presented in Figure 5.15. The image shows an aerial view of the the south west view (south-spur). The pink colour code is merely for visualisation of the x,y,z return from the laser scanner which colours the concrete wall and dolos units. The data are imported into the 3D reshaper CAD software package for rendering points to surfaces using triangulations. It is also used to extract cross-sections for interpretation of the depth of cover between the design and present profiles. Once the surface triangulations have been completed the volumetric surface-to-surface difference calculations are determined.

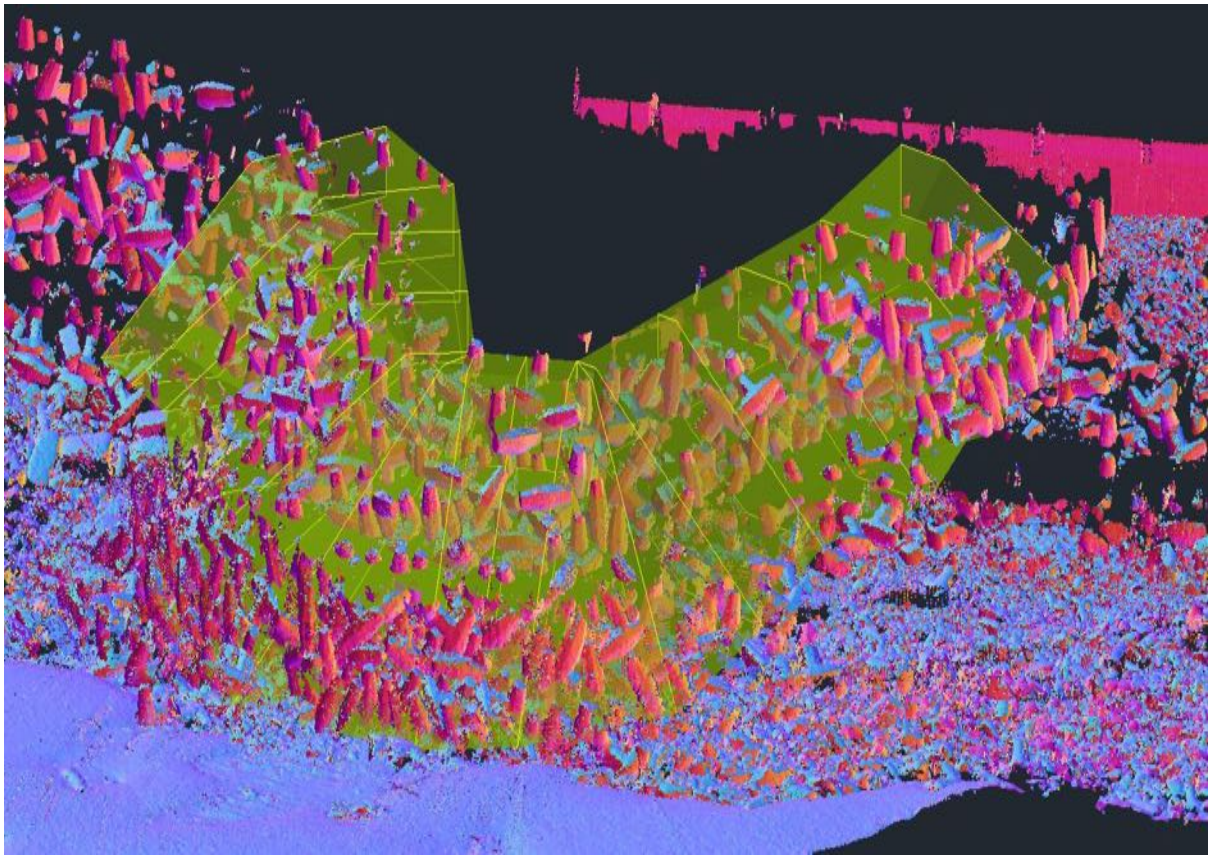

Figure 5.15: Multibeam and laser scanner south west aerial view

The as-built design is converted from 2D cross-sections into 3D trapezoidal shapes by converting 2D view to 3D isometric views in Autodesk Civil 3D. The 2D view provides the area of a cross-section and 3D view the volume of the as-built station by joining two sections by the distance between. This is exported from CAD as a surface and overlaid to match the dolos point data in 3D Reshaper. The point data are geo-referenced to the control points on the wall. The result of the importation is shown in Figure 5.16.

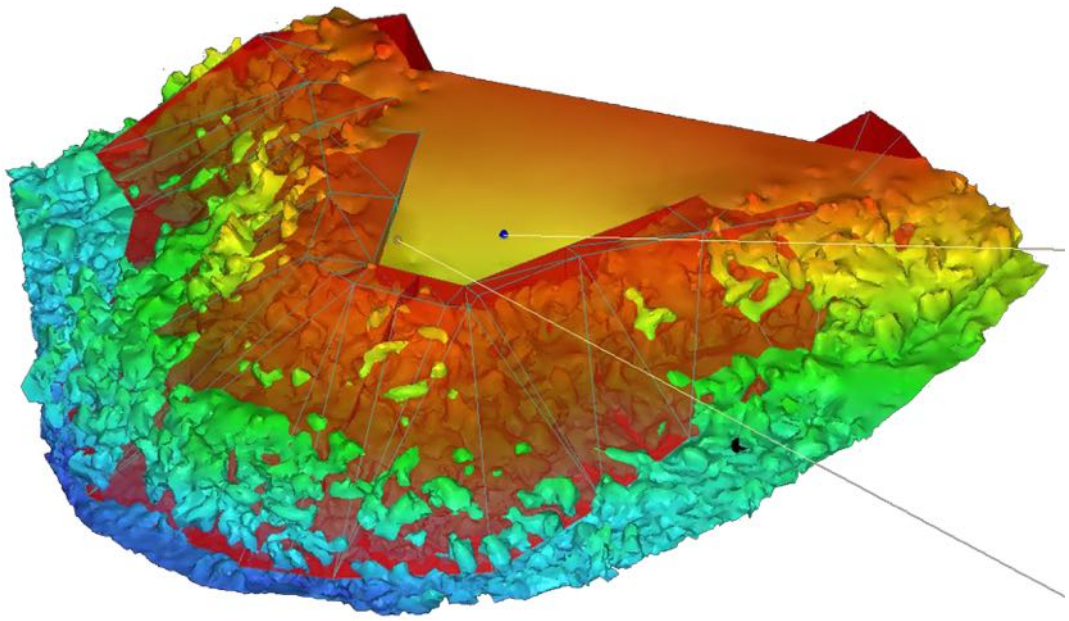

Figure 5.16: Multibeam and mobile laser scan processed with as-built cross-section overlay The red colour indicates the theoretical 3D surface cover surface and the rainbow of orange, yellow, green and blue the surface created from the three dimensional point data.

A cross-section is taken through the station to calculate depth of cover. The cross-sections are taken at intervals of D_n and presented in Appendix B. A typical cross-section extracted from CAD with the 3D data is presented in Figure 5.17. The cross-section shows the design profile (blue line) and a dolos profile (red line) above water and below the water surface to the toe. It should be noted that the cross-section line are very thin lines extracting data points of the surface and may appear irregular as explained earlier in Section 3. It should be viewed in correlation with the 3D overlay as shown in Section 3.2.3. The cross-section section is done after the 3D data points are converted to a surface. The area between the design profile (blue line) to dolos profile (red line) can be extracted to provide the area of erosion. This is useful in identifying whether the underlayer or core is near to exposure.

The accuracy of the mesh resolution was dependent on the point data captured. The scanner was set to capture data continuously through a 100 degree view with an interval spacing of 10 mm at a distance of 100 m. The data captured, therefore have a maximum resolution of 10 mm or better depending on the time spent at a specific point. The data resolution was further improved by applying a triangulation to the data points of 5 mm wherever possible. The mesh of the dolos surface created is shown in Figure 5.18.

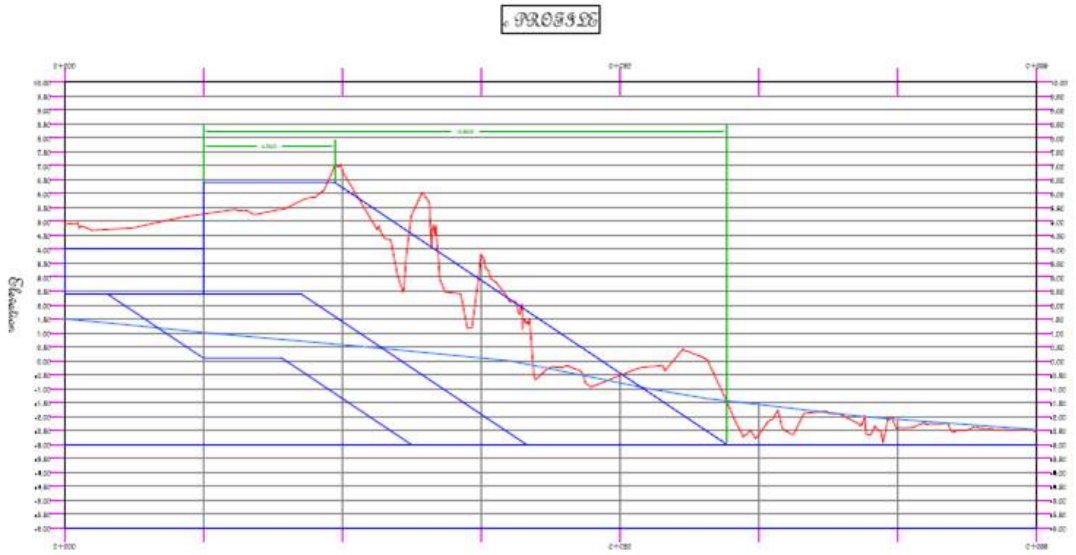

Figure 5.17: Cross-section view through station providing depth of cover Design profile in blue and dolos profile in red

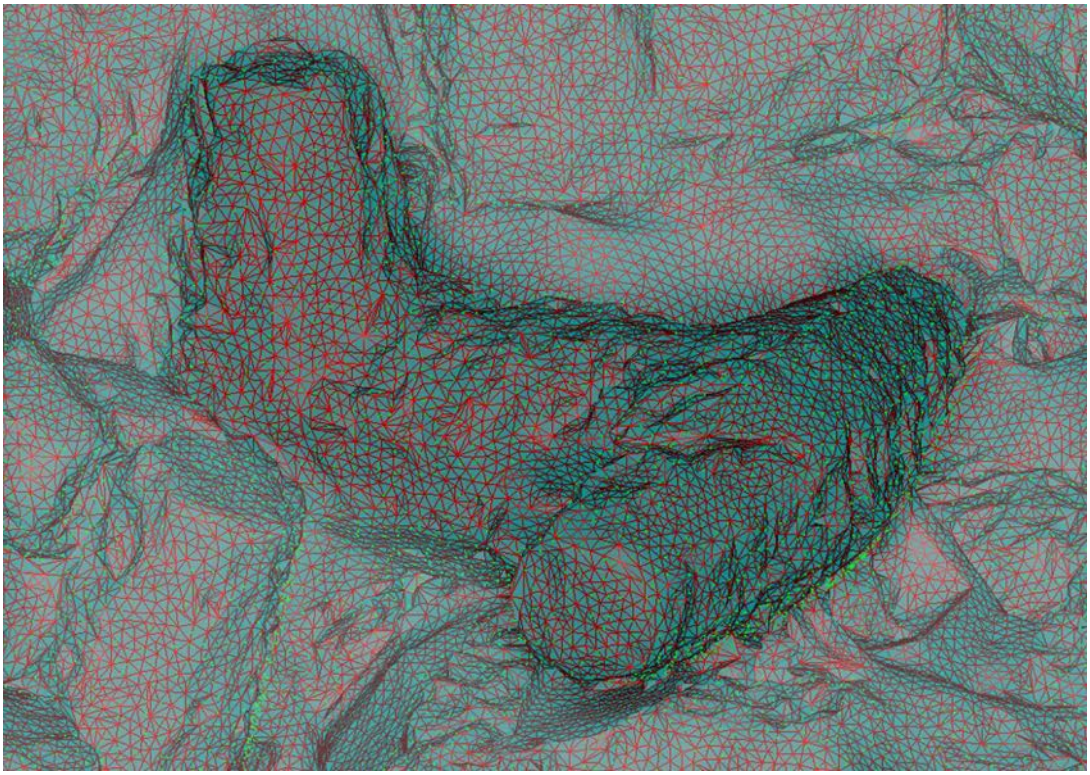

Figure 5.18: Prototype scan capture of 10 mm by 10 mm and mesh resolution

After the mesh has been generated and resolution assessed to be acceptable showing good definition of the dolos unit, the view in "3D reshaper" is changed to smooth+wire to show the result of the meshing in Figure 5.19. Measurements of the dolos can now be done. The accuracy of the measurement is ± 20 mm in prototype across the length of a 3.9

m dolos fluke. This is calculated from the mean absolute error, measuring the height of dolos flukes in prototype and in the computer model.

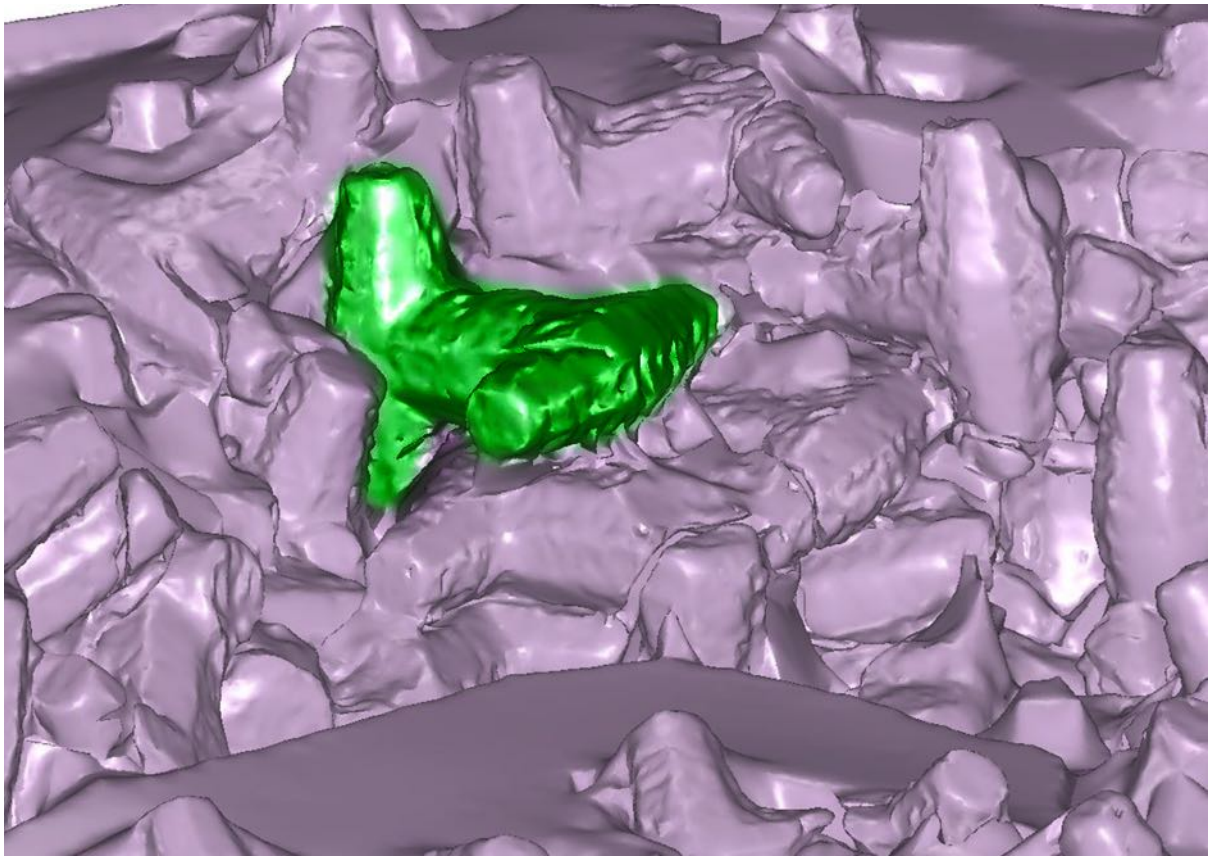

Figure 5.19: Smooth+wire mesh of dolos surface

For the comparison evaluating the performance of the visual damage analysis method against the three dimensional eroded volume method, given by Equation 3.2. Table 5.6 presents the results of the analysed station. The volume of station cover is the as-built volume of the cross-section determined using CAD. This is depicted in 3D by Figure 5.20. The volume of the erosion is computed by extracting the void between the two surfaces. This is presented in Table 5.6 and depicted in Figure 5.20. The result is expressed in Equation 5.1;

$$S_{3D}D\% = \frac{781.250m^3}{1094.262m^3}\ x\ 100 = 71.4\% \tag{5.1}$$

Table 5.6: Station volume calculation

Mass of unit	25000	kg
Density of unit	2400	kg/m^3
Volume of unit	10.41667	m^3
Dn	2.183951	m
11Dn (station width)	24.02346	m
Volume of station cover	1572.216	m^3
$V_{station}$ packing density (approx. 30.4 units per 100 m)	0.696	
V_e = volume extraction from 3D data		
$V_{station}$ = Average area of two cross-sections x 11Dn x packing density	1094.262	m^3

Table 5.7: Scanned percentage eroded volume

Year	Ve	V_{eroded}	$S_{3D}D(\%)$
1991	0.00	0.00	0.0
2014	0.00	781.25	71.4

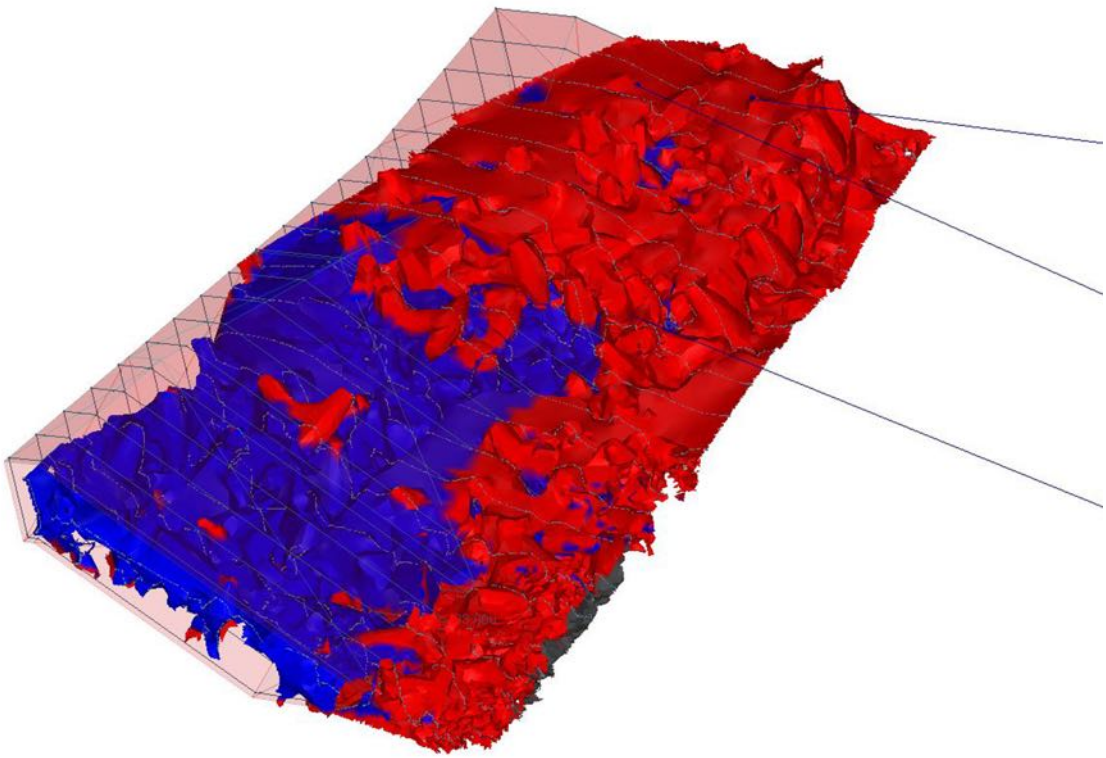

Figure 5.20: As-built station design (transparent pink) and scanned station surface (red and blue) in 3D

The result of the photographic analysis indicates the present damage to the breakwater is 65.8%. The three dimensional eroded volume analysis indicates the damage to be 71.4%. The difference between the results of two calculation methods is 5.6%. The data are

plotted in Figure 5.21. The figure shows the cumulative percentage damage over time. This figure can be updated in future to track the performance of the two methods.

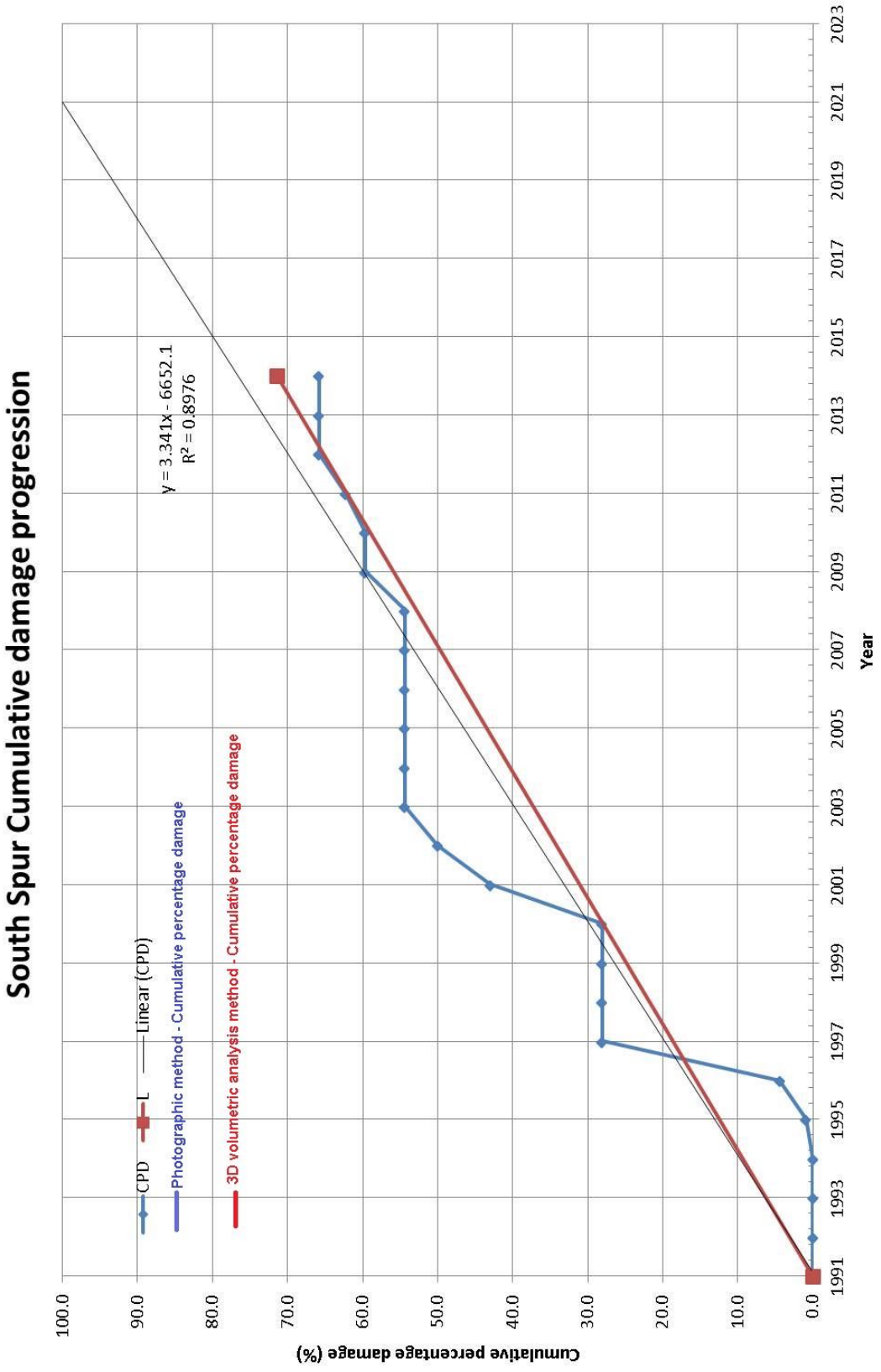

Figure 5.21: South spur damage progression determined according to the eroded volume method

Chapter 6

Discussion of results

6.1 General

The results obtained for each of the experiments from the scaled model accuracy check to the surveys in prototype using the photographic method compared to LIDAR and multi-beam data are described in this chapter.

The scaled physical model results are presented by comparing photographic movement recorded against LIDAR scanned movement with reference to rotations, minor displacements, settlement and large voids compared with the volume of material removed within a section of the breakwater armoured with dolos units. This comparison is carried out to determine the accuracy and suitability of using 3D data for damage analysis instead of the currently employed visual techniques.

Section 3 presents the results from the *experimental verification* obtained from photographic displacements recorded using the armour track method in comparison with the LIDAR (*3D Method*) volumetric difference of material lost of the slope in the physical model. This is done to verify that the three dimensional data captured can be interpreted similar to the photographic method which is presently the norm in measuring armour movement. This is followed by a *3D physical model of the Cape Town Spur Breakwater* experiment in Section 4.11 to assess damage progression measurement by wave action.

Section 5.2 focuses on the *aerial photographic* investigation hindcast data as well as the most recent survey conducted on the south spur damage in prototype. Historical data is collated to produce a cumulative damage table.

Section 5.4 presents the results from the *multi-beam and LIDAR survey* of the prototype section of the south spur and calculates the damage as a percentage of the slope that is lost.

6.2 Accuracy measurements

During the model and prototype investigation it was possible to measure the dolos units physically, including capture data using the 3D scanner for minor, moderate and large movements. The accuracy check was initially done by measuring the height and waist of the dolos units and the repeatability of scan measurements. Thereafter, this was expanded into measurements of voids as a result of rotations and major displacements.

The average dolos height measurement was 3900 mm (prototype) and 73.9 mm (model) while the waist measurement was 1300 mm (prototype) and 24.46 mm (model). The mean absolute error between the five units was ± 0.22 mm for the height and ± 0.12 mm for their waist. The units were then scanned and measured using the CAD software package. The results from the scanned data and actual measurements indicate minor deviations when measurements are made to the nearest whole number (Table 3.12). The average model dolos height was measured at 74.00 mm and waist at 24.60 mm. The mean absolute error was zero for the height measurement and ± 0.48 mm for the waist measurement when comparing the physical error in Table 3.11 and scanned error in Table 3.12

The ability to track the intricate shape of the dolos unit was tested and cross-sections were taken at intervals of 1Dn, 0.5 Dn, 0.25 Dn, 0.125 Dn, 0.0625 Dn and 0.03125 Dn. The most similar results were found between 0.5 Dn, 0.25 Dn. However, for this application the optimal spacing was 0.25 Dn. Software and computers in the future will be able to handle finer grid spacing. However this was not possible with the presently available equipment.

Tests were carried out to quantify the expected damage percentage that can be associated with displacement, rotation and settlement using the eroded volume method. This was compared with the visual method. Damage classification was according to Van der Meer (1988) for the damage parameter $D\%$ Equation 2.9. Damage percentages for both methods are plotted in Figure 3.11. The methods show that there is a slight variation between the two methods, however the results interweave one another. Both methods are able to track difference to the slope if there is settlement, minor displacements and rotations and provide a damage percentage in relation to the first scan or first image. The data processing can be further refined to improve edge detection on armour units to improve intricate surfaces for the eroded volume calculations by improving on the captured data from a bird eye view or movable platform.

In the 3D physical model section 4.11 the scanned section as shown in Figure 6.1 is zoomed in to visualise the mesh shape and displacements which have occurred. The figure shows the meshed surface with blue and red dolos units. The blue units represent the before test location of the dolos units as the reference position and the red, the position to which the dolos has been displaced. This erosion void is recorded as the percentage damage from the two surfaces and tabulated in Table 4.6.

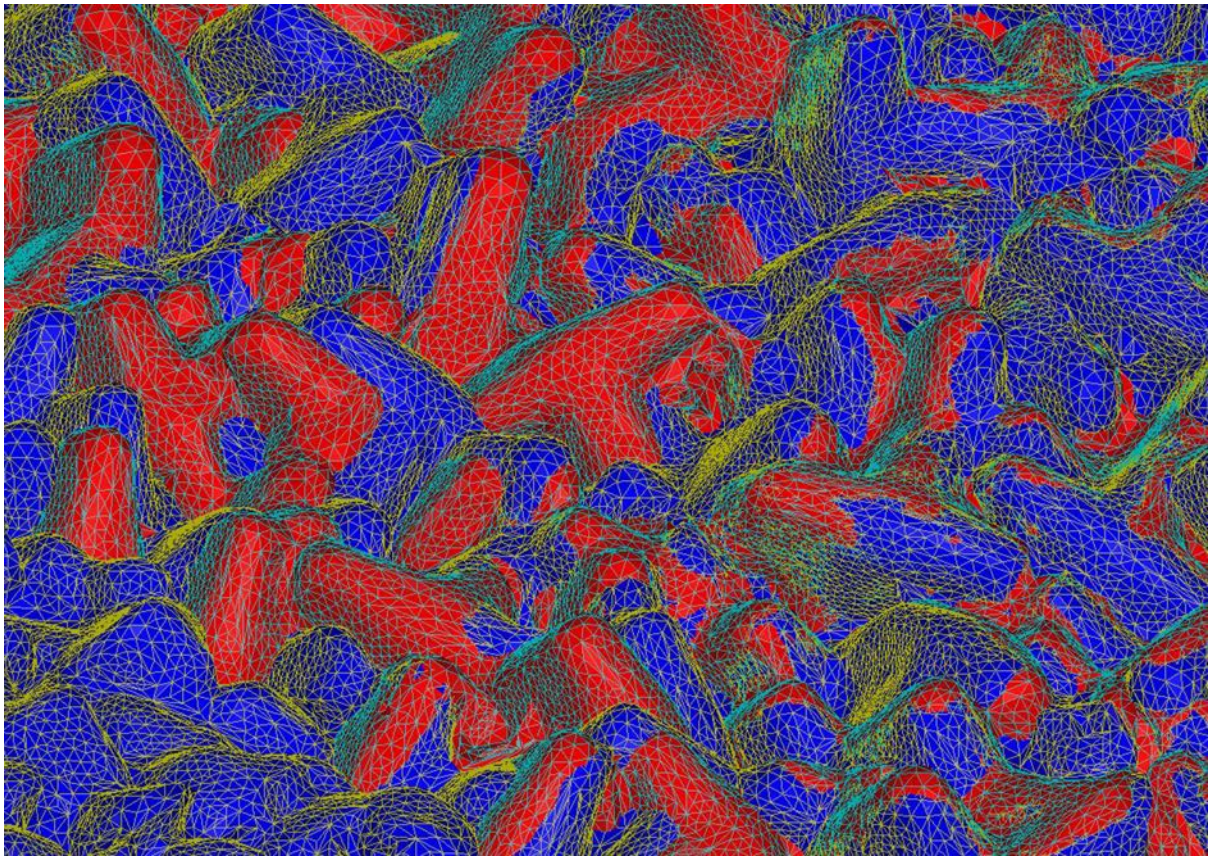

Figure 6.1: 3D surface volume overlay of before test 3(blue) and after test 3(red) Blue dolos units represent the pre-test situation and the red units are those that have been displaced in the test.

There is a similar trend between the comparison of the cumulative damage progression monitored by the 2D visual photographic method and that calculated by the 3D scanned eroded volume method plotted in Figure 3.20 and Figure 4.11. This also applies to the small settlements and larger displacements although variability exists between the visual analysis and scanned volume eroded, which may be due to the nature of the recording displacement manually and the variability of the mesh being generated for the two methods. In the four Test cases in Section 4.1, the 3D scanned damage percentages are higher than the visual method. Individual tests can be a factor of three times larger.

Table 4.6 shows that in this controlled experiment the 3D eroded volume method has a mean damage percentage of 12% over the four tests with a exceedance of 3.48% for test 2. This also confirms that the combination of settlement and displacement as derived from the automated 3D volumetric method is slightly higher in comparison with the visual method. However, a comparison of the cumulative percentage damage during the largest wave condition (Test 3) the comparison indicates that the difference of 1.89% between the 2D visual method and 3D scanned eroded volume method compares well, with the 2D visual method results indicating a slightly smaller percentage damage. This indicates that the 3D scanned eroded volume method, in general, be considered as slightly conservative

in comparison with the 2D visual method results, but that during larger displacements the cumulative percentage damage are comparable for these specific tests.

From the comparison of the prototype scanned damage progression, as determined by the aerial photographic analysis, with that calculated using the 3D multibeam and LIDAR scanned data there can be a correlation between the two methods. The cumulative percentage damage from the 3D scanned method records has a 5.6% exceedance. This is higher than the photographic method and is only one data record using the 3D method. This indicates that the settlement and displacement voids are being recorded as well as the breakwater slope from toe to crest and are often higher in comparison with the aerial photographic analysis method in prototype which is calculated visually by counting the above water movements only. The result shows that the scanned data in prototype is able to provide information of the entire slope rather than just the above water portion. The cumulative damage trend of the photographic method and that of the 3D method need to be investigated further to track the trend over time. Although only the results of one 3D field survey was possible the results accord with those from the 2D method. The 3D is more conservative and consequently provides a better assessment of damage. The consern is merely the cost of equipment and time to process the data which may influence a descision towards the 2D aerial photograpic method.

The comparison of the 2D photograph as shown in Figure 4.10 to Figures 5.10 and the 3D image of the dolos slope, with those obtained by the 3D scanner and echo-sounder and as plotted, produce good definition of the complex shape.

The 3D scanned eroded volume method and the 2D photographic analysis methods realistically reflect the quantification of damage progression (Figure 3.20) and (Figure 4.11). It can also be accepted that the accuracy between the 3D scanned volumetric method and 2D photographic method correctly record damage independently.

The conclusion from the comparison of the two methods is that the 3D scanned eroded volume method produces results similar to those from the photographic analysis with respect to the quantification of cumulative percentage damage.

For the prototype comparison to be more relevant with regard to damage progression, more records of scanned data is needed. This would lead to better accuracy checks in differentiating between scanned and photographic analysis methods for prototype measurements. Therefore breakwaters that have been recorded using the photographic method should be simultaneously recorded using the new 3D method to gather more data.

This study has shown that the combination of laser scan and multi-beam measurements from a mobile platform can replace the aerial photographic procedures especially if data is required between the intertidal zone down to the toe thereby creating a seamless dataset above and below water. For breakwater maintenance and repair the 3D method

can provide a seamless / more complete assessment than the "old" 2D method. Aerial photography will still remain an important tool for port planning but should not be necessary for breakwater repair and maintenance. Both monitoring methods complement one another in order to support the decision making processes for the maintenance of the port infrastructure with high resolution aerial photographs providing a bird's eye view and 3D scanned data for quantification of damage.

Chapter 7

Summary, conclusions and recommendations

7.1 Summary

This study addresses a breakwater damage assessment method using three dimensional survey data established from above-water mapping using a terrestrial laser scanner in addition to a multi-beam echo sounder mounted on a boat.

The prototype photographic method is compared with the prototype multi-beam and laser scanned data. The photographic method provides sufficient historic data for it to be used as a baseline for the comparison. The procedure was applied to a scaled physical model study in order to track movement of dolos armour units using the armour track program and compared with the movement recorded using the 3D laser scanner processed by the 3D Reshaper program and laser scanning data acquisition software.

Chapters 1 - 2 introduce the topic of quantifying damage to, and failure of prototype rubble mound breakwaters. It is noted that the methods are relatively complex and time consuming and the spatial concentration of damage is generally not clearly representative of the profile shape as the prototype cross-sections computes average depth profiles.

Chapter 2 reviews the monitoring and measurement techniques to provide condition assessments. The best monitoring approach being either counting the number of displacements, breakages or measurement of profiles along the structure.

Chapter 3 describes an experimental set up to evaluate the accuracy of the photographic and 3D scanning techniques in assessing breakwater damage. The experiment was conducted to investigate damage deterioration using 3D data points on the surface of the breakwater. By adapting the relative eroded area method described by (Broderick, 1982), the 3D eroded volume method was developed to analyse the design station.

The volumetric equation is used to compute the damage over a specific station length ($11D_n$) of a breakwater station re-written here as Equation 7.1. The physical model measurements are used to validate the use of this equation:

$$S_{3D}D\% = \frac{V_{station\ erosion}}{V_{station\ design}} \times 100 \tag{7.1}$$

The experimental verification of the 3D method considered tests with minor movement to major displacement. The displacements were carried out by hand to control small movements, rotations, settlement and complete exposure down to the underlayer. The tracking of damage progression from minor movement, to rotational displacements and major movement produced similar damage percentage trends to the photographic visual method. The findings of the cumulative percentage damage assessment indicates that the difference between the 2D visual method damage level by D(%) and 3D scanned eroded volume method $S_{3D}D(\%)$ follow a similar damage progression trend however, some individual results differ for example Test 19 which can differ in magnitude of three times the damage level.

Chapter 4 presents the results of the 3D physical model set-up for the Cape Town spur breakwater as it was also scanned in prototype to test the method.

In the physical model, the damage quantification was tested within quantifying damage using the armour track method (photographic method) as described in (Holtzhausen et al. (2000)) which tracks the distance model dolos units have travelled to calculate damage using Equation 4.9 in which dolos damage is the recorded damage, "H" is the height of a Dolos fluke and 0.5H is half the height of a dolos fluke length. This is compared with the (3D method) volumetric damage using $S_{3D}D\%$ which uses 3D surface to surface void difference over the station to quantify damage by equation 3.2. $S_{3D}D\%$ being the recorded damage, $V_{station\ erosion}$ is the void created after dolos displacement has occurred, and $V_{station\ design}$ is the volume of the station before damage has occurred. The result of the two equations (equation 7.1 and equation 4.9) are calculated as percentage damage that has occurred on the breakwater slope.

Chapter 5 presents the results of the field experiment using the Aerial photographic method with that of the 3D LIDAR data and multi-beam data.

The results from the aerial photographic monitoring is superior for monitoring damage above water, and estimates the damage below water as being 1.5 times the damage recorded above the waterline as indicated by the (PACD) percentage adjusted cumulative damage described in Phelp (1995) due to the absence of good underwater data. When calculating damage using 3D data, it provides a complete data set of above and below water in 3D point data. This is beneficial for quantifying toe damage and movement of units underwater.

7.2 Conclusions

The ultimate objective is to have sufficient prototype breakwater data (of dolos structures in this case), to combine with the recorded wave conditions, to create a basis for validating design formulae which are, thus far, predominantly based on results from physical model tests.

Ongoing monitoring of breakwaters using the latest technologies such as laser scanning and multi-beam echo soundings help record damage to breakwaters. This should help prevent costly unnoticed failures. From the comparison of the two methods, the aerial photographic method and the 3D method, the following observations are drawn:

Advantages of Aerial Photographic Investigations (Presently the usual way to determine breakwater damage)

- Photographic investigations provide superior quality visual information of the above water condition of breakwater stations.
- Photographic investigations can be done within 1 hour during spring low tide and data is processed immediately as compared to the Crane and Ball and boat based surveys.
- Data are mostly visual and can be interpreted instantaneously by a trained assessor.
- It is quick to set up and can be carried out easily as long as there is a helicopter available.

Disadvantages of Aerial Photographic Investigations

- The photographic record is dependent on the skill of the helicopter pilot to hover at an arbitrary point on the seaward side of the breakwater and imposes safety problems with hovering at a height of 60 m above the water surface.
- The ability of the photographer to spot the required area of interest within a spilt second to capture the slope at the most exposed moment during wave draw-down.
- Since the data are mostly visual, it requires antrained eye for movement and understanding of the type of units that are analysed.
- Minor settlement of armour units is only noticed in photographs if breakage has occurred Phelp and Zwamborn (2000).
- The photographic record is only useful for above water movements and not suitable for below water analysis.

Advantages of 3D LIDAR and multi-beam data

- 3D data provides full coverage of above and below water to the toe of the breakwater.
- Data processing does not necessarily require a trained assessor and can be run using scripts programmed into the software.
- Captured data quantifiable with reference to dimension and volume.
- As-built cross-sections can be compared easily by creating a 3D theoretical design to compare latest scan data.
- Data processing in future can be automated to be included with remotely piloted aerial or boat based systems.

Disadvantages of 3D LIDAR and multi-beam data

- Requires a high performance computer to process the 3D data.
- Data are captured at a slower rate at a cruising speed of a boat and can take up to a day to collect data.
- Large data storage for handling data is required.

The physical model experimental application compared the results including progressive damage calculated by the 3D method with the photographic method of a 1:1.5 dolos slope in a controlled environment. The test program was carried out in stages from minor movement less than 0.5 Dn (Test 1 to Test 6) , rotations of an individual unit until displacement out of the slope (Test 7 to Test 16) followed by settlement tests (Test 17 to Test 19) and finally major changes to the slope with units displaced to expose the underlayer (Test 20 to Test 24). The findings of the cumulative percentage damage indicates that the difference between the 2D visual method damage level by D(%) and 3D scanned eroded volume method $S_{3D}D(\%)$ follow a similar damage progression trend however, some individual results differ for example Test 19 which can differ in magnitude of three times the damage level.

It is however essential that model damage be verified further by monitoring of prototype breakwaters for interpretation of progressive damage over time. This is especially important because of the detailed displacement data, which is now easily produced by 3D techniques. It is also very important that strict quality control be applied to both model and prototype investigations, to further reduce the variations between design and prototype performance using 3D scanning technology which also requires skilled personnel.

The prototype application calculated using the 3D method compared with the damage determined by the 2D photographic method, compares well, thus confirming the suitability of the 3D method in prototype. This also confirms that the settlement and displacement voids of the entire breakwater slope from toe to crest are being recorded. This also indicates that the 3D analysis method results in prototype are conservative. The trend line of the photographic method and that of the 3D method correlate well. This method has shown that the combination of laser scan and multi-beam measurements from a mobile platform can replace the aerial photographic procedures especially if data is required from the intertidal zone, down to the toe.

The 3D scanned eroded volume method (3D method) realistically reflects the quantification of damage progression accurately. The accuracy of the 3D method and 2D photographic methods follow a similar trend.

7.3 Recommendations

The results from the model tests emphasised the complexity of tracking movement of armour units on breakwaters. As a consequence, the accuracy in the observed damage varies when comparing the photographic visual method with the 3D method. It is therefore recommended that further research be done to improve the accuracy of the scanned data of small scale breakwater stability studies which are scanned using the 3D method to track damage. However, the accuracy of the data is determined by visibility and shadows should be minimised when recording data from different angles ie. the more data the better the mesh accuracy.

This method has shown that the 3D method is able to capture the shape of a dolos unit which is fairly complex. There are approximately 50 types of armour units worldwide, of which some are documented in Appendix D. The method therefore should be applied to Accropodes, Xbloc, Core-locs, Antifer cubes, rock and other complex shape concrete armour units.

The recommendations for future research should focus on categorising levels of percentage damage to a breakwater slope to reflect initial damage, medium damage and failure trends.

Further studies can be carried out since the shape of the armour unit is now captured, 3D armour units can be fitted automatically by shape recognitions to build the structure using CAD.

This can be further studied for wave and structure interactions in numerical models. Structure life cycle predictions can be computed using this new damage analysis method to track changes over time.

Bibliography

Bradbury, A. and Allsop, W., 1989. Monitoring techniques for armoured coastal structures, Technical report, Hydraulics Research Ltd, Wallingford, United Kingdom.

Brock, J. and Purkis, S., 2009. 'The emerging role of lidar remote sensing in coastal research and resource management', *Journal of Coastal Research* (Special issue 53), 1–5.

Broderick, L., 1982. 'Rip-rap stability scale effects', pp. 82–3.

Brouwer, M., 2013. The influence of the under layer on the stability of single layer armour units, Master's thesis, Delft University of Technology, Netherlands.

Burcharth, H., D'Angremond, K., van der Meer, J. and Liu, Z., 2000. 'Empirical formula for breakage of dolosse and tetrapods', *Coastal Engineering* **40**(3), 183–206.

Burcharth, H. F., Kramer, M., Lamberti, A. and Zanuttigh, B., 2006. 'Structural stability of detached low crested breakwaters', *Coastal Engineering* **53**(4), 381–394.

Burcharth, H. F. and Liu, Z., 1992. Design of Dolos armour units, *in* '23 International Conference on Coastal Engineering'.

Cialone, M. A., 1984. Monitoring rubble-mound coastal structures with photogrammetry, Technical report, US Army Engineer Waterways Experiment Station, Vicksburg,MS.

CIRIA, CUR and CETMEF, 2007. The use of rock in hydraulic engineering, *in* 'The Rock Manual', chapter Chapter 10, pp. 642–646 & 795–797.

Collin, A., Long, B. and Archambault, P., 2011. 'Benthic classifications using bathymetric LIDAR waveforms and integration of local spatial statistics and textural features'.

Cornett, A., 1995. A study of wave-induced forcing and damage of rock armour on rubble-mound breakwaters, PhD thesis, University of British Columbia.

CSIR, 2015. Port of Cape Town Wavenet (IPOSS) Annual Summary Report: 2013/2014, Technical report, Council for scientific and industrial research, Stellenbosch, Cape Town.

DAngremond, K., Verhagen, H. and Roode, F., 2009. *Breakwaters and closure dams*, Delft University of Technology, Netherlands.

Davies, M. M. E. and Cornett, A., 1994. 'Damage analysis for rubble mound breakwaters', *Coastal Engineering Proceedings* **1**(24), 1001–1015.

Drake, L., 2007. Comparison of two profile survey techniques on the submerged portion of a rubble mound breakwater in a laboratory model, Technical report, Stellenbosch University.

Flener, C., Vaaja, M., Jaakkola, A., Krooks, A., Kaartinen, H., Kukko, A., Kasvi, E., Hyyppä, H., Hyyppä, J. and Alho, P., 2013. 'Seamless mapping of river channels at high resolution using mobile liDAR and UAV-photography', *Remote Sensing* **5**(12), 6382–6407.

Hedar, P. A., 1960. Stability of rock-fill breakwaters, PhD thesis, University of Goteborg, Sweden.

Hedar, P. A., 1986. 'Armor layer stability of rubble mound breakwaters', *Waterway, port, coast, and ocean engineering, ASCE 112(3)* pp. 343–350.

Holthuijsen, L. H., 2007. *Waves in oceanic and coastal waters*, World Scientific Publishing Co. Pty. Ltd.

Holtzhausen, A., Retief, G. d. F. and Zwamborn, J. A., 2000. Physical Modelling of Dolos Breakwaters: The Coega Results and Historical Perspective, *in* 'Coastal Engineering 2000', pp. 1536–1549.

Holtzhausen, and Zwamborn, J., 1992. New Stability Formula for Dolosse, *in* 'Coastal Engineering', pp. 1231–1244.
URL: *http://ascelibrary.org/doi/abs/10.1061/9780872629332.093*

Hough, G. and Phelp, D., 1999. Digital Image processing techniques for the aerial field monitoring of harbour breakwaters, *in* 'Coastal Engineering Proceedings', pp. 1789–1799.

Hudson, R., 1959. 'Laboratory investigation of rubble-mound breakwaters', *Waterway, port, coast, and ocean engineering, ASCE* **85**, 93–121.

Hudson, R. Y., 1958. Design of quarry-stone cover layers for rubble-mound breakwaters, Technical report, U.S. Army Engineer Waterways Experiment Station, Vicksburg,MS.

Hughes, S., 1993. *Physical models and laboratory techniques in coastal engineering*, World Scientific Publishing Co. Pty. Ltd.

Iribarren, C., 1938. Una formula para el calculo de los diques en escoller (A formula for the calculation of rock-fill dikes)Translated by D. Heinrich, Technical report, Fluid Mech. Lab., Univ. of Calif., Berkeley, CA.

Jenson, O., 1984. A monograph on rubble-mound breakwaters, Technical report, Danish Hydraulic Institute, Horsholm, Denmark.

Kendall, T., 1989. Analysis of 42-ton dolos motions at Crescent City, *in* 'International Conference on Coastal Engineering', American Society of Civil Engineers, Malaga, pp. 2129–2143.

Kluger, J., 1982. Monitoring of rubble mound breakwaters stability using photographic survey method, *in* 'International Conference on Coastal Engineering, Cape Town', American Society of Civil Engineers, Cape Town.

Kluger, J., 1988. Monitoring of 9t dolos test section on Table Bay harbour breakwater, November 1986 to July 1987, Technical report, CSIR, Stellenbosch, South Africa.

Kucharski, W. and Clausner, J., 1989. Side scan sonar for inspection of coastal strructures., Technical report, US Army Engineer Waterways Experiment Station, vicksburg,MS.

Kucharski, W. and Clausner, J., 1990. Underwater inspection of coastal structures using commercially available sonars, Technical report, US Army Engineer Waterways Experiment Station, Vicksburg,MS.

Kukko, A., 2013. Mobile laser scanning system development, performance and applications, PhD thesis, Finnish Geodetic Institute,Finland.

Lomónaco, P., Vidal, C., Medina, J. and Gómez, M., 2009. 'Evolution of damage on roundheads protected with cube and cubipod armour units', *Proceedings of Coastal, ...* pp. 1–12.

Marujo, Nuno Ricardo, C. S., Trigo-Teixeira, A., Sanches-Valle, A., Araújo, M. A. V. C. and Caldeira, J., 2013. An improved and integrated monitoring methodology for breakwaters Application to the Ericeira Breakwater, *in* '6th SCACR International Short Course/ Conference on Applied Coastal Research'.

Melby, J., 1999. Damage progression on rubble-mound breakwaters, PhD thesis, University of Delaware.

Melby, J. and Kobayashi, 1998. 'Progression and variability of damage on rubble mound breakwaters', *Waterway, Port, Coastal and Ocean Engineering* **124**(6), 286–294.

Monfort, C. L. and Lippmann, T. C., 2011. 'Assimilation of airborne imagery with a wave model for bathymetric estimation', *Journal of Coastal Research* pp. 40–49.

Morang, Larson and Gorman, 1997. 'Monitoring the coastal environment Part III, geophysical and research methods', *Journal of Coastal Research* **13**(4), 1064–1085.

N. Marujo, A. Trigo-Teixeira, A. Sanches do Valle, M. A. Araújo, J. C., 2007. 'An improved and integrated monitoring metholody for rubble mound breakwaters', *International short course and Conference on applied coastal research* pp. 1–2.

Owen, M., and Allsop, W., 1983. 'Hydraulic modelling of rubble mound breakwaters', *Breakwaters: Design and construction,Institute of Civil Engineers* .

Parsons, L.E. and Lilycrop, W., 1988. The SHOALS system - a comprehensive surveying tool., Technical report, US Army Engineer Waterways Experiment Station, Vicksburg,MS.

Peyronnin, N., Green, M., Richards, C. P., Owens, A., Reed, D., Chamberlain, J., Groves, D. G., Rhinehart, W. K. and Belhadjali, K., 2013. 'Louisianas 2012 coastal master plan : Overview of a science-based and publicly informed decision-making process', *Journal of Coastal Research* **Sp.Issue**(67), 1–15.

Phelp, D., 1995. Field monitoring of dolos breakwaters, Master's thesis, University of Cape Town.

Phelp, D., Luger, S., Van Tonder, A. and Holtzhausen, A., 1994. 'Results of extensive field monitoring of dolos breakwaters', *Coastal Engineering Proceedings* **24**(1), 1511–1525. **URL:** *http://journals.tdl.org/icce/index.php/icce/article/view/5053/4731*

Phelp, D. and Tulsi, K., 2006. Digital image technology as a measurement tool in physical models, *in* 'International Conference on the Application of Physical Modelling in Coastal and Port Engineering and Science', pp. 21–31.

Phelp, D. and Zwamborn, J., 2000. 'Correlation between model and prototype damage of dolos breakwater armouring', *Coastal Engineering 2000* pp. 1–13. **URL:** *http://ascelibrary.org/doi/abs/10.1061/40549(276)120*

Pope, J., 1992. Our Ageing coastal infrastructure, *in* 'Coastal Engineering Practice', American Society of Civil Engineers, New York, pp. 1055–1068.

Prickett, T., 1996. Coastal structure underwater inspection technologies, Technical report, US Army Engineer Waterways Experimental Station, Vicksburg,MS.

Reif, M. K., Macon, C. L. and Wozencraft, J. M., 2011. 'Post-Katrina Land-Cover , Elevation , and volume change assessment along the south shore of lake Pontchartrain', *Journal of Coastal Research* pp. 2005–2006.

RIEGL, 2009. 'RIEGL VZ-400', pp. 1–7.

RIEGL, 2012. '3D Terrestrial Laser Scanner, RIEGL VZ-400 / RIEGL VZ-1000'.

Risser, R., 2011. Data analysis of a new 3D laser scanning technique used for computing profiles of damages armour slopes on a laboratory rubble breakwater model, Technical report, Stellenbosch university.

Rossouw, M., Terblanche, L., Moes, J. and Africa, S., 2013. 'General Characteristics of Long Waves around the South African Coast'.

Schawlow, A. L. and Townes, C. H., 1958. 'Infrared and optical masers', *Physics Review* **112**(6), 1940–1949.

Thies, T., 2011. A Vessel-Based Mobile Mapping System From Sensor Integration to Multipurpose Products, PhD thesis, University Hamburg, Germany. **URL:** *http://www.riegl.com/uploads/tx_pxpriegldownloads/Thies_Thomas__2011_-_A_Vessel-Based_Mobile_Mapping_System__Master_Thesis__HafenCity_University_-Hamburg__Germany_part1.pdf*

Thompson D. and Shuttler R., 1975. Riprap design for wave attack a laboratory study in random waves., wallingford, United Kingdom.

Thompson, D. and Shuttler R., 1976. Design of rip-rap slope protection against wind waves, London, United Kingdom.

Tomlinson, B. Olliver, G. and Cooke, R, 2001. Emerging acoustic techniques for monitoring the condition and performance of underwater structures - as applied to Peterhead Breawkater, *in* T. Telford, ed., 'Proceedings of Breakwater Coastal Structure and Coastlines.', pp. 345–357.

Torum, A. Mathiesen, B. Escutia, R., 1979. 'Reliability of breakwater model tests', *Coastal Structures* pp. 454–469.

Tulsi, K. and Phelp, D., 2009. Monitoring and maintenance of breakwaters which protect port entrances, *in* '28th Annual Southern African Transport Conference', number July, pp. 317–325.
URL: *http://hdl.handle.net/2263/12016*

USACE, 2006. [CEM] Engineer Manual, *in* W. CHL-ERDC, ed., 'Coastal engineering manual', Vicksburg,MS, pp. 1110–2–1100.

Van der Meer, J. W., 1988. Rock slopes and gravel beaches under wave attack, PhD thesis, Delft Hydrulics Laboratory, Emmeloord, The Netherlands.

Vanlishout, V., Verhagen, H. J. and Troch, P., 2011. 'Oblique wave transmission through rough impermeable rubble mound submerged breakwaters'.

Vidal, C., Losada, M., and Medina, R., 1991. Stability of mound breakwater's head and trunk, Vol. 117(6), pp. 570–587.

Wallingford, H. R. Ltd., 1990. Rock armouring for coastal and shoreline structures, Technical report, H.R. Wallingford, United Kingdom.

Wehr, A. and Lohr, U., 1999. 'Airborne laser scanningan introduction and overview'.

Weymouth, O. and Magoon, O., 1968. Stability of quadripod coverlayers, *in* J. Johnson, ed., 'Proceedings of the Coastal Engineering Conference', American Society of Civil Engineers, London,U.K.

Wüst, I., 2012. Application of a 3D laser scanner to laboratory model of breakwater with various armour units to create cross-sections for use in damge assessment, Technical report, Stellenbosch University.

Appendix A

Appendix A

A.1 Field Data Aerial Photographic survey

This section contains the data gathered from the aerial photographic survey, multi-beam survey and caisson survey of the western breakwater of the Port of Cape Town was carried out during 29 October 2014 and 27 November 2014. The data record provides for a visual qualitative state of the breakwater for every station. The images show the state of the dolos cover in 1999 and adjacent to it the 2014 aerial image.

Table A.1: Helicopter centre positions of each photographic station

Clarke1880 Lo19			
Figure Number	Station Number	Northing (m)	Easting (m)
1	365	3752220	52608.1
2	390	3752228	52632.3
3	415	3752236	52655.6
4	440	3752244	52679.4
5	465	3752252	52703
6	490	3752260	52726.8
7	515	3752268	52750.4
8	540	3752277	52775
9	565	3752284	52797.6
10	590	3752292	52821.8
11	615	3752304	52844.9
12	640	3752313	52867.3
13	665	3752321	52890.9
14	690	3752329	52914.6
15	715	3752337	52938.3
16	740	3752345	52962
17	765	3752353	52985.7
18	790	3752361	53009.6
19	815	3752369	53033.4
20	840	3752377	53057.3
21	865	3752387	53080.2
22	N. Spur	3752395	53100.8
23	M. Spur	3752398	53115.1
24	S. Spur	3752430	53134.9
Ref. station		3752445	53983.5

Table A.2: Damage Table for trunk of breakwater November 2014

		Displaced Dolosse				Damaged Dolosse		New Damage	Prev Damage	Cum Damage	No of Dolos
Figure No.	Station No.	0 - 0.5m (A)	0.5 - 1.5m (B)	> 1.5m (C)	Total (D)	Broken (E)	Lost (F)	ND (C+E+F)	Dec-12 PD	Nov-14 CD (ND+PD)	N
1	365								4	4	78
2	390								1	1	166
3	415								1	1	108
4	440								4	4	116
5	465								1	1	117
6	490								3	3	116
7	515								0	0	121
8	540								1	1	112
9	565								3	3	114
10	590								3	3	119
11	615		1						3	3	118
12	640					1			4	4	105
13	665								2	2	108
14	690								7	7	112
15	715								6	6	117
16	740								7	7	113
17	765								6	6	122
18	790								2	2	114
19	815								5	5	115
20	840								8	8	125
21	865								16	16	118
TOTAL		0	1	0	0	1	0	0	87	87	2434

Table A.3: Damage Table for trunk of breakwater November 2014 Continued

		No of Dolos	% Damage					
Figure No.	Station No.	N	New PND (ND/N*100)	Previous PPD (PD/N*100)	Cum PCD (PND + PPD)	Adjusted Cum PACD (PCD*1.5)	Nod (CD/11.8)	Adjusted Damage (Nod*1.5)
1	365	78	0.00	5.13	5.13	7.69	0.34	0.51
2	390	166	0.00	0.60	0.60	0.90	0.08	0.13
3	415	108	0.00	0.93	0.93	1.39	0.08	0.13
4	440	116	0.00	3.45	3.45	5.17	0.34	0.51
5	465	117	0.00	0.85	0.85	1.28	0.08	0.13
6	490	116	0.00	2.59	2.59	3.88	0.25	0.38
7	515	121	0.00	0.00	0.00	0.00	0.00	0.00
8	540	112	0.00	0.89	0.89	1.34	0.08	0.13
9	565	114	0.00	2.63	2.63	3.95	0.25	0.38
10	590	119	0.00	2.52	2.52	3.78	0.25	0.38
11	615	118	0.00	2.54	2.54	3.81	0.25	0.38
12	640	105	0.00	3.81	3.81	5.71	0.34	0.51
13	665	108	0.00	1.85	1.85	2.78	0.17	0.25
14	690	112	0.00	6.25	6.25	9.38	0.59	0.89
15	715	117	0.00	5.13	5.13	7.69	0.51	0.76
16	740	113	0.00	6.19	6.19	9.29	0.59	0.89
17	765	122	0.00	4.92	4.92	7.38	0.51	0.76
18	790	114	0.00	1.75	1.75	2.63	0.17	0.25
19	815	115	0.00	4.35	4.35	6.52	0.42	0.64
20	840	125	0.00	6.40	6.40	9.60	0.68	1.02
21	865	118	0.00	13.56	13.56	20.34	1.36	2.03
TOTAL		2434	0.00	3.57	3.57	5.36	0.35	0.53

Figure A.1: Aerial photographic survey 1999 station 365

Figure A.2: Aerial photographic survey 2014 station 365

Figure A.3: Aerial photographic survey 1999 station 390

Figure A.4: Aerial photographic survey 2014 station 390

Figure A.5: Aerial photographic survey 1999 station 440

Figure A.6: Aerial photographic survey 2014 station 440

Figure A.7: Aerial photographic survey 1999 station 490

Figure A.8: Aerial photographic survey 2014 station 490

Figure A.9: Aerial photographic survey 1999 station 490

Figure A.10: Aerial photographic survey 2014 station 490

Figure A.11: Aerial photographic survey 1999 station 515

Figure A.12: Aerial photographic survey 2014 station 515

Figure A.13: Aerial photographic survey 1999 station 540

Figure A.14: Aerial photographic survey 2014 station 540

Figure A.15: Aerial photographic survey 1999 station 565

Figure A.16: Aerial photographic survey 2014 station 565

Figure A.17: Aerial photographic survey 1999 station 590

Figure A.18: Aerial photographic survey 2014 station 590

Figure A.19: Aerial photographic survey 1999 station 615

Figure A.20: Aerial photographic survey 2014 station 615

Figure A.21: Aerial photographic survey 1999 station 640

Figure A.22: Aerial photographic survey 2014 station 640

Figure A.23: Aerial photographic survey 1999 station 665

Figure A.24: Aerial photographic survey 2014 station 665

Figure A.25: Aerial photographic survey 1999 station 690

Figure A.26: Aerial photographic survey 2014 station 690

Figure A.27: Aerial photographic survey 1999 station 715

Figure A.28: Aerial photographic survey 2014 station 715

Figure A.29: Aerial photographic survey 1999 station 740

Figure A.30: Aerial photographic survey 2014 station 740

Figure A.31: Aerial photographic survey 1999 station 765

Figure A.32: Aerial photographic survey 2014 station 765

Figure A.33: Aerial photographic survey 1999 station 790

Figure A.34: Aerial photographic survey 2014 station 790

Figure A.35: Aerial photographic survey 1999 station 840

Figure A.36: Aerial photographic survey 2014 station 840

Figure A.37: Aerial photographic survey 1999 station 865

Figure A.38: Aerial photographic survey 2014 station 865

Figure A.39: Aerial photographic survey 1999 station North Spur

Figure A.40: Aerial photographic survey 2014 station North Spur

Figure A.41: Aerial photographic survey 1999 station Mid Spur

Figure A.42: Aerial photographic survey 2014 station Mid Spur

Figure A.43: Aerial photographic survey 1999 station South Spur

Figure A.44: Aerial photographic survey 2014 station South Spur

Appendix B

Appendix B

B.1 Field data mobile LIDAR multi-beam survey

An aerial photographic survey, multi-beam survey and caisson survey of the western breakwater of the Port of Cape Town was carried out during 29 October 2014 and 27 November 2014. The data recorded from the LIDAR multi-beam investigation provides a quantitative state of the breakwater for every station. The figures presented show the voids between the as-built (1989) section and the present state (2014) of the breakwater.

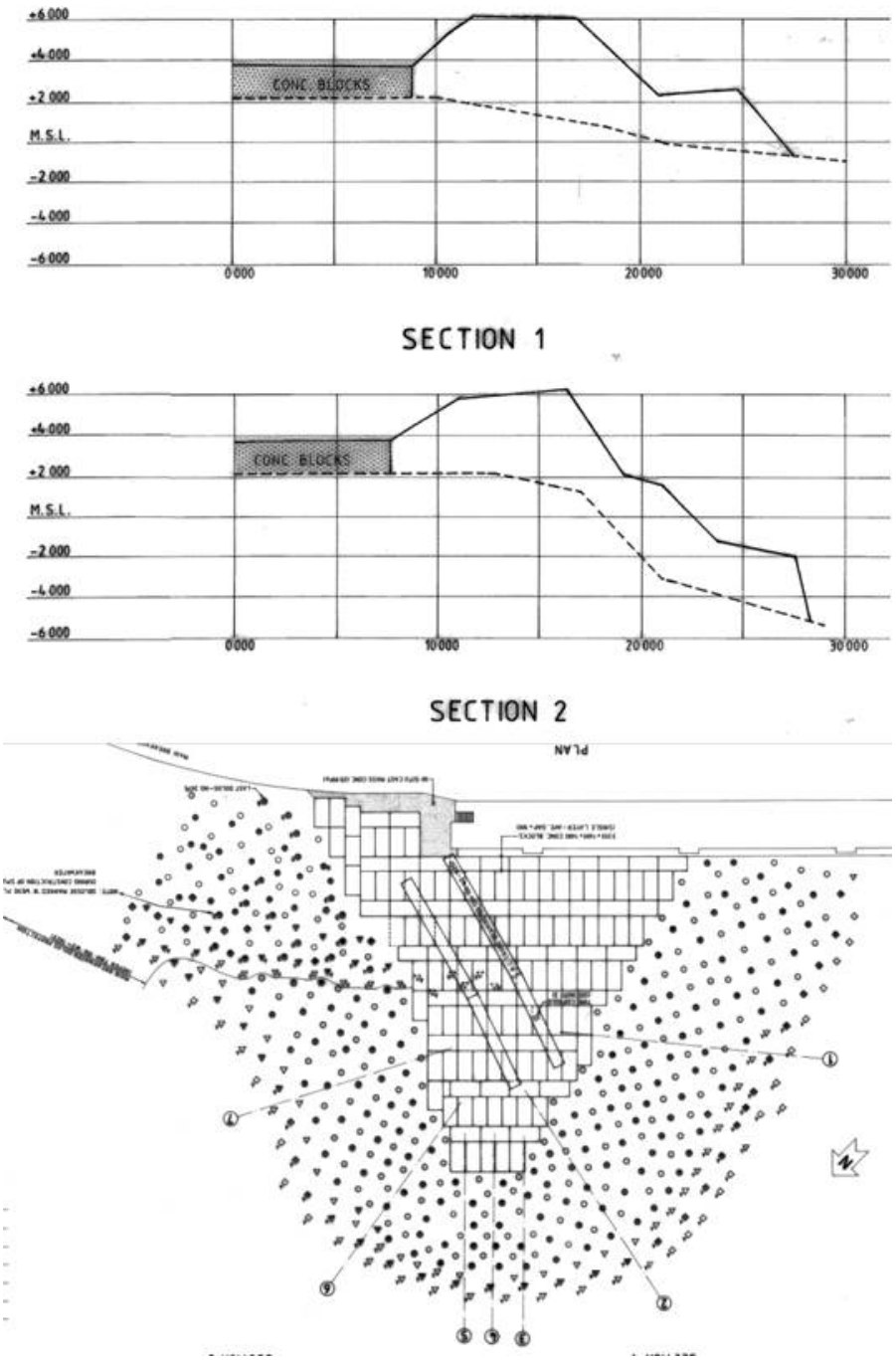

Figure B.1: As-built cross-section on either side of the south spur station

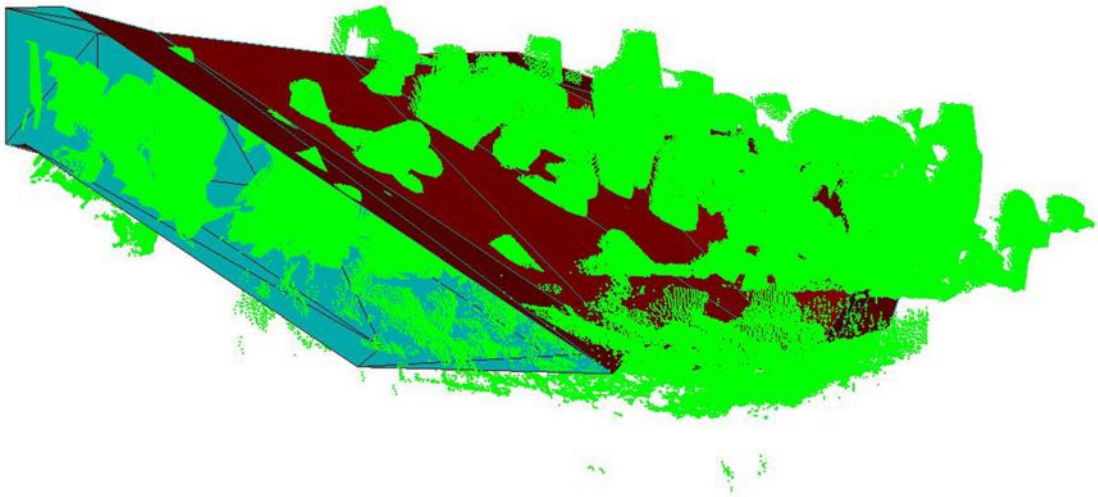

Figure B.2: View through the station

B.2 Cross-section of the spur breakwater from LIDAR Multi-beam scan for the S-Spur

The data cross-section collected from the as built survey are presented in this section.

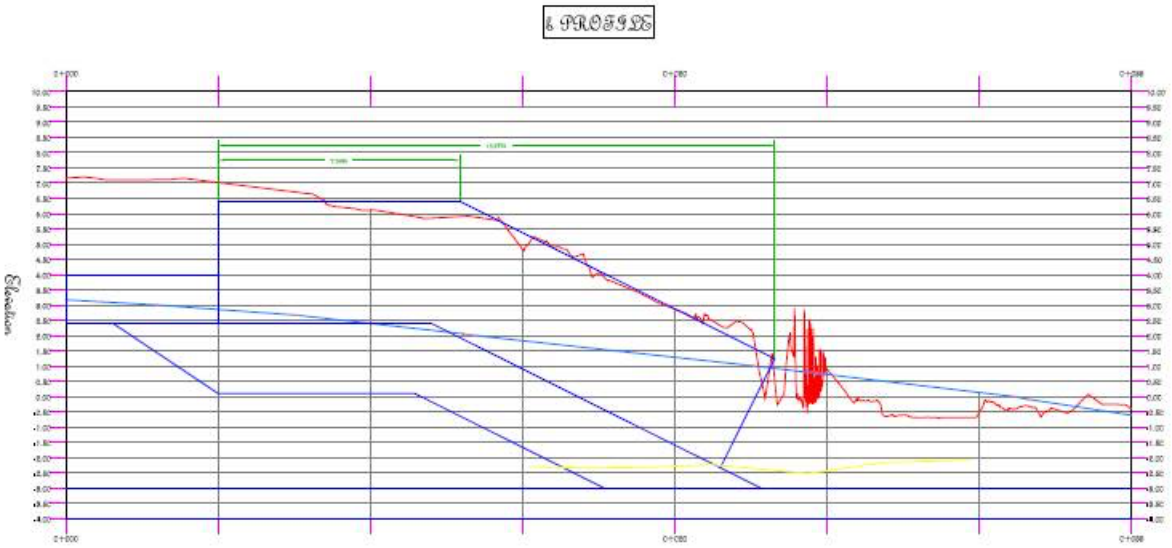

Figure B.3: Cross-section through section B from the LIDAR multi-beam scan

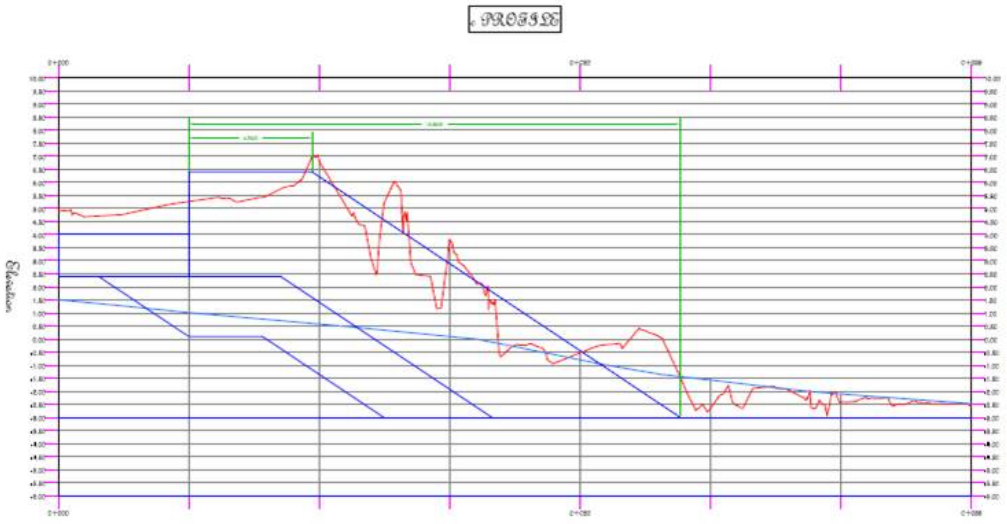

Figure B.4: Cross-section through section C from the LIDAR multi-beam scan

Figure B.5: Cross-section through section D from the LIDAR multi-beam scan

Figure B.6: Cross-section through section E from the LIDAR multi-beam scan

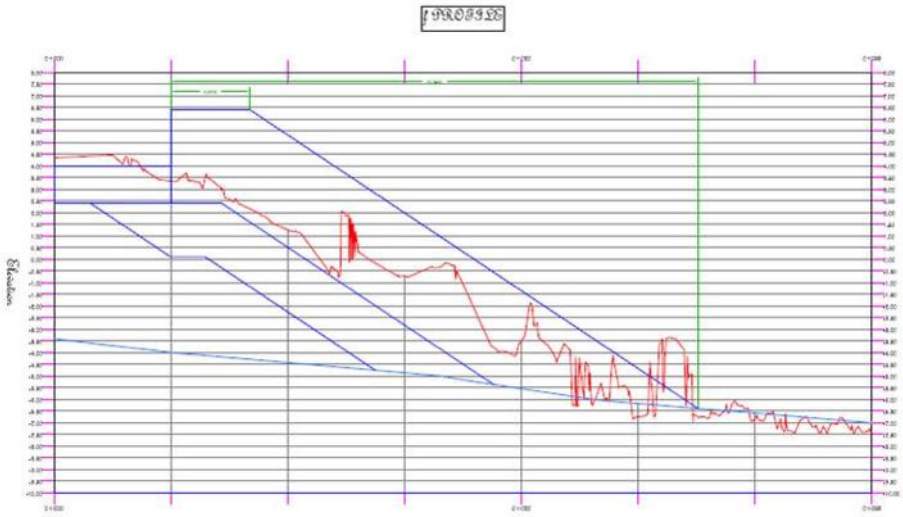

Figure B.7: Cross-section through section F from the LIDAR multi-beam scan

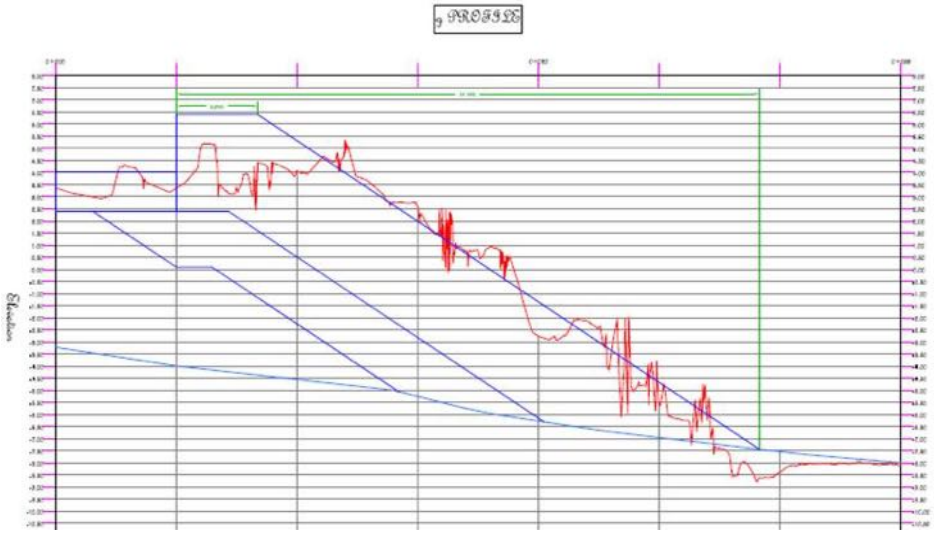

Figure B.8: Cross-section through section G from the LIDAR multi-beam scan

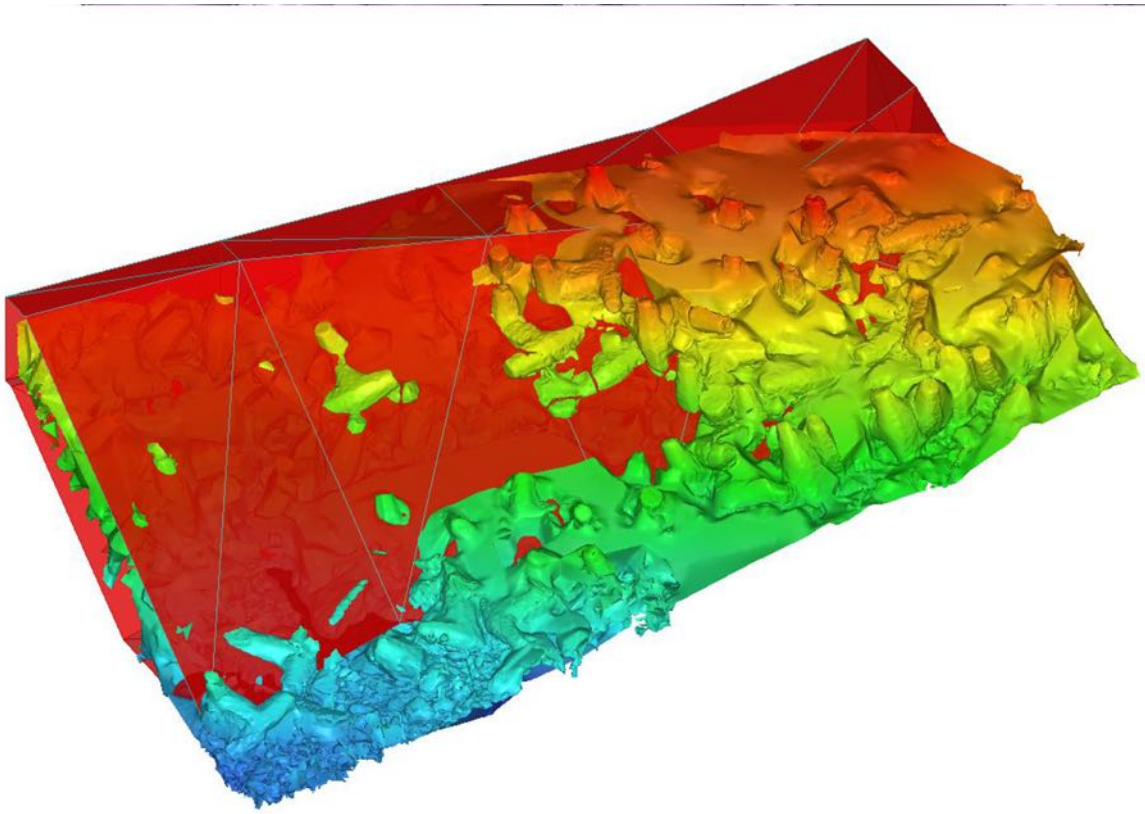

Figure B.9: 3D view of south spur station indicating as-built surface overlay

Appendix C

Appendix C

C.1 Data from model study

The figures presented indicate the records from the armour track software. Lines are drawn to show the distance a unit has moved. The before image is a repeat of the after image from the previous test for Test 2 to Test 4.

C.1.1 Data from spur breakwater model tests

Figure C.1: Image before Test 1.1

Figure C.2: Image after Test 1.1

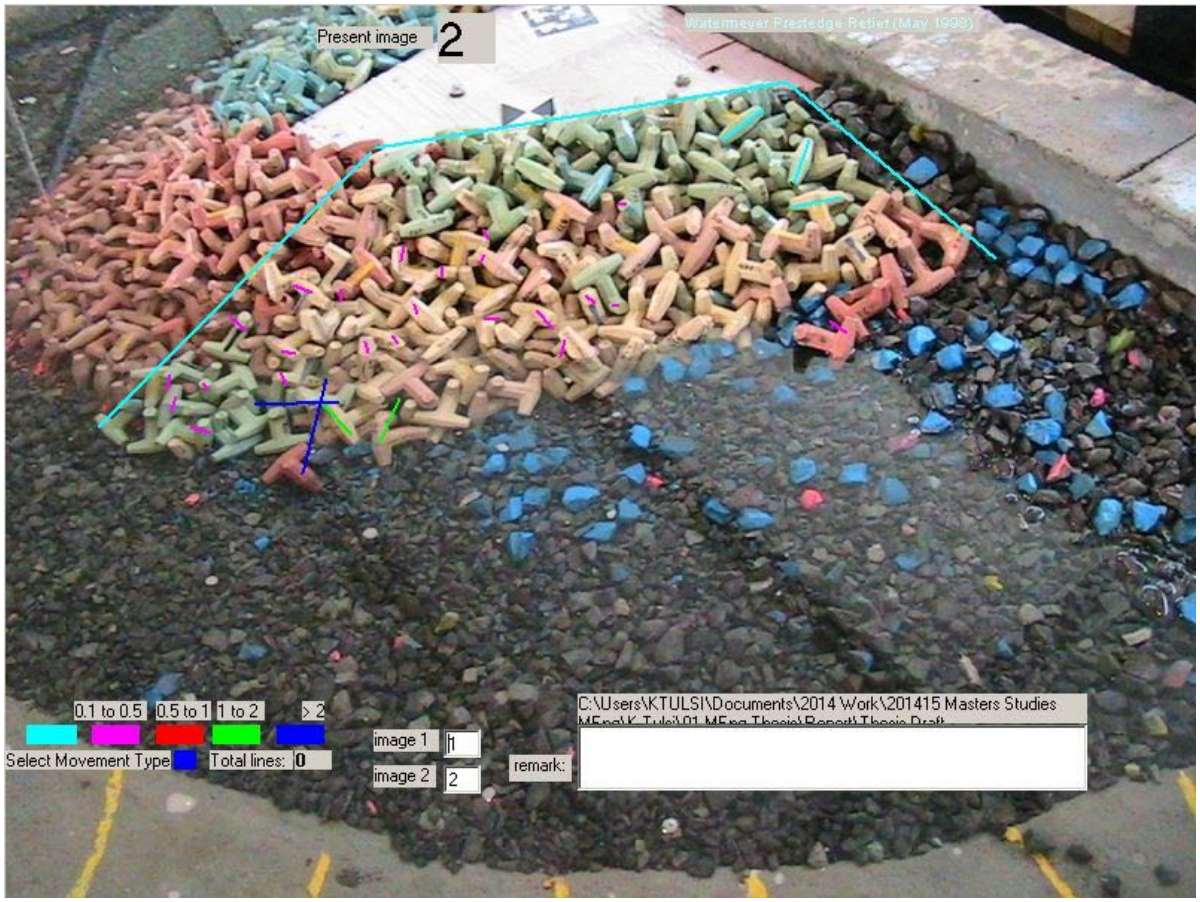

Figure C.3: Recorded displacement for Test 1.1

Figure C.4: Image before Test 2.1

Figure C.5: Image after Test 2.1

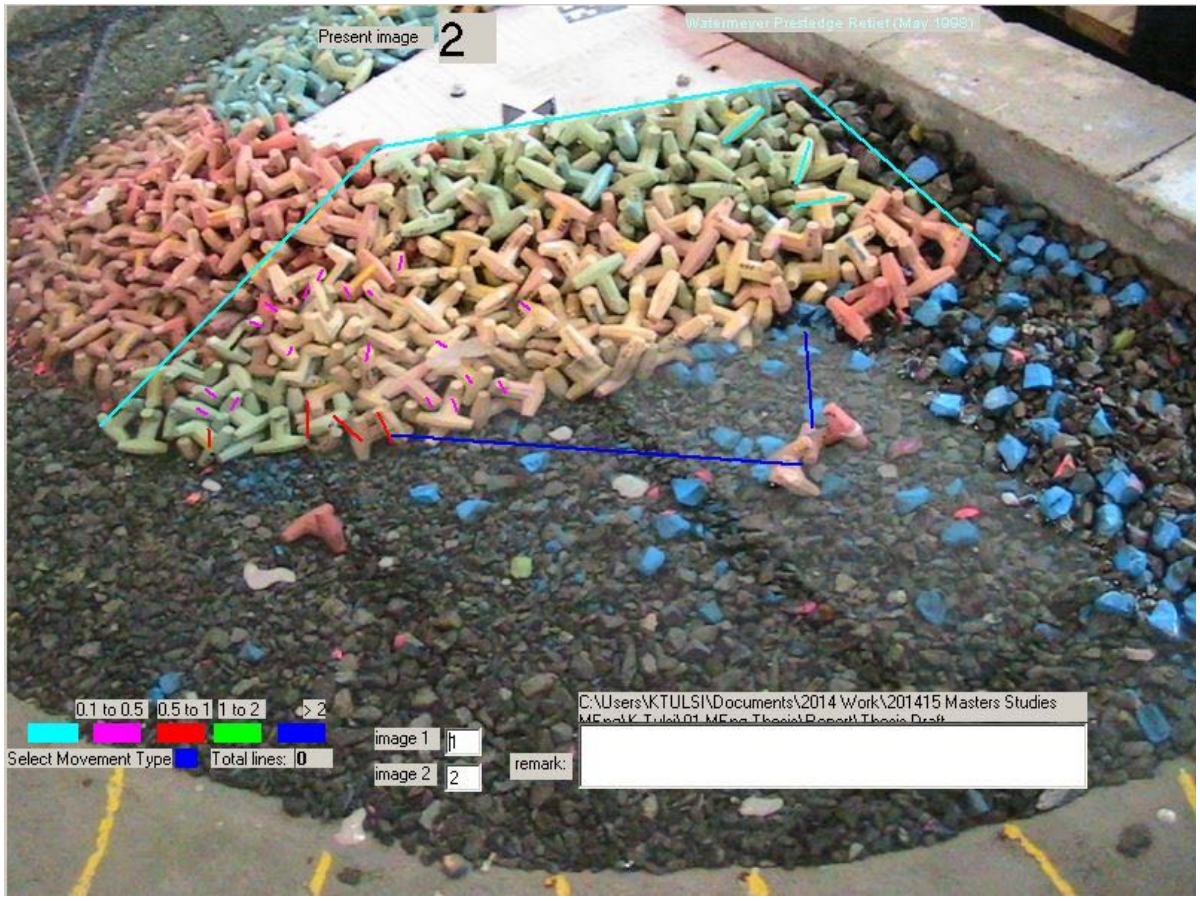

Figure C.6: Recorded displacement for Test 2.1

Figure C.7: Image before Test 3.1

Figure C.8: Image after Test 3.1

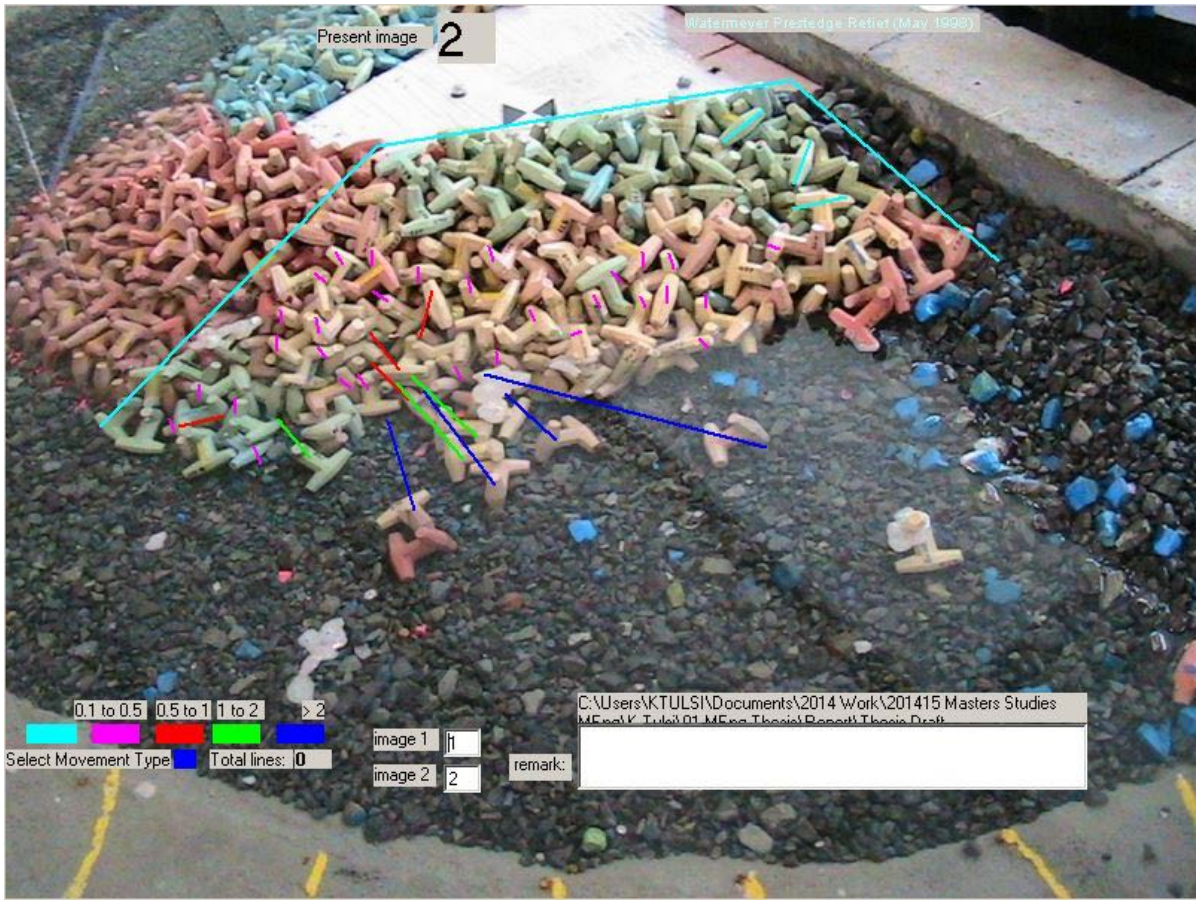

Figure C.9: Recorded displacement for Test 3.1

Figure C.10: Image before Test 4.1

Figure C.11: Image after Test 4.1

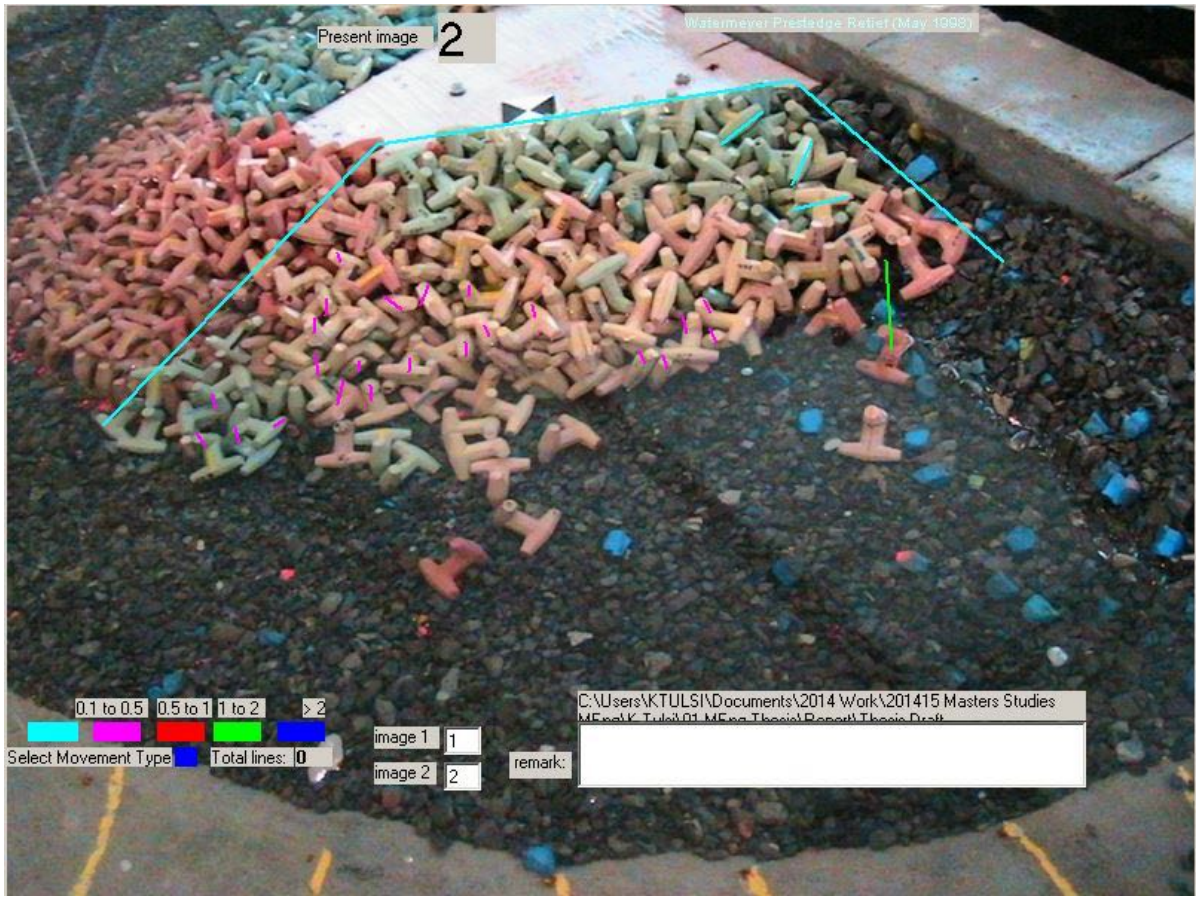

Figure C.12: Recorded displacement for Test 4.1

The data recorded from the LIDAR scanning provides a quantitative state of the breakwater for every station. Scanned data from tests

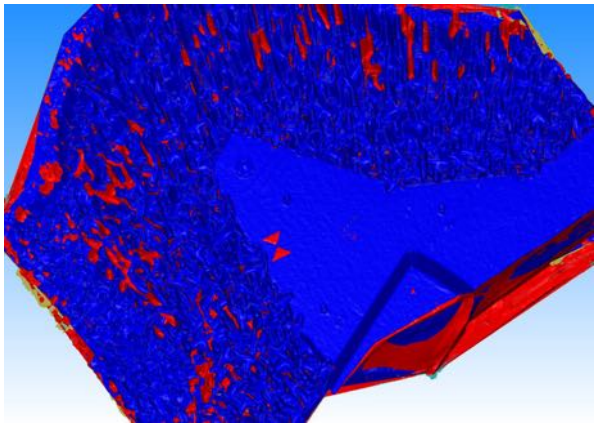

Figure C.13: Scanned spur top view

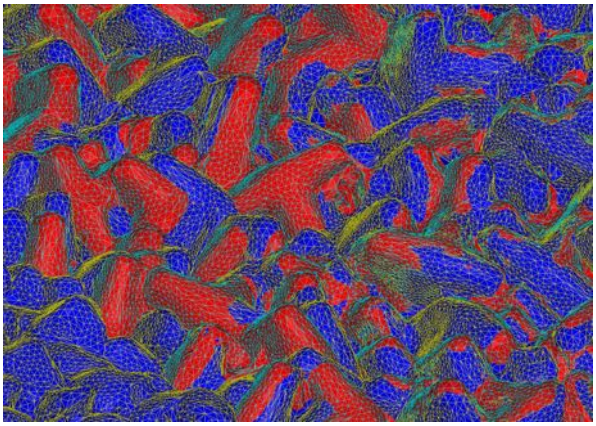

Figure C.14: Zoomed in view showing mesh and movement between tests

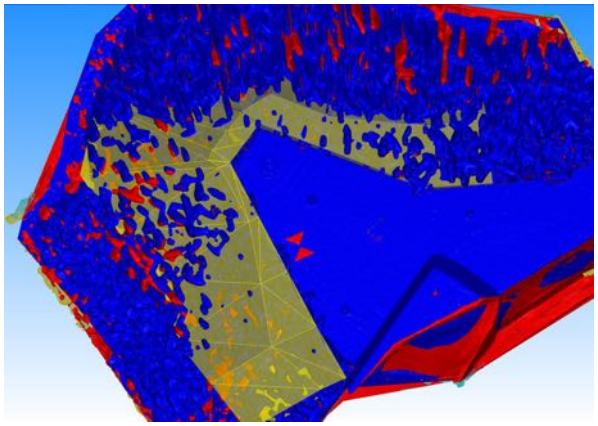

Figure C.15: Spur with as-built design overlay

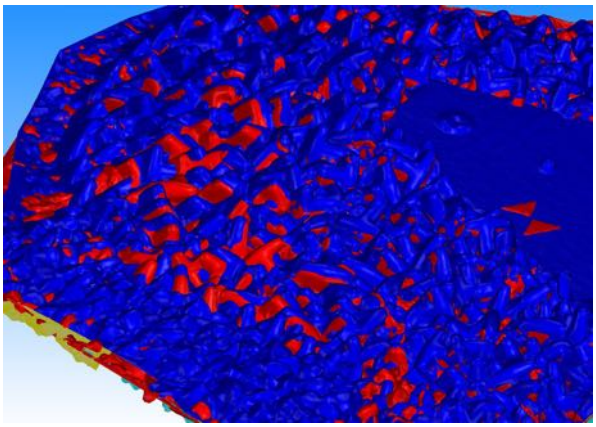

Figure C.16: Zoomed in section showing movement after Test 2

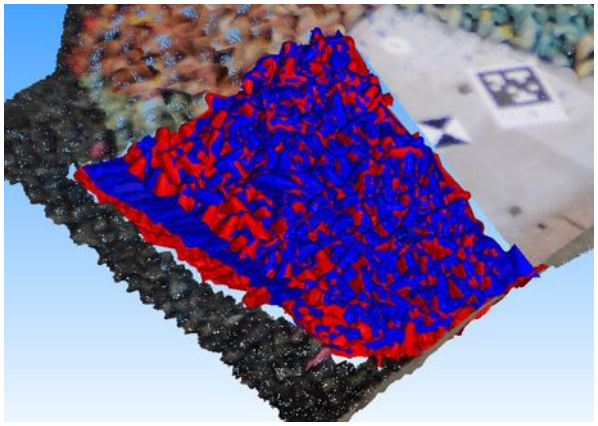

Figure C.17: View showing area of interest

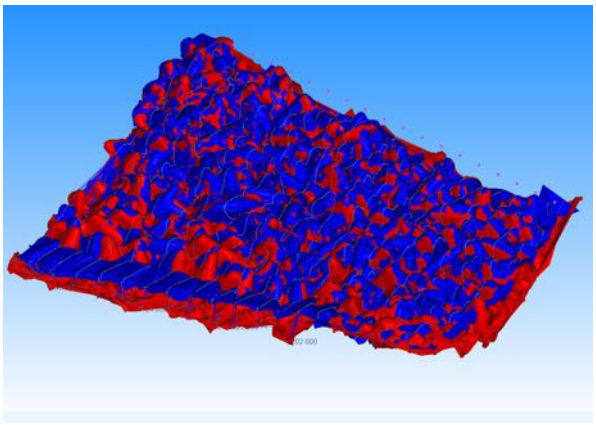

Figure C.18: View showing extracted station for further analysis

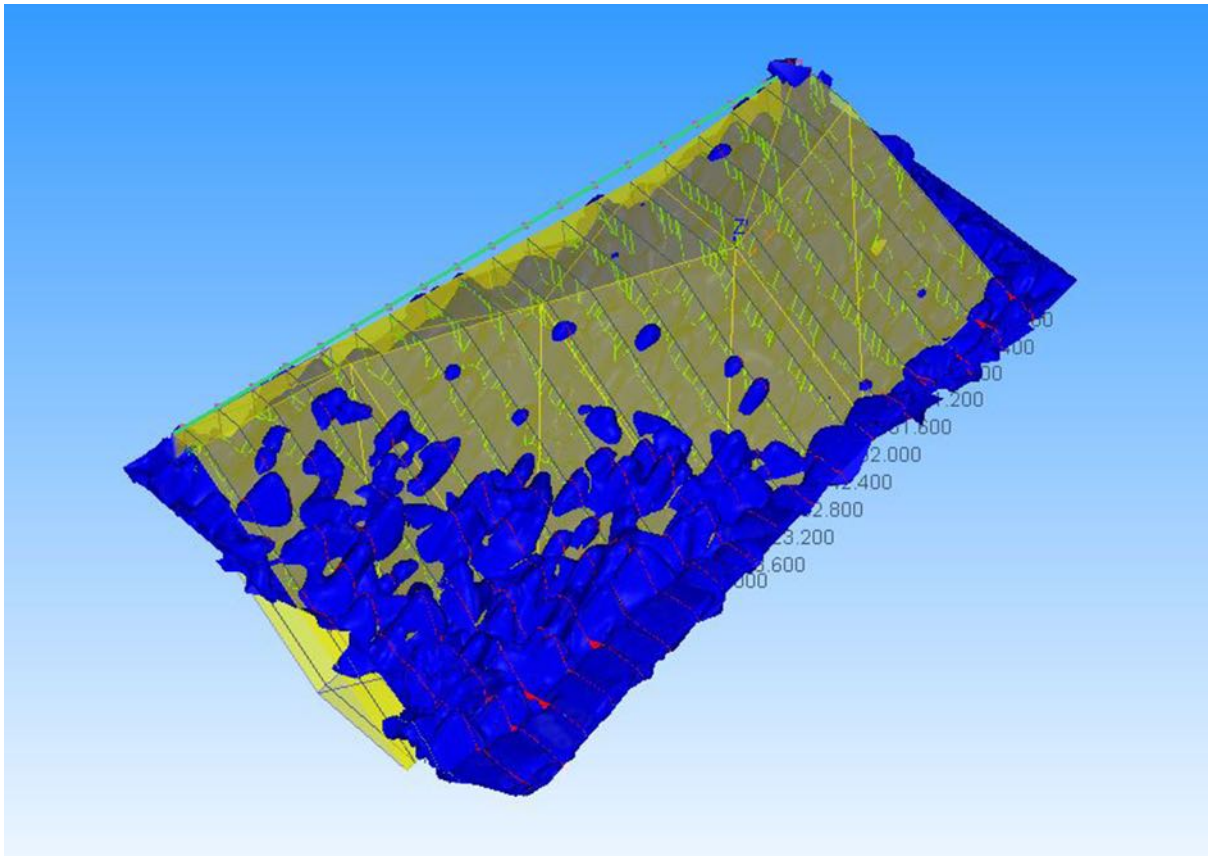

Figure C.19: View showing location of cross-section and as-built design

C.1.2 Sensitivity test comparing scanned data to photographic method

The images and scans of the displacement, rotation and settlement tests are presented below in Figure C.20 and Table C.67. The tests descriptions are indicated in Table C.1

Table C.1: Test conditions

Dolos displacement Test	Initial	Intermediate	Failure
Damage Level criteria	0-2%		≥15%
Test Description	Test 1 to 6	Test 7 to Test 19	Test 20 to Test 24

Figure C.20: Visual image from photographic method T1.1

Figure C.21: Visual image from scaned method T1.1

Figure C.22: Visual image from photographic method T1.2

Figure C.23: Visual image from scaned method T1.2

Figure C.24: Visual image from photographic method T1.3

Figure C.25: Visual image from scaned method T1.3

Figure C.26: Visual image from photographic method T1.4

Figure C.27: Visual image from scaned method T1.4

Figure C.28: Visual image from photographic method T1.5

Figure C.29: Visual image from scaned method T1.5

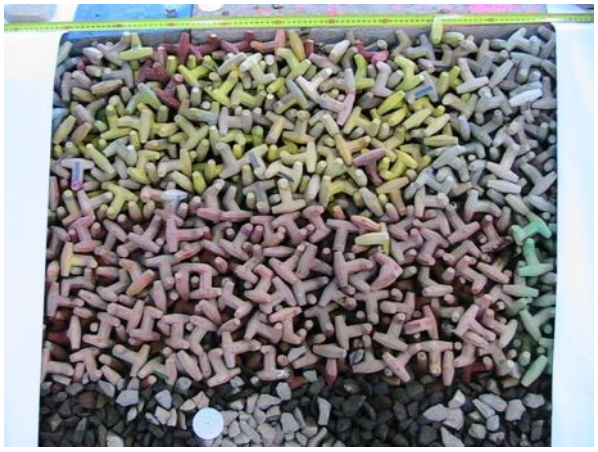

Figure C.30: Visual image from photographic method T1.6

Figure C.31: Visual image from scaned method T1.6

Figure C.32: Visual image from photographic method T2.1

Figure C.33: Visual image from scaned method T2.1

Figure C.34: Visual image from photographic method T2.2

Figure C.35: Visual image from scaned method T2.2

Figure C.36: Visual image from photographic method T2.3

Figure C.37: Visual image from scaned method T2.3

Figure C.38: Visual image from photographic method T2.4

Figure C.39: Visual image from scaned method T2.4

Figure C.40: Visual image from photographic method T2.5

Figure C.41: Visual image from scaned method T2.5

Figure C.42: Visual image from photographic method T2.6

Figure C.43: Visual image from scaned method T2.6

Figure C.44: Visual image from photographic method T2.7

Figure C.45: Visual image from scaned method T2.7

Figure C.46: Visual image from photographic method T2.8

Figure C.47: Visual image from scaned method T2.8

Figure C.48: Visual image from photographic method T2.9

Figure C.49: Visual image from scaned method T2.9

Figure C.50: Visual image from photographic method T2.10

Figure C.51: Visual image from scaned method T2.10

Figure C.52: Visual image from photographic method T3.1

Figure C.53: Visual image from scaned method T3.1

Figure C.54: Visual image from photographic method T3.2

Figure C.55: Visual image from scaned method T3.2

Figure C.56: Visual image from photographic method T3.3

Figure C.57: Visual image from scaned method T3.3

Figure C.58: Visual image from photographic method T4.1

Figure C.59: Visual image from scaned method T4.1

Figure C.60: Visual image from photographic method T4.2

Figure C.61: Visual image from scaned method T4.2

Figure C.62: Visual image from photographic method T4.3

Figure C.63: Visual image from scaned method T4.3

Figure C.64: Visual image from photographic method T4.4

Figure C.65: Visual image from scaned method T4.4

Figure C.66: Visual image from photographic method T4.5

Figure C.67: Visual image from scaned method T4.5

Appendix D

Appendix D

D.1 Conference abstract

THREE DIMENSIONAL METHOD FOR MONITORING DAMAGE TO DOLOS BREAKWATERS

Kishan Tulsi, Council for Scientific and Industrial Research, South Africa, ktulsi@csir.co.za,
Koos Schoonees, Stellenbosch University, South Africa, kooss@sun.ac.za

INTRODUCTION

The inter-tidal zone on a breakwater slope is commonly where damage occurs. However, it is the most difficult data capture zone particularly for visibility. Nowadays, high resolution acoustic and laser scanning technology are available to inspect above and underwater using bathymetric multi-beam echo sounders with light detection and ranging (LIDAR) methods. The advantages of this technologies are that it can be accomplished relatively inexpensively compared to aerial photographic methods.

Traditionally, breakwater inspections have been done using aerial photographs, and underwater imaging to accomplish condition inspections. Large infrastructures like breakwaters are systematically broken up into inspection stations and photographs are taken. The photographs are then visually compared with the previous inspection photograph to identify the changes. This is time consuming and requires a good visual understanding of the damage to breakwaters and most often the information gathered is qualitative. A method representing quantity of material lost is generally required.

OBJECTIVE

The objective of this study is to test the three-dimensional (3D) method by evaluating the accuracy of using the LIDAR (laser) and multi-beam echo sounder data to quantify damage to dolos breakwaters above and below the water surface (including the intertidal zone). Thus, this comparison is aimed towards the development of the 3D method.

A physical model is set-up comparing the accuracy of the photographic displacement and eroded volume. Damage is created manually and measured. The scanned section is shown in Figure 1. Thereafter, a physical model of a prototype breakwater comparing damage to dolos armour units is carried out to assess damage progression by wave action.

This was followed by obtaining an extensive dataset of photographs between 1991 and 2014 from the CSIR. This consisted of aerial photographic data of the Port of Cape Town.

Thereafter the bathymetric multi-beam and LIDAR breakwater survey data is collected and processed to create a 3D mesh of the scanned surface. Thereafter the as-built design profiles are re-created in the 3D environment. The two surfaces are then subtracted to determine the eroded volume per station (Figure 2).

Figure 1: Laser scanned slope in physical model

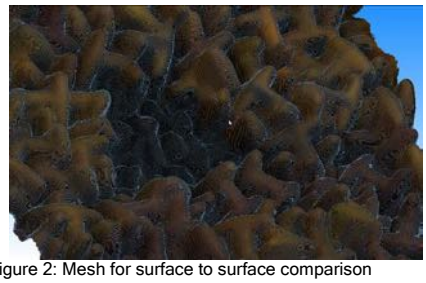

Figure 2: Mesh for surface to surface comparison

CONCLUSION

This has led to quantifiable assessments for large damage to breakwaters with concrete armour.
The eroded volume method used to assess the extent of damage to a breakwater was compared against the conventional damage number method viz. counting the number of units displaced.
A good comparison between the two methods is seen, however further field inspections using both methods are required to create a database of this technology.

REFFERENCES

Phelp et al, (1994). “Results of Extensive Field Monitoring of Dolos Breakwaters.” *Coastal Engineering Proceedings* 24

Holtzhausen et al, (2000). “Physical Modelling of Dolos Breakwaters: The Coega Results and Historical Perspective.” In *Coastal Engineering 2000*, 1536-49.

Figure D.1 indicates some of the existing concrete armour units used globally.

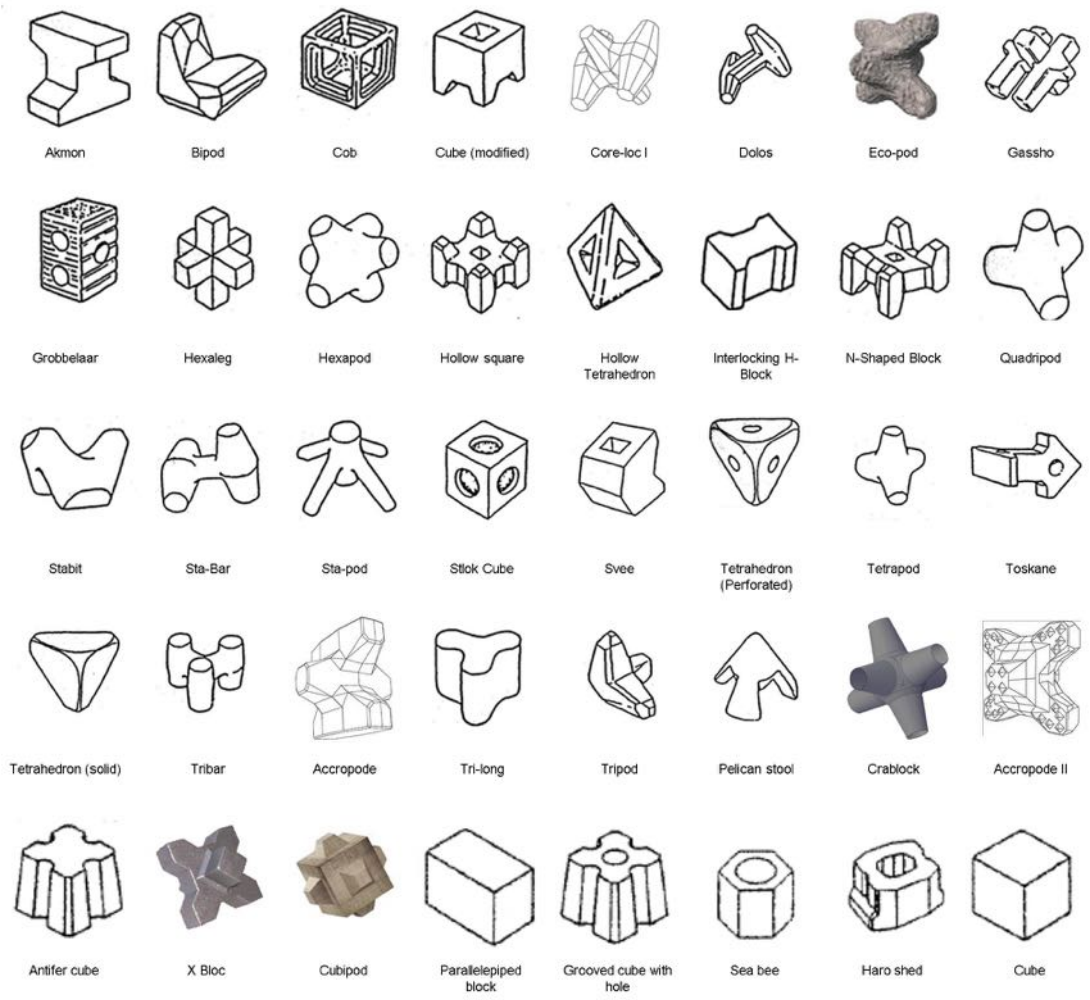

Figure D.1: Breakwater concrete armour units